The impact of electron acceptor variation and reactive oxygen species on microbial respiration rates

Dissertation

zur Erlangung des Grades eines Doktors der Naturwissenschaften

- Dr. rer. nat. –

am Fachbereich Biologie/Chemie der Universität Bremen

Olivia Bourceau

May 2024

Die vorliegende Arbeit wurde in der Arbeitsgruppe Mikrosensoren am Max-Planck-Institut für Marine Mikrobiologie in Bremen angefertigt.

1. Gutachter: Dr. Dirk de Beer
2. Gutachter: Dr. Timothy Ferdelman

1. Prüfer: Prof. Dr. Michael Friedrich
2. Prüfer: Dr. Judith Klatt

Datum des Promotionskolloquiums: 16.07.2024

Table of Contents:

Summary……1

Zusammenfassung……3

Introduction……...5

Redox conditions……...5
Changing environments……10
Denitrification and DNRA……12
Sulfate reduction……15
ROS formation and distribution……...18
Effect of ROS on microbes and the environment……..21
Environments investigated in this thesis……22
Thesis Aims and Research Questions……..24

Manuscript 1: Simultaneous sulfate and nitrate reduction in coastal sediments……35

Manuscript 2: Reactive oxygen species affect the potential for mineralization processes in permeable intertidal flats ……47

Manuscript 3: The effects of ROS and short oxygenation periods on sulfate and nitrate reduction in intertidal sediments……..59

Manuscript 4: High resolution functional analysis and community structure of photogranules……81

Discussion……....93

The impact of electron acceptor variation on respiration ……..93
Environmental implications……97
ROS in photogranules……...……98
Follow up questions……...99
Conclusion ……101

Acknowledgments……104

Contributions to manuscripts..……105

Versicherung an Eides Statt...……106

Erklärungen zur elektronischen Version und zur Überprüfung einer Dissertation……107

Summary:

Dynamic environments are often hotspots of microbial activity that differs from the metabolic activity in more stable environments. Frequent shifts in redox environments pose unique challenges to microbes, who often change their energy metabolism as electron acceptors become depleted or available. In addition to requiring energy to produce new proteins and switch metabolisms, proteins driving e-transfer from reduced electron donors to terminal electron acceptors may become damaged by an influx of more oxidized compounds. For example, the methanogenic protein methyl coenzyme-A is rapidly damaged by oxygen (Mahlert *et al.*, 2002). Further, shifts in redox environments, and particularly oxic-anoxic transitions, can produce reactive oxygen species, which may damage cells (Page *et al.*, 2012; Tong *et al.*, 2016). All of these challenges demand that microbes adapt their behaviors to maximize their fitness.

This thesis investigates how redox fluctuations in environments with chemical gradients, and the reactive oxygen species often produced by such fluctuations, affect microbial metabolism in permeable sediments in the German Wadden Sea and wastewater photogranules. **Manuscript 1** finds that sulfate and nitrate reduction occur simultaneously, and that sulfate reduction rates are correlated with rates of dissimilatory nitrate reduction to ammonia in permeable sediments from the German Wadden Sea, possibly as both processes are driven by the same strains. **Manuscript 2** finds that enzymatically removing reactive oxygen species from incubations of Wadden Sea sediments increases rates of sulfate and iron reduction and well as aerobic respiration. Furthermore, H_2O_2 was found in the upper sediments, controlling early diagenesis. **Manuscript 2** also finds that while sulfate reduction does not occur simultaneously to oxygen consumption in permeable Wadden Sea sediments, it recovers instantly upon anoxia, meaning that the cells and their metabolic apparatus are not damaged by oxygen. **Manuscript 3** finds that the removal of reactive oxygen species does not affect rates of denitrification or dissimilatory nitrate reduction to ammonia. It also finds that pretreatment of sediments with oxygen can increase sulfate reduction in the subsequent anoxic period. Furthermore, it finds that ROS can decrease sulfate reduction even in sediments that have not been recently exposed to oxygen. **Manuscript 4** finds that wastewater photogranules are well adapted to extreme changes in nutrient and oxygen concentrations, performing carbon fixation over a large range of nutrient concentrations. It also finds evidence of aerobic denitrification. The photogranules would not be

suitable for the degradation of recalcitrant substances by ROS, as no ROS production was found, and granules were capable of consuming large quantities of hydrogen peroxide.

Overall, this thesis finds that resident microbes are well adapted to environments with frequent redox changes, and exhibit "braided" use of electron acceptors. It nonetheless finds that the reactive oxygen species produced over oxic-anoxic transitions can substantially decrease microbial activity.

Zusammenfassung:

Dynamische Umgebungen sind oft Hotspots mikrobieller Aktivität, die sich von der Stoffwechselaktivität in stabileren Umgebungen unterscheidet. Häufige Veränderungen in Redox-Umgebungen stellen Mikroben vor besondere Herausforderungen, da sie häufig ihren Energiestoffwechsel ändern, wenn Elektronenakzeptoren erschöpft oder verfügbar werden. Neben dem Energiebedarf für die Produktion neuer Proteine und die Umstellung des Stoffwechsels können Proteine, die den Elektronentransfer von reduzierten Elektronendonatoren zu terminalen Elektronenakzeptoren steuern, durch den Zufluss von mehr oxidierten Verbindungen beschädigt werden. So wird beispielsweise das methanogene Protein Methyl-Coenzym-A durch Sauerstoff schnell beschädigt (Mahlert et al., 2002). Darüber hinaus können Verschiebungen im Redox-Milieu und insbesondere oxische/anoxische Übergänge reaktive Sauerstoffspezies erzeugen, die Zellen schädigen können (Page et al., 2012; Tong et al., 2016). All diese Herausforderungen erfordern, dass Mikroben ihre Verhaltensweisen anpassen, um ihre Fitness zu maximieren.

In dieser Arbeit wird untersucht, wie Redox-Schwankungen in Umgebungen mit chemischen Gradienten und die dabei häufig entstehenden reaktiven Sauerstoffspezies den mikrobiellen Stoffwechsel in durchlässigen Sedimenten im deutschen Wattenmeer und in Abwasser-Photogranulaten beeinflussen. Manuskript 1 zeigt, dass Sulfat- und Nitratreduktion gleichzeitig stattfinden und dass die Sulfatreduktionsraten mit den Raten der dissimilatorischen Nitratreduktion zu Ammoniak in durchlässigen Sedimenten aus dem deutschen Wattenmeer korreliert sind, möglicherweise weil beide Prozesse von denselben Stämmen angetrieben werden. In Manuskript 2 wird festgestellt, dass die enzymatische Entfernung reaktiver Sauerstoffspezies aus Wattenmeersedimenten die Sulfat- und Eisenreduktionsraten sowie die aerobe Atmung erhöht. Darüber hinaus wurde H2O2 in den oberen Sedimenten gefunden, was die frühe Diagenese kontrolliert. In Manuskript 2 wird auch festgestellt, dass die Sulfatreduktion in durchlässigen Wattenmeersedimenten zwar nicht gleichzeitig mit dem Sauerstoffverbrauch stattfindet, sich aber bei Anoxie sofort erholt, was bedeutet, dass die Zellen und ihr Stoffwechselapparat nicht durch Sauerstoff geschädigt werden. In Manuskript 3 wird festgestellt, dass die Entfernung reaktiver Sauerstoffspezies keinen Einfluss auf die Geschwindigkeit der Denitrifikation oder der dissimilatorischen Nitratreduktion zu Ammoniak hat. Es wird auch festgestellt, dass die Vorbehandlung von Sedimenten mit Sauerstoff die Sulfatreduktion in der anschließenden anoxischen Periode erhöhen kann. Darüber hinaus wird festgestellt, dass ROS

die Sulfatreduktion auch in Sedimenten verringern können, die keinem Sauerstoff ausgesetzt waren. In Manuskript 4 wird festgestellt, dass Abwasser-Photogranula gut an extreme Veränderungen der Nährstoff- und Sauerstoffkonzentrationen angepasst sind und Kohlenstoff über einen großen Bereich von Nährstoffkonzentrationen fixieren. Es gibt auch Hinweise auf aerobe Denitrifikation. Die Photogranula eignen sich nicht für den Abbau widerspenstiger Substanzen durch ROS, da keine ROS-Produktion festgestellt wurde und die Granula in der Lage waren, große Mengen an Wasserstoffperoxid zu verbrauchen.

Insgesamt zeigt diese Arbeit, dass die ansässigen Mikroben gut an Umgebungen mit häufigen Redoxwechseln angepasst sind und eine "geflochtene" Nutzung von Elektronenakzeptoren aufweisen. Es wird jedoch festgestellt, dass die reaktiven Sauerstoffspezies, die bei oxischen/anoxischen Übergängen entstehen, die mikrobielle Aktivität erheblich verringern können.

Introduction

Redox conditions

Oxidation-reduction reactions, or redox reactions, where one compound donates an electron to another compound, are the most significant reactions for transforming environmental potential chemical energy into energy useable by cells. While animals and plants rely exclusively on molecular oxygen as their primary electron acceptor, and will die in its absence, microbes can use a diverse range of electron acceptors. The most common of these are, besides oxygen, nitrate/nitrite, iron III, manganese, sulfate, and carbon dioxide. Based on how readily a compound accepts an additional electron, i.e. its electrode potential, a different amount of energy is released when each electron acceptor is paired with the same electron donor (**Table 1**). The reduction products of these redox reactions can theoretically serve as inorganic electron donors for processes with higher electrode potentials. The actual amount of chemical energy stored by microbes in each reaction, however, also depends on the enzymatic machinery used to perform these reactions as well as the activation energy required for the reaction (Flamholz *et al.*, 2013; Nelson and Cox, 2013). Different reactions, or even the same reaction performed by different microorganisms, require different numbers of enzymes, which generate a proton gradient with different levels of efficiency (Flamholz *et al.*, 2013; Nelson and Cox, 2013; Madigan *et al.*, 2015). The proton gradient drives ATP formation by membrane-bound ATPases that couple proton transport to ATP conversion (these enzymes are reversible, and thus can also generate a proton gradient from ATP). As the ATP:H^+ stoichiometry of the H^+ ATPases is normally fixed, the number of translocated protons directly determines the amount of ATP generated in respiratory reactions (Madigan *et al.*, 2015). The consequence of this strict coupling, described in the chemiosmotic theory (Mitchell, 1961) is that the amount of biologically conserved energy (ATP) is not determined by the thermodynamics of the driving process, but by its detailed mechanism. A crucial consequence is that, even when the thermodynamics of two process are close, both the ATP yield per transferred electron and the growth rate of the organisms can drastically differ.

It is often hypothesized that the growth yield on the limiting substrates ultimately determines the winners of the competition for these substrates and the community will move towards the most efficient use of substrates for growth(Roller and Schmidt, 2015). As a consequence, microorganisms performing aerobic respiration will outcompete those performing, for example, denitrification or sulfate reduction. The ecological consequence is that, in

environments with stable gradients, microbes use the most favorable electron acceptor until its depletion, then in deeper zones proceed to the next-most favorable acceptor (**Figure 1 A,B)** (Richards *et al.*, 1965; Fenchel and Jørgensen, 1977; Froelich *et al.*, 1979). Sequential depletion of electron acceptors consistent with this pattern has been observed over time in wastewater treatment (Heukelekian, 1943; McKinney and Conway, 1957) and cell cultures(Seitz and Cypionka, 1986; Krekeler and Cypionka, 1995; Unden and Bongaerts, 1997), and with increasing depth in sediments (Bender *et al.*, 1977; Froelich *et al.*, 1979; Canfield *et al.*, 1993), soils, ground water, and enclosed and stratified water basins (Richards *et al.*, 1965). The sequential use of the strongest oxidant extracts the most energy per molecule of electron donor, which should result in the highest possible production of biomass (McKinney and Conway, 1957; Chen *et al.*, 2017). The hierarchy of electron acceptor use is thought to be preserved by competitive exclusion, where microbes using the most favorable electron acceptor are able to outcompete microbes using less favorable acceptors for electron donor (Lovley and Phillips, 1987; Lovley and Goodwin, 1988). Additionally, the presence of some electron acceptors, especially oxygen, can directly inhibit the expression or function of enzymes involved in the reduction other electron acceptors (Lin and Iuchi, 1991).

Reduction half-reaction	**E°'**
$O_2 + 4e^- + 4H^+ \rightarrow H_2O$	+.815
$Fe^{3+} + e^- \rightarrow Fe^{2+}$	+.771
$NO_3^- + 5e^- + 6H^+ \rightarrow N_2 + 3H_2O$	+.748
$NO_3^- + 8e^- + 9H^+ \rightarrow NH_3 + 3H_2O$	+.717
$NO_3^- + 2e^- + 2H^+ \rightarrow NO_2^- + H_2O$	+.433
$CH_2O + 4e^- + 4H^+ \rightarrow CH_4 + H_2O$	-.213
$SO_4^{2-} + 8e^- + 9H^+ \rightarrow HS^- + 4H_2O$	-.234
$CO_2 + 8e^- + 8H^+ \rightarrow CH_4 + 2H_2O$	-.263
$2H^+ + 2e^- \rightarrow H_2$	-.431
$CO_2 + 4e^- + 4H^+ \rightarrow CH_2O + H_2O$	-.482

Table 1 Electrode potentials of common electron acceptors Values take from (Seager *et al.*, 2012), and represent standard electrode potentials against a hydrogen electrode at pH7.

The thermodynamic energy yield of a reaction, however, does not indicate the kinetics, or rate, of the reaction (Madigan *et al.*, 2015). In some cases, even extremely thermodynamically favorable reactions, such as the reaction of H_2 and O_2, are very slow (Madigan *et al.*, 2015). Enzymes can dramatically increase the rate of reactions, serving as efficient catalysts for a variety of reactions and lowering the required activation energy (Madigan *et al.*, 2015). Predicting what reactions are actually occurring in an environment, must thus also take into account the factors, both inducers and inhibitors, regulating what enzymes are present and active in a system (Nelson and Cox, 2013).

Metabolic activity by one microbe can directly inhibit the metabolism of other community members, and this effect is modulated by the surrounding chemical environment, its history, and the sensitivity of the target organism (Litchman *et al.*, 2015). For example, high concentrations of ammonium can be potently toxic at low pH but is much less so at neutral or alkaline pH (Kater *et al.*, 2006), and both pH and ammonium concentration are themselves directly affected by microbial metabolism. Similarly, in the presence of reduced iron, the oxygenation of an anerobic environment can prove particularly lethal for microbes, due to the production of ROS(Ma *et al.*, 2019; Zhang *et al.*, 2020). Oxygen in general is toxic to many microbes, as it reacts with reduced metal cofactors to produce ROS intracellularly, and production of enzymes for anaerobic metabolism are often inhibited by oxygen (Imlay, 2019; Pandey *et al.*, 2020). In a similar fashion, the reaction of Fe(II) with oxygen inhibits the capacity for oxidation of Mn(II) in the same environment, due to the production of Fe(III) oxyhydroxides and, at high concentrations, ROS (Tong *et al.*, 2022). and microbes required significant adaptations to allow survival of the great oxygenation event (Sessions *et al.*, 2009). Similarly, high concentrations of sulfide or nitric oxide such as produced by sulfate reduction or nitrogen cycling, respectively, inhibit other microbes and thereby shape the community (Brunet and Garcia-Gil, 1996; Fida *et al.*, 2018).

The argument that the order of electron acceptor usage mirrors the order of its depletion, which in turn reflects a decreasing energetic yield, is not without controversy. Instead, some propose that the depletion of electron acceptors is better explained by a partial equilibrium between inorganic electron acceptors and their reduction products and the fermentation products which serve as electron donors (Postma and Jakobsen, 1996; Jakobsen and Postma, 1999). This is because the rate limiting step of most anaerobic processes is fermentation and the breakdown of organic carbon, not the redox reaction of the terminal electron acceptor and

fermentation product (Postma and Jakobsen, 1996; Jakobsen and Postma, 1999). Furthermore, reduction products of less energetic processes can serve as electron donor to the more energetic processes, masking the presence of a less energetic process in an oxidized zone e.g. iron II can serve as an electron donor for nitrate reduction. "Cryptic" cycling, where reduction products from less energetic processes are so quickly oxidized as to be undetectable, has been observed in stratified environments (Canfield *et al.*, 2010). This rapid cycling cannot be detected from concentration profiles, and may mask "unexpected" microbial metabolism. Additionally, overlapping zones of iron reduction and sulfate reduction, sulfate reduction and methaneogenesis and iron reduction and methanogenesis, have been observed in range of environments (Jakobsen and Postma, 1999). It should be noted, however, that the case of overlapping iron and sulfate reduction is special, because the favorability iron reduction depends strongly on the form of iron available, so whether sulfate or iron reduction is more thermodynamically favorable varies according to the minerology of microsites within sediments (Postma and Jakobsen, 1996). Finally, even in culture, some microbes do not preferentially use the most thermodynamically favorable electron acceptor available(Lorenzen *et al.*, 1993; Dalsgaard and Bak, 1994; Marietou *et al.*, 2009).

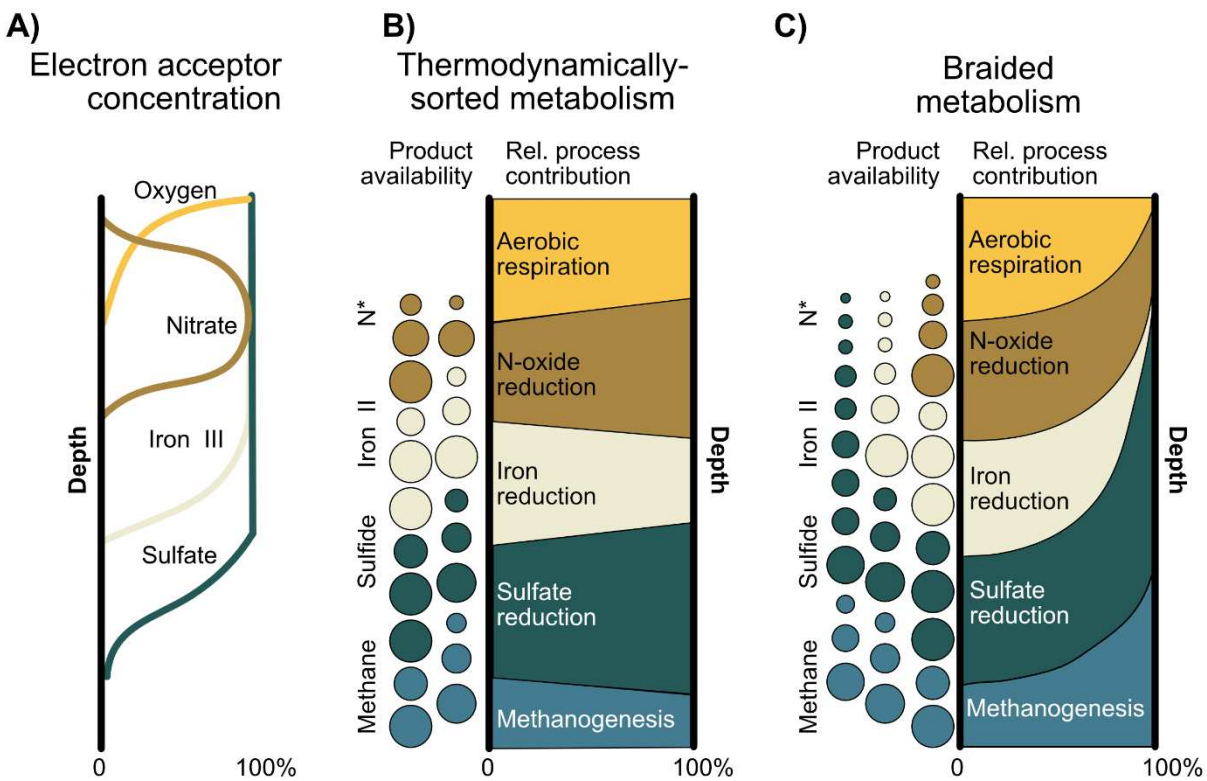

Figure 1: Distribution of metabolic activity in sediment A) The distribution of electron acceptors in stratified, unmixed sediment with increasing depth is displayed, from 0 to 100% of its maximum concentration. B) The distribution of bacterial metabolism according to thermodynamic sorting, where the most thermodynamically favorable metabolism excludes other metabolisms from its area, in stratified, unmixed sediment is displayed on a scale of 0-100% of the total metabolism at a given depth, to the right of the bolded line. To the left of the bolded line are the products of microbial metabolism available for potential oxidation by more favorable electron acceptors. C) The distribution of bacterial metabolism with "braided" metabolism, where multiple thermodynamically favorable metabolisms co-occur rather than only the most favorable metabolism, in a stratified sediment is displayed on a scale of 0-100% of the total metabolism at a given depth, to the right of the bolded line. To the left of the bolded line is as in B).

In environments with variable electron acceptor availability, it seems that the typical pattern of electron acceptor use and depletion is even less stringently followed (**Figure 1 C**). Instead, electron acceptors may be used in a "braided" fashion, where multiple electron acceptors are used simultaneously, and the products of one metabolism are used for another(Chen *et al.*, 2017). Denitrification in the presence of oxygen has been observed in cultures grown under alternating redox conditions, intertidal sands, and wastewater treatment plants (Frette *et al.*, 1997; Patureau *et al.*, 2000; Gao *et al.*, 2010), and intermittent oxygen exposure increased the capacity for aerobic denitrification (Marchant *et al.*, 2017). Additionally, enrichment cultures of intertidal sands provided oxygen or nitrate failed to exclude microbes performing less energetically favorable metabolisms, suggesting that multiple redox metabolisms with different energy yields proceeded simultaneously (Chen *et al.*, 2017). Fluctuating soil redox conditions resulted in co-occurring iron reduction, N_2O production and methanogenesis (DeAngelis *et al.*, 2010).

Variable redox conditions can also allow sediments to "recharge" and fuel later anaerobic respiration. Reduced compounds are reoxidized by compounds with higher electrode potentials, especially oxygen, providing a refreshed pool of electron acceptors(Bayley *et al.*, 1986; Dowrick *et al.*, 2006; Knorr *et al.*, 2009). Within sediments there are a number of substances with redox-active metastable phases (RAMPS), structures consisting of a mixture of substance with different redox potentials or structure e.g. humic acids and magnetite(Peiffer *et al.*, 2021). As the RAMPS age in a stable environment, their redox states become more uniform, thereby making them less reactive (Peiffer *et al.*, 2021). Redox cycling slows or prevents the aging process, boosting the reactivity of the RAMPs, and allowing them to serve as "biogeobatteries" to fuel anaerobic metabolism (Peiffer *et al.*, 2021). This includes iron hydroxides which are reduced, retained in the sediment as solid iron II, then rapidly reoxidized back to iron III upon oxygenation (Zhou *et al.*,

2023). Iron containing RAMPS formed from tide-induced redox cycling are also potent sources of ROS upon oxygenation (Zhao *et al.*, 2023).

Changing Environments

Organisms thrive by adapting to their habitat. When their habitat changes, as happens frequently in nature, they must adapt once again. Fortunately, compared to animals and other multicellular life, microbes are supremely adaptable on both a lineage and individual level. At the lineage scale, genomic imprinting, rapid cellular division, plasmid uptake, and a higher replication error rate, among other factors, allow for the emergence and selection of well adapted microbes from previously poorly adapted ancestors on very short timescales (Shade *et al.*, 2012; Xue and Leibler, 2016). At the individual level, microbes have a high level of metabolic diversity, and can often subsist using a range of different carbon sources and/or electron acceptors. Nevertheless, environmental changes can be life threatening, especially if they involve a change in nutrient availability, and microbes must adopt strategies to cope.

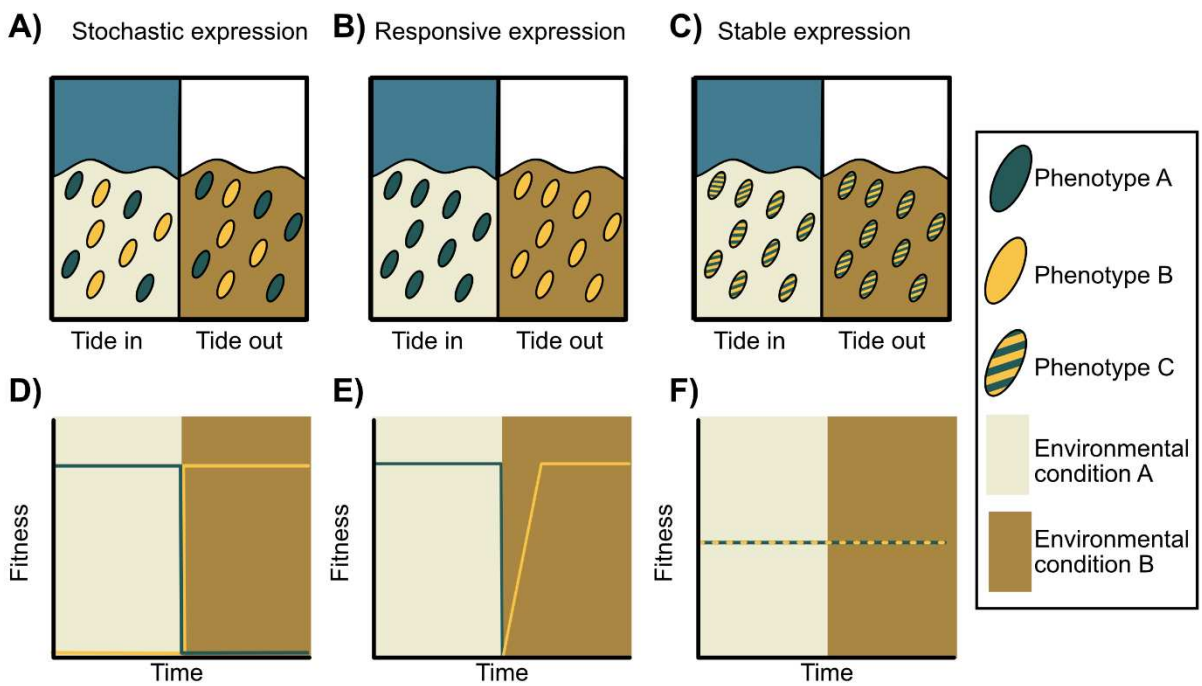

Figure 2: Methods of coping with environmental variation Three different ways of coping with environmental fluctuation, and their impact on organismal fitness are visualized. Phenotypic expression of one species of bacteria where bacteria: **A)** randomly vary their phenotype to be optimized for either environmental condition A or B; **B)** vary their phenotype according to environmental signals; or **C)** stably express an intermediate phenotype that is not optimized for either environmental condition A or B. The effect of these different strategies on fitness are displayed in panels D-F.

Most short-term microbial strategies to cope with environmental change fall into three fundamental categories: responsive expression of well-adapted phenotypes, stochastic expression of well- and poorly-adapted phenotypes (phenotypic variation), and stable expression of intermediate phenotypes (**Figure 2**). All three strategies are widespread among bacteria, and employed simultaneously for different traits, or combined to regulate a single trait. Under responsive expression, a trait is directly regulated through a mechanism sensitive to environmental or intracellular signals. The classic example of responsive expression is switching metabolisms based on changing nutrient availability(New *et al.*, 2014; Chu, 2017). However, responsive expression comes with the cost of environmental sensing machinery, as well as lag time as the cell changes its phenotype(Geisel, 2011; New *et al.*, 2014; Grimbergen *et al.*, 2015). Under stochastic expression, the expression of a trait is semi-randomly regulated, such that a portion of a population is mal-adapted to the present conditions at all times, but well adapted to an alternative potential environment(Lagage and Uphoff, 2020). The size of the well- versus poorly adapted subpopulations is sensitive to both environmental history and the higher growth rate of the well-adapted subpopulation(Martins and Locke, 2015; de Groot *et al.*, 2023). Nutrient limitation, changes in environmental conditions over time, and gradients all increase heterogeneity of phenotype expression within microbial populations (de Jong *et al.*, 2011; Schreiber and Ackermann, 2020). In fluctuating environments, phenotypic variation enables "bet-hedging," a trade-off between the temporal variance of the fitness of a population and its mean fitness, where although the mean fitness of a population is decreased, the geometric mean of the fitness over generations is higher (Philippi and Seger, 1989; Morawska *et al.*, 2022). Bet-hedging is particularly successful in randomly varying environments with relatively long duration between changes, but can also be successful under alternative conditions (Kussell and Leibler, 2005; Acar *et al.*, 2008; de Groot *et al.*, 2023). Finally, the expression of an intermediate phenotype which is sub-optimally adapted to multiple environments may sometimes serve microbes, especially by minimizing the lag time associated with changing a cell's phenotype (Geisel, 2011; Mao *et al.*, 2015). What may seem to be the expression of an intermediate phenotype at the population level may, however, actually be caused by phenotypic heterogeneity between individual cells.

In habitats with variable redox environments a combination of responsive, stochastic, and constant phenotype expression can also improve fitness (Carey *et al.*, 2018; Lycus *et al.*, 2018). For example, stable expression of part of the denitrification pathway (NOS) ensures that cells will have enough energy to synthesize the rest of the pathway upon anoxia(Lycus *et al.*, 2018). Simultaneously, the random expression of upstream enzymes (NIR) tide to a feedback loop ensures that a portion of the population can instantaneously take advantage of anoxia(Lycus *et al.*, 2018). In contrast, in intertidal permeable sediments, nitrate reductase (NAP) was constantly expressed over a tidal cycle, while NOS expression varied (Marchant *et al.*, 2017). Random variation in expression of trimethylamine oxide respiration, which is generally repressed by oxygen, ensures that a portion of the *E. coli* populations are constantly prepared for anoxia(Carey *et al.*, 2018). Similarly, rather than increasing responsiveness, nutrient variability appears to favor some degree of stochastic and "leaky" expression, where random expression of genes can allow bacteria to take advantage of brief environmental shifts, especially when responsive expression times are slow (Thattai and van Oudenaarden, 2004; New *et al.*, 2014). Nutrient limitation also increases phenotypic heterogeneity such that a portion of the population is better prepared for a nutrient regime shift, such as from low-nitrogen to nitrogen-depletion(Schreiber *et al.*, 2016; Zimmermann *et al.*, 2018).

Denitrification and DNRA

Nitrogen is one of the basic building blocks of life, and the availability of fixed nitrogen limits growth in both agriculture and broad regions of the ocean. Nitrogen fertilizers have become widespread in agriculture, causing a nitrogen excess in downstream rivers and coastal regions. This excess of fixed nitrogen can lead to oxygen depletion and algal blooms in waterbodies, which directly and dramatically affect the surrounding ecosystems. The transformation of nitrogen is therefore of great ecological and societal interest. The ammonia and urea contained within fertilizers is partially converted to nitrate (NO_3^-) by microbial communities and waters through the aerobic process of nitrification. A portion of the nitrate incorporated to biomass growth, and the rest either accumulates or is reduced through dissimilatory pathways. These pathways are the competing processes of denitrification, dissimilatory nitrate reduction to ammonia (DNRA), and anaerobic ammonia oxidation (anammox). Anammox is not relevant in the intertidal sediments investigated in this thesis and so is not discussed further (Marchant *et al.*, 2014).

Reaction	ΔfG° (kJ/mol)
$2NO_3^- + 5H_2 + 2H^+ \rightarrow N_2 + 6H_2O$	-560
$NO_3^- + 4H_2 + 2H^+ \rightarrow NH_4^+ + 3H_2O$	-600
$2CH_2O + NO_3^- + H_2O \rightarrow NH_4^{\mp} + 2HCO_3^-$	-316

Table 1 Equations for denitrification and DNRA, with their free energy yield. Values from (Porubsky *et al.*, 2009; Austin *et al.*, 2016)

Denitrification and dissimilatory nitrate reduction to ammonia both start with the respiratory conversion of nitrate to nitrite, but release different end products (Pandey *et al.*, 2020). DNRA fully reduces nitrate and nitrite to ammonia, first reducing nitrate to nitrite then to ammonia via the unreleased intermediates of nitric oxide and hydroxylamine. This retains fixed nitrogen in the environment, which can be advantageous in agricultural soils, but usually harmful in waterways. DNRA can be either fermentative or respiratory, though the first step, converting nitrate to nitrite, is always respiratory (Pandey *et al.*, 2020). In contrast, denitrification is a multistep respiratory process that ultimately produces dinitrogen gas. Each step of denitrification requires separate enzymes and produces intermediates that can escape to the environment. First nitrate is reduced to nitrite (NO_2^-), then to nitrous oxide (N_2O), then nitric oxide (NO), then finally dinitrogen gas (N_2) (**Figure 3 A**).

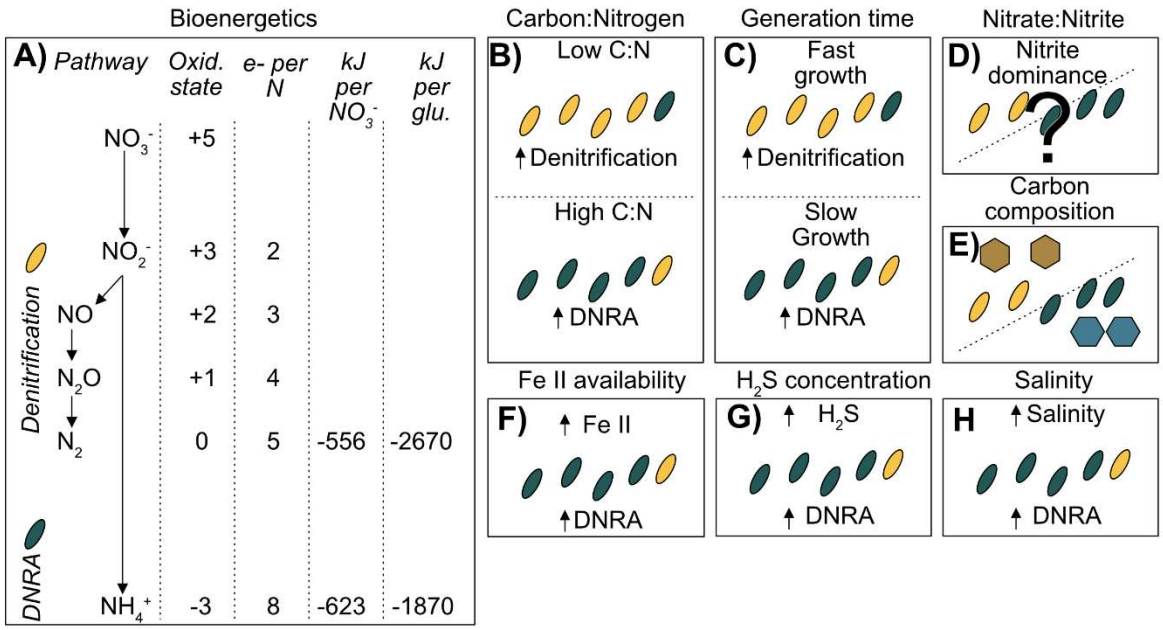

Figure 3 Factors controlling the DN:DNRA ratio Seven of the most commonly considered factors controlling the ratio of DNRA to denitrification are outlined. **A)** The bioenergetics of DNRA versus denitrification in term of total electrons accepted per nitrogen reduced, as well as the Gibbs free energy change of each pathway per mole of nitrate or per mole of glucose, have been used to argue why DNRA or denitrification should be favored under different carbon and nitrogen regimes. Values taken from (Pandey *et al.*, 2020). **B)** The carbon:nitrate/nitrite ratio is very frequently found to explain DNRA rates, with a high C:N ratio favoring DNRA and a low ratio favoring denitrification. **C)** Generation time has also been found to control nitrite partitioning in continuous bioreactors, with slow growth favoring DNRA. **D)** The ratio of nitrate:nitrite has occasionally been found to influence nitrite partitioning, with conflicting results. **E)** Carbon composition can directly control which nitrogen reduction process is favored, where fermentable carbon favors DNRA. Increased **F)** iron II availability, **G)** sulfide, and **H)** salinity have all been found to increase DNRA rates.

There are many competing hypotheses as to what controls how nitrate is divided between denitrification and DNRA (**Figure 3**). The hypotheses that consider drivers in the microenvironment and are either based on bioenergetics or oxygen sensitivity. The most popular proposal, based on bioenergetics, is that the ratio of carbon to nitrate/nitrite determines which pathway is more fruitful in a given environment (Tiedje *et al.*, 1983; Kraft *et al.*, 2014; van den Berg *et al.*, 2015) though this is not consistently found (Behrendt *et al.*, 2014). DNRA is thought to be favorable under high carbon to nitrate/nitrite ratios, as it fully uses the oxidative capacity of nitrate, reducing it fully to ammonia using 8 electrons, while denitrification uses only 5 (Tiedje *et al.*, 1983). The Gibs free energy change per molecule of nitrate is similarly higher for DNRA than denitrification (Tiedje *et al.*, 1983; Pandey *et al.*, 2020). Furthermore, starting from nitrite a net 6 protons are translocated under denitrification, versus 12 under DNRA (Vuono *et al.*, 2019) and microbes performing DNRA seem to have a higher affinity for nitrate (van den Berg *et al.*, 2016). In contrast, denitrification is thought to be favored under nitrate/nitrite excess and carbon limitation because it is more energetically favorable, per molecule of electron donor (Tiedje *et al.*, 1983; Pandey *et al.*, 2020) (**Figure 3 A)** and seems to have a higher affinity for carbon (van den Berg *et al.*, 2016). Alternatively, the total substrate concentration (Vuono *et al.*, 2019) or carbon composition (Akunna *et al.*, 1993; Carlson *et al.*, 2020; Albert *et al.*, 2021) may also control DNRA vs denitrification partitioning. Some studies find that the dominant electron acceptor, nitrate vs nitrite, influence nitrogen partitioning (Kraft *et al.*, 2014; Yoon, Sanford, *et al.*, 2015), but others find that this had no effect under electron acceptor-limiting conditions (van den Berg *et al.*, 2017). High iron II availability has also been found to favor DNRA in lakes, streams, and wetlands (Roberts *et al.*, 2014; Robertson *et al.*, 2016; Robertson and Thamdrup, 2017). Generation time, pH, and temperature have also been found to influence the fate of nitrate/nitrite (Kraft *et al.*, 2014; Yoon, Cruz-García, *et al.*, 2015). Sulfide can also affect N

partitioning by both stimulating DRNA and inhibiting the last step of denitrification, nitrous oxide reduction (Sørensen, 1987; Brunet and Garcia-Gil, 1996; An and Gardner, 2002).

Oxygen availability and concentration may also affect partitioning between denitrification and DNRA. While both process are generally anaerobic, they have been detected despite aerobic conditions in numerous environments (Lloyd *et al.*, 1987; Patureau *et al.*, 2000; Cojean *et al.*, 2019). All complete denitrifiers are also capable of aerobic respiration, which may give them a metabolic advantage in periodically oxygenated environments (Chen and Strous, 2013). Furthermore, denitrification and aerobic respiration share many elements of their electron transport chain, namely NADH dehydrogenase, the quinone pool, the bc_1 complex and cytochrome c, allowing for simultaneous nitrate and oxygen respiration (Bonin and Gilewicz, 1991; Chen and Strous, 2013). This may also enable rapid changes in metabolism as the environmental oxygen availability changes in fluctuating environments (Frette *et al.*, 1997; Chen and Strous, 2013; Marchant *et al.*, 2017). However, oxygen deactivates nitrous oxide reductase (Pomowski *et al.*, 2011) and inhibits the transcription of enzymes in both the DNRA and denitrification pathway (Pandey *et al.*, 2020). In contrast, DNRA uses an entirely different respiratory chain, which also differs based on whether it is performed via a fermentative or respiratory process (Pandey *et al.*, 2020). Nevertheless, DNRA is typically found to be less sensitive to oxygenation than denitrification in most environments (Fazzolari *et al.*, 1998; Morley and Baggs, 2010; Cojean *et al.*, 2019).

The microbial community composition itself, rather than thermodynamics or kinetics may also control partitioning between denitrification and DNRA (Merz *et al.*, 2021). In many cases no firm driver for DNRA or denitrification may be pinpointed. It seems that the environment can select for organisms that perform DNRA or denitrification, on grounds more complicated than simple energetics or inhibiton. For example, if the environment is suitable for typical DNRA performing organisms like *Beggiatoaceae* or diatoms, perhaps at a boundary between sulfide and nitrate or under high light, DNRA will occur, simply because that is the nitrate reduction pathway in these organisms. If the environment is unsuitable for such organisms, denitrification may be dominant.

Sulfate reduction

Sulfate reduction is responsible for up to half of total carbon respiration on continental shelves, despite releasing relatively little energy per molecule reduced. This is largely because the

concentration of sulfate in seawater (~28 mM) is orders of magnitude higher than that of most other electron acceptors, such as oxygen (~200 μM) or nitrate (0-100 μM) (Jørgensen *et al.*, 2019). The high concentration of sulfate supports sulfate reduction until deep in the sediment (Jørgensen *et al.*, 2019). Sulfate reducers are extremely metabolically diverse, and can often respire multiple different electron acceptors using a variety of electron donors(Cypionka, 2000). Possible acceptors individual sulfate reducers may be capable of using include sulfate, nitrate/nitrite, manganese, iron, thiosulfate, carbon dioxide, arsenate, uranium, and chromate, and possible electron donors include hydrogen, various fatty acids, alcohols, methane, or inorganic sulfur compounds, though no one microbe can use all of these acceptors donors (Cypionka, 2000).

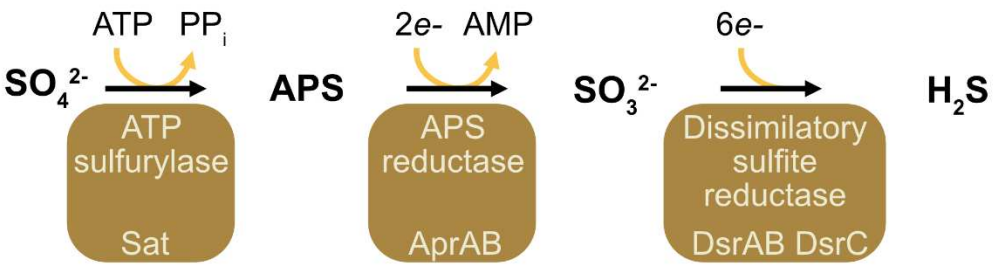

Figure 4: The dissimilatory sulfate reduction pathway. First sulfate activated by ATP sulfurylase using 1 ATP to produce adenosine-5'-phosphosulfate (APS). Next APS is reduced to sulfite by APS reductase. Finally, sulfite is reduced to sulfide by dissimilatory sulfite reductase.

Sulfate reducers are typically considered to be obligately anaerobic, as oxygen is directly toxic and inhibits their growth (Cypionka, 2000; Dolla *et al.*, 2006). The interaction between oxygen and the reduced metal enzymes within sulfate reducers can produce reactive oxygen species that inactivate enzymes and cause cellular damage (Dolla *et al.*, 2006). Nevertheless, many sulfate reducers live in aerobic or periodically aerobic environments and have developed strategies to cope with this stress (Sass *et al.*, 1997; Krekeler *et al.*, 1998; Dolla *et al.*, 2006). Some sulfate reducers may form aggregates or associate with aerobic bacteria to reduce oxygen availability, others migrate away from high oxygen concentrations, still others directly respire oxygen (Dilling and Cypionka, 1990; Sass *et al.*, 2002; Dolla *et al.*, 2006). While oxygen respiration may be coupled to ATP generation in sulfate reducers, it is generally not coupled to growth and most likely serves as a detoxification mechanism (Dannenberg *et al.*, 1992; Cypionka, 2000; Dolla *et al.*, 2006). Sulfate reduction is usually inhibited by oxygen, though it has been detected in a number of aerobic environments(Canfield and Des Marais, 1991; Jørgensen, 1994; Cypionka,

2000). The ability to reduce nitrate has also been suggested as a mechanism of improving oxygen tolerance in sulfate reducers by providing an alternative metabolism when oxygen concentrations are too high to allow sulfate reduction (Marietou, 2016).

Due to the corrosive, toxic, and odorous effects of sulfide, prevention and elimination of sulfide build-up is of interest to many industries(Gieg *et al.*, 2011). Nitrate effectively inhibits sulfide accumulation in various industrial environments (Jenneman *et al.*, 1986; Bødtker *et al.*, 2008; Schwermer *et al.*, 2010). A combination mechanisms have been proposed to explain this inhibition (**Figure 5**), with the best supported including: the oxidation of sulfide by nitrate reducing microbes(Montgomery *et al.*, 1990; Mclnerney *et al.*, 1992; Londry and Suflita, 1999); competition for electron donors resulting in competitive exclusion of sulfate reducing microbes by nitrate reducing microbes(Hitzman and Sperl, 1994; Hubert *et al.*, 2003; Grigoryan *et al.*, 2008); direct inhibition of sulfate reduction by nitrate and its reduction intermediates, nitrite and nitric oxide (Greene *et al.*, 2003; Haveman *et al.*, 2004, 2005); and sulfate reducing microbes switching their metabolism to nitrate reduction (Seitz and Cypionka, 1986; Marietou, 2016). The direct inhibition of sulfate reduction by nitrate and its reduction products each act via different mechanisms (**Figure 5**). In very high concentrations, nitrate inhibits ATP sulfurylase, which activates sulfate with ATP, and may also leak into the cell via thiosulfate transporters (Korte *et al.*, 2014; Stoeva and Coates, 2019). Nitrite can competitively inhibit sulfite reductase, which slowly converts it to ammonium(Wolfe *et al.*, 1994). Nitric oxide can nitrosate 4Fe-4S proteins, which are common in sulfate reducers, including sulfite reductase (Chautrand *et al.*, 2022). Some sulfate reducers also have the ability to perform DNRA, and though some will preferentially reduce nitrate/nitrite, others preferentially reduce sulfate despite the presence of nitrate/nitrite (Mitchell *et al.*, 1986; Haveman *et al.*, 2005; Marietou *et al.*, 2009). The possession of nitrite reductase confers nitrite resistance and improves sulfate reducers competition with other nitrate/nitrite reducing microbes(Greene *et al.*, 2003; Haveman *et al.*, 2004; Rajeev *et al.*, 2015).

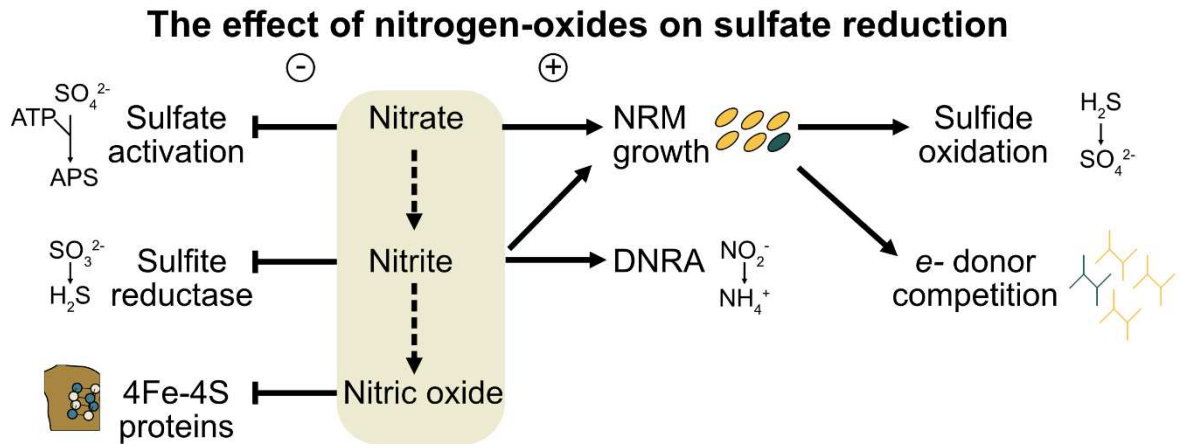

Figure 5: The effect of nitrogen-oxides on sulfate reduction. Nitrate can directly bind and inhibits sulfate activation via ATP sulfurylase, which produces adenosine 5' phosphosulfate, in high concentrations(Stoeva and Coates, 2019). Nitrate can be reduced to nitrite, which competitively inhibits dissimilatory sulfite reductase (DsrAB), the energy-generating step of sulfate reduction. Finally, nitrite can be reduced to nitric oxide, which damages 4Fe-4S clusters in proteins, which are abundant in sulfate reducers. Both nitrate and nitrite stimulate the growth of nitrate/nitrite reducing microorganisms (NRM), which can then effectively compete with sulfate reducers for carbon and micronutrients, as well as oxidize sulfide, the product of sulfate reduction. In sulfate reducers capable of DNRA, nitrite can induce this pathway.

ROS formation and distribution

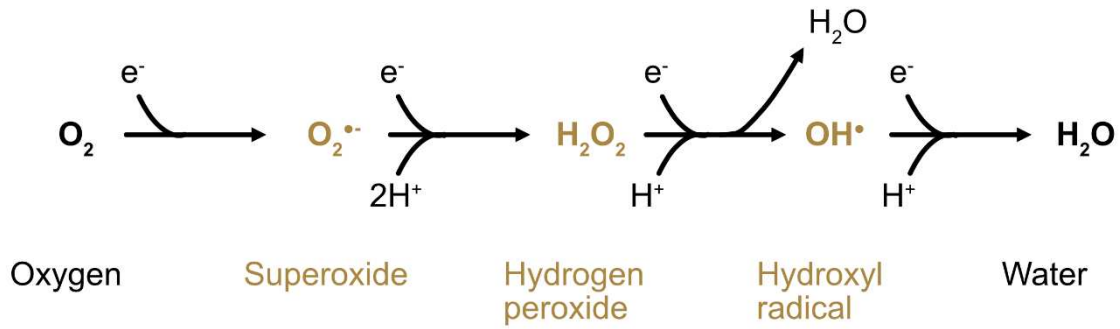

Figure 6: Reactive oxygen species The sequential formation of ROS from one electron reductions of oxygen is outlined. Modeled on (Hansel and Diaz, 2021).

Reactive oxygen species are highly reactive small oxygen-containing molecules, formed from sequential one electron reductions of oxygen, or oxidations of water (**Figure 6**) (Morris *et al.*, 2022). They include superoxide, hydrogen peroxide, and the hydroxyl radical and are oxidants, with the exception of superoxide, which can also be a mild reductant at neutral pH (Morris *et al.*, 2022). They are formed at different rates in most reactions involving oxygen, especially in combination with metals like iron. ROS can be produced intracellularly as a

byproduct of both photosynthesis and respiration, and in non-specific reactions between oxygen and metaolloproteins (Imlay, 2019; Morris *et al.*, 2022). They are also released extracellularly by microbes, seaweeds, and corals to improve iron acquisition, as pathogen defense, for energy dissipation, and signaling, among other reasons (Saragosti *et al.*, 2010; Hansel and Diaz, 2021). Microbes also serve as the primary sink for hydrogen peroxide in the water column (Morris *et al.*, 2022). Abiotically, they are produced at high rates when light reacts with colored organic matter, nitrate or nitrite, or certain metals (Gligorovski *et al.*, 2015; Morris *et al.*, 2022). ROS are also produced when reduced iron reacts with hydrogen peroxide, in a cycle named the Fenton or pseudo-Fenton reactions, depending on whether the iron is soluble or solid, and when sulfide and reduced iron react with oxygen (Garrido-Ramírez *et al.*, 2010; Gligorovski *et al.*, 2015; Murphy *et al.*, 2016). The reaction of humic acids with oxygen can also produce substantial amounts of ROS (Page *et al.*, 2012). ROS can also be formed anaerobically, with the reaction of water with immobilized iron on the surface of pyrite (Borda *et al.*, 2001; Cohn *et al.*, 2006; Ling *et al.*, 2021). Adding to the complexity of studying ROS, the sources of one ROS can also be their sink, or the sink of another ROS, leading to cycling (Goldstone and Voelker, 2000).

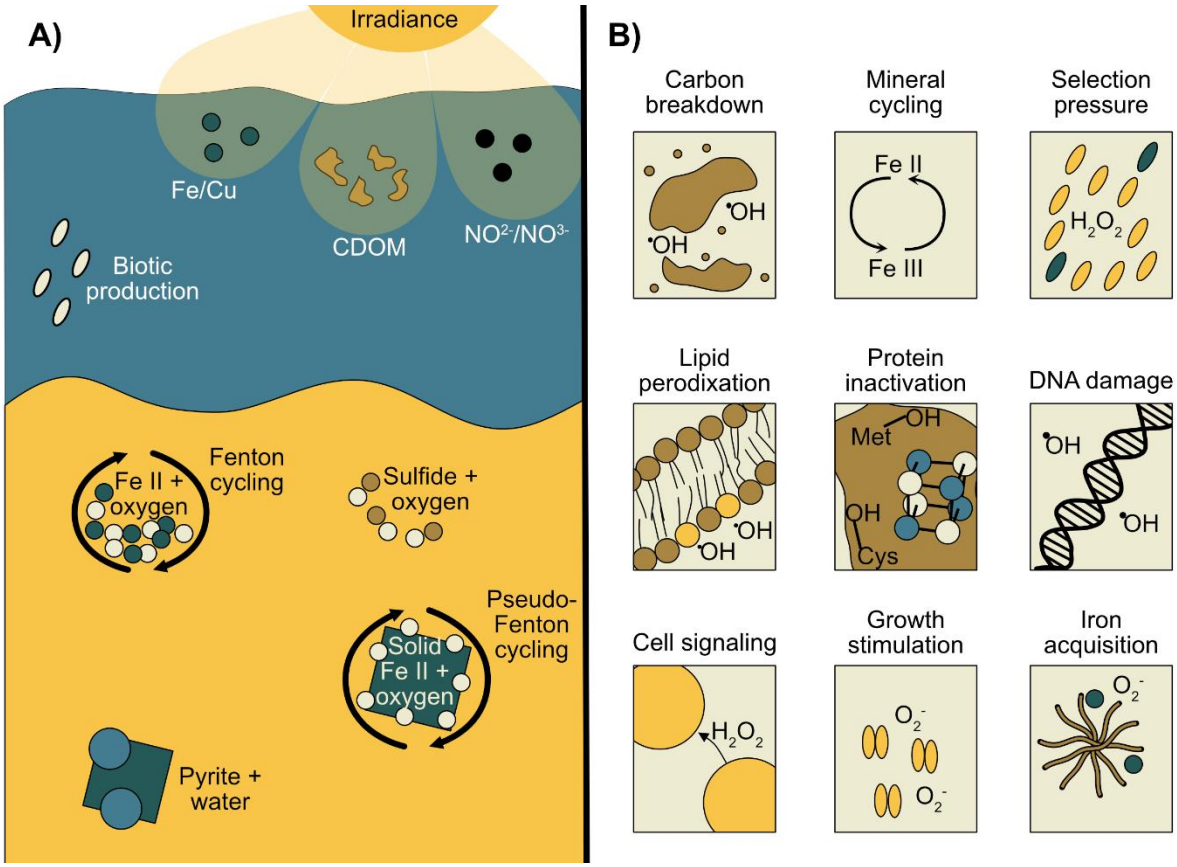

Figure 7 ROS in the environment Known sources of ROS in the environment are illustrated (A) and include solar irradiance of iron and copper, colored organic matter and nitrate/nitrite; biotic extracellular production; Fenton cycling; pseudo-Fenton cycling; the reaction of sulfide with oxygen in the presence of hydrous ferric oxides; and the reaction of pyrite with water. Potential effects of environmental ROS on microbes are outlined (B) and include: carbon break down, mineral cycling, selection pressure, lipid peroxidation, protein inactivation, DNA damage, cell signaling, growth stimulation, and iron acquisition. (Borda *et al.*, 2001; Murphy *et al.*, 2016; Ezraty *et al.*, 2017; Imlay, 2019; Hansel and Diaz, 2021; Morris *et al.*, 2022)

In the water column, ROS concentrations are often highest in the upper lit waters and follow a diel and seasonal cycle, but are also produced and cycled in deeper, dark waters (Zhang *et al.*, 2016; Sutherland *et al.*, 2020; Morris *et al.*, 2022). Levels of hydrogen peroxide are correlated with the concentration of dissolved organic matter, and thus higher in terrestrially influenced regions (Morris *et al.*, 2022). Oxic-anoxic interfaces are expected to produce substantial ROS, as reduced iron and sulfide come into contact with oxygen (Imlay, 2019). Anaerobic soils and sediments have been shown to produce ROS to substantial levels upon oxygenation (Page *et al.*, 2014; Tong *et al.*, 2016; Trusiak *et al.*, 2018). Similarly, coastal soils subject to tidal cycling produce ROS according to tide-induced oxygen and redox cycling (Zhao *et al.*, 2022) as do sediments subject to seasonal flooding-drought cycles (Du, Cao, *et al.*, 2021; Du, Wang, *et al.*,

2021). The area around the roots of marine plants, and in the burrows of marine worms are also expected to have high levels of ROS as they sit at oxic-anoxic interfaces (Abele *et al.*, 1998; Dias *et al.*, 2016).

Fenton Cycle
$Fe^{2+} + H_2O_2 \rightarrow FeOH^{2+} + \bullet OH$
$\rightarrow Fe^{3+} + OH^- + \bullet OH$
$Fe^{2+} + \bullet OH \rightarrow FeOH^{2+}$
$\rightarrow Fe^{3+} + OH^-$
$H_2O_2 + \bullet OH \rightarrow HO_2\bullet + H_2O$
$FeOH^{2+} + HO_2\bullet / O_2\bullet \rightarrow Fe^{2+} + O_2 + H_2O / OH^-$
$FeOH^{2+} + H_2O_2 \rightarrow Fe^{2+} + H_2O + HO_2\bullet$

Table 2: The Fenton Cycle Reactions in the Fenton cycle, as outlined in (Gligorovski *et al.*, 2015) are displayed. The Fenton reaction is triggered by the reaction of hydrogen peroxide and iron II at low pH (~<pH3) and produces hydroxyl radicals. The products of this reaction, iron hydroxides/iron III and hydroxyl radicals, cycle through a cascade of downstream reactions until reactants are depleted. Similar reactions also occur in the pseudo-Fenton reactions, where solid iron hydroxides serve as catalysts, and which can occur at circum-neutral pH.

Effect of ROS on microbes and the environment

Intracellular ROS concentrations are tightly controlled, as they have the potential to seriously damage cellular machinery. Superoxide and hydrogen peroxide can both react with free iron and iron contained within proteins, ultimately producing more potent radicals which can permanently damage enzymes (Imlay, 2019; Morris *et al.*, 2022). Superoxide and the hydroxyl radical can also react with cysteine and methionine amino acids to produce additional radicals that inactivate enzymes (Ezraty *et al.*, 2017). Hydroxyl radicals react very rapidly and indiscriminately with organic carbon, and can substantially damage lipids and DNA (Morris *et al.*, 2022). Hydroxyl radicals are so reactive there are no enzymes able to detoxify them, while there are a variety of effective enzymes to cope with hydrogen peroxide and superoxide (Mishra and Imlay, 2012).

ROS can directly shape communities and community behaviors. In simple communities, lactic acid bacteria will produced hydrogen peroxide to inhibit the growth of other bacteria(Imlay, 2019). Similarly, certain marine organisms are particularly sensitive to hydrogen peroxide, such as *Procholorococcus* and *Thaumarchaeota*, and may rely on symbioses with other

bacteria to tolerate high-ROS environments or else be excluded from these regions (Morris *et al.*, 2022). Redox cycling in sediments leading to ROS production directly impacts the survival and activity of some microbes and alters community structure (Ma *et al.*, 2019; Zhang *et al.*, 2020). High hydrogen peroxide concentrations may prevent toxic algal blooms (Morris *et al.*, 2022). ROS can also be used for nutrient acquisition, such as with superoxide improving iron uptake, or inhibition of nutrient acquisition, such as with hydrogen peroxide inhibiting iron uptake (Rose, 2012; Morris *et al.*, 2022). Hydrogen peroxide can even be used as a terminal electron acceptor in the absence of oxygen (Khademian and Imlay, 2017). The hydroxyl radical can react with organic carbon, breaking it down into smaller molecules or even all the way back to CO2 (Page *et al.*, 2014; Trusiak *et al.*, 2018). The hydroxyl radical may be especially relevant in the degradation of resistant organics such as lignin and phenolics (Yu and Kuzyakov, 2021). This has the potential to indirectly shape the microbial community, by controlling the quality and quantity of organic carbon available for respiration.

The impact of ROS on microbial communities has been the subject of substantial research, but only a fraction of this focused on environmental communities. Environmental research on this topic has grown considerably in the past decade, but the impact or ROS on geochemical cycling is underexplored, especially for marine sediments.

Environments investigated in this thesis

The Wadden Sea

The Wadden Sea is the worlds largest intertidal area, covering 8000 km² and with a width between 10 and 30 km and mean depth of 2-3 m (van Beusekom *et al.*, 1999). Approximately half of that area is composed of tidal flats, which are flooded twice daily (van Beusekom *et al.*, 1999). The Wadden Sea is sandwiched between the North Sea and barrier islands on one side, and the German, Dutch and Danish coast on the other, and is fed by multiple rivers (van Beusekom *et al.*, 1999). The coast line, and especially the Dutch coastline, has been substantially impacted by human activity, particularly draining wetlands, "reclaiming" land, and building dykes (Wolff, 1992). Removing wetlands results in a higher-energy coastline, with sand flats increasingly replacing mudflats (Delafontaine *et al.*, 2000; Mai and Bartholomä, 2000; Reise, 2005). The Wadden Sea nevertheless serves as an effective "biocatalytic filter" that removes more fixed nitrogen and carbon than it produces, taking carbon and nitrogen inputs both from coastal rivers and the North Sea (van Beusekom *et al.*, 1999). This helps limit eutrophication of the North Sea.

Because the sea is so shallow and dominated by tidal flats, sediments play a disproportionately large role in mineralization compared to the North Sea, with about 50 vs 10% of respiration occurring in the sediment (van Beusekom *et al.*, 1999).

Sediment permeability has a dramatic impact on nutrient cycling, directly impacting both the standing stock of nutrients and the flux of nutrients through the system (Huettel *et al.*, 2014). While standing stocks of organic carbon are lower in permeable sediments, advective flushing results in a large flux of nutrients through the sediment, supplying active microbial communities(Huettel *et al.*, 2014). In intertidal flats, this results in redox cycling according to the tides, with oxygen penetration varying between a few millimeters and centimeters (de Beer *et al.*, 2005; Werner *et al.*, 2006; Jansen *et al.*, 2009). This redox cycling results in limited amounts of aerobic denitrification (Gao *et al.*, 2010; Marchant *et al.*, 2017), and "braided" fermentative and respiratory activity (Chen *et al.*, 2017). It is not clear to what extent redox cycling affects sulfate reduction in this environment, and nor the effects of reactive oxygen species on biogeochemical turnover.

Wastewater photogranules

Wastewater treatment is necessary to prevent excess fixed carbon, nitrogen, and other pollutants from eutrophying natural waters. Unfortunately, this process can be extremely energy intensive, due to the need to aerate wastewater to provide oxygen for nitrification and organic matter mineralization (Maktabifard *et al.*, 2018). Recently, researchers have attempted to reduced the need for aeration by incorporating photosynthetic microbes in the wastewater stream, developing self-aggregating photosynthetic biogranules, or photogranules, within batch reactors (Abouhend *et al.*, 2018; Trebuch *et al.*, 2020). These photogranules are subject to large fluxes in nutrient concentrations, which also result in redox fluctuations. While it is known that the photogranules effectively remove organic carbon and fixed nitrogen, it is not clear how redox fluctuations effect microbial activity within the granule. Similarly, it is not known whether these granules are a source or sink of ROS. This would be useful to know, as ROS can be employed for the degradation of organic wastewater contaminants (Bracamontes-Ruelas *et al.*, 2022).

Thesis Aims and Research Questions

The overall aim of this thesis was to investigate how regular changes in redox environments affect microbial metabolism and nutrient cycling. The consequences of exposure to reactive oxygen species, which are generated during oxic-anoxic transitions, received special attention. The Janssand tidal flat behind the barrier island Spiekeroog in the German Wadden Sea was investigated in the first three manuscripts. In the fourth manuscript the activity of wastewater photogranules grown in batch reactors was investigated.

The main research questions investigated in this research were:

1. *Does frequent redox switching result in overlapping, "braided" use of electron acceptors?*
2. *Do reactive oxygen species accumulate in environments subject to frequent redox switching?*
3. *How do reactive oxygen species affect microbial respiration?*

These questions are addressed over five chapters. **Manuscript 1** focuses on research question 1 and investigates how variations in nitrate availability affect sulfate and nitrate respiration in the Janssand tidal flat. **Manuscript 2** examines all three research questions, determining standing concentrations of hydrogen peroxide in the Janssand tidal flat (question 2) and how removal of ROS affected rates of sulfate and iron reduction (question 3). It also tests sediments for evidence of the simultaneous use of oxygen and sulfate respiration, i.e. oxic sulfate reduction (question 1). **Manuscript 3** addresses question 3, testing how ROS removal affected rates of nitrate respiration and how anaerobically formed ROS affects sulfate reduction in sediments from the Janssand tidal flat. **Manuscript 4** addresses question 1, investigating the rates of carbon fixation, nitrification, and denitrification in wastewater photogranules subject to different nutrient and oxygen exposure.

Abele, D., Großpietsch, H., and Pörtner, H.O. (1998) Temporal fluctuations and spatial gradients of environmental PO2, temperature, H2O2 and H2S in its intertidal habitat trigger enzymatic antioxidant protection in the capitellid worm Heteromastus filiformis. *Mar Ecol Prog Ser* **163**: 179–191.

Abouhend, A.S., McNair, A., Kuo-Dahab, W.C., Watt, C., Butler, C.S., Milferstedt, K., et al. (2018) The Oxygenic Photogranule Process for Aeration-Free Wastewater Treatment. *Environ Sci Technol* **52**: 3503–3511.

Acar, M., Mettetal, J.T., and van Oudenaarden, A. (2008) Stochastic switching as a survival strategy in fluctuating environments. *Nat Genet* **40**: 471–475.

Akunna, J.C., Bizeau, C., and Moletta, R. (1993) Nitrate and nitrite reductions with anaerobic sludge using various carbon sources: Glucose, glycerol, acetic acid, lactic acid and methanol. *Water Res* **27**: 1303–1312.

Albert, S., Bonaglia, S., Stjärnkvist, N., Winder, M., Thamdrup, B., and Nascimento, F.J.A. (2021) Influence of settling organic matter quantity and quality on benthic nitrogen cycling. *Limnol Oceanogr* **66**: 1882–1895.

An, S. and Gardner, W.S. (2002) Dissimilatory nitrate reduction to ammonium (DNRA) as a nitrogen link, versus denitrification as a sink in a shallow estuary (Laguna Madre/Baffin Bay, Texas). *Mar Ecol Prog Ser* **237**: 41–50.

Austin, D., Scharf, R., Carroll, J., and Enochs, M. (2016) Suppression of hypolimnetic methylmercury accumulation by liquid calcium nitrate amendment: redox dynamics and fate of nitrate. *Lake Reserv Manag* **32**: 61–73.

Bayley, S.E., Behr, R.S., and Kelly, C.A. (1986) Retention and release of S from A freshwater wetland. *Water Air Soil Pollut* **31**: 101–114.

Behrendt, A., Tarre, S., Beliavski, M., Green, M., Klatt, J., de Beer, D., and Stief, P. (2014) Effect of high electron donor supply on dissimilatory nitrate reduction pathways in a bioreactor for nitrate removal. *Bioresour Technol* **171**: 291–297.

Bender, M.L., Fanning, K.A., Froelich, P.N., Heath, G.R., and Maynard, V. (1977) Interstitial Nitrate Profiles and Oxidation of Sedimentary Organic Matter in the Eastern Equatorial Atlantic. *Science* **198**: 605–609.

van den Berg, E.M., Boleij, M., Kuenen, J.G., Kleerebezem, R., and van Loosdrecht, M.C.M. (2016) DNRA and Denitrification Coexist over a Broad Range of Acetate/N-NO3− Ratios, in a Chemostat Enrichment Culture. *Front Microbiol* **7**:.

van den Berg, E.M., van Dongen, U., Abbas, B., and van Loosdrecht, M.C. (2015) Enrichment of DNRA bacteria in a continuous culture. *ISME J* **9**: 2153–2161.

van den Berg, E.M., Rombouts, J.L., Kuenen, J.G., Kleerebezem, R., and van Loosdrecht, M.C.M. (2017) Role of nitrite in the competition between denitrification and DNRA in a chemostat enrichment culture. *AMB Express* **7**: 91.

van Beusekom, J.E.E., Brockmann, U.H., Hesse, K.-J., Hickel, W., Poremba, K., and Tillmann, U. (1999) The importance of sediments in the transformation and turnover of nutrients and organic matter in the Wadden Sea and German Bight. *Dtsch Hydrogr Z* **51**: 245–266.

Bødtker, G., Thorstenson, T., Lillebø, B.-L.P., Thorbjørnsen, B.E., Ulvøen, R.H., Sunde, E., and Torsvik, T. (2008) The effect of long-term nitrate treatment on SRB activity, corrosion rate and bacterial community composition in offshore water injection systems. *J Ind Microbiol Biotechnol* **35**: 1625–1636.

Bonin, P. and Gilewicz, M. (1991) A direct demonstration of "co-respiration" of oxygen and nitrogen oxides by Pseudomonas nautica: some spectral and kinetic properties of the respiratory components. *FEMS Microbiol Lett* **80**: 183–188.

Borda, M.J., Elsetinow, A.R., Schoonen, M.A., and Strongin, D.R. (2001) Pyrite-Induced Hydrogen Peroxide Formation as a Driving Force in the Evolution of Photosynthetic Organisms on an Early Earth. *Astrobiology* **1**: 283–288.

Bracamontes-Ruelas, A.R., Ordaz-Díaz, L.A., Bailón-Salas, A.M., Ríos-Saucedo, J.C., Reyes-Vidal, Y., and Reynoso-Cuevas, L. (2022) Emerging Pollutants in Wastewater, Advanced Oxidation Processes as an Alternative Treatment and Perspectives. *Processes* **10**:.

Brunet, R.C. and Garcia-Gil, L.J. (1996) Sulfide-induced dissimilatory nitrate reduction to ammonia in anaerobic freshwater sediments. *FEMS Microbiol Ecol* **21**: 131–138.

Canfield, D.E. and Des Marais, D.J. (1991) Aerobic Sulfate Reduction in Microbial Mats. *Science* **251**: 1471–1473.

Canfield, D.E., Jørgensen, B.B., Fossing, H., Glud, R., Gundersen, J., Ramsing, N.B., et al. (1993) Pathways of organic carbon oxidation in three continental margin sediments. *Mar Sediments Burial Pore Water Chem Microbiol Diagenesis* **113**: 27–40.

Canfield, D.E., Stewart, F.J., Thamdrup, B., De Brabandere, L., Dalsgaard, T., Delong, E.F., et al. (2010) A Cryptic Sulfur Cycle in Oxygen-Minimum–Zone Waters off the Chilean Coast. *Science* **330**: 1375–1378.

Carey, J.N., Mettert, E.L., Roggiani, M., Myers, K.S., Kiley, P.J., and Goulian, M. (2018) Regulated Stochasticity in a Bacterial Signaling Network Permits Tolerance to a Rapid Environmental Change. *Cell* **173**: 196-207.e14.

Carlson, H.K., Lui, L.M., Price, M.N., Kazakov, A.E., Carr, A.V., Kuehl, J.V., et al. (2020) Selective carbon sources influence the end products of microbial nitrate respiration. *ISME J* **14**: 2034–2045.

Chautrand, T., Souak, D., Chevalier, S., and Duclairoir-Poc, C. (2022) Gram-Negative Bacterial Envelope Homeostasis under Oxidative and Nitrosative Stress. *Microorganisms* **10**:.

Chen, J., Hanke, A., Tegetmeyer, H.E., Kattelmann, I., Sharma, R., Hamann, E., et al. (2017) Impacts of chemical gradients on microbial community structure. *ISME J* **11**: 920–931.

Chen, J. and Strous, M. (2013) Denitrification and aerobic respiration, hybrid electron transport chains and co-evolution. *Evol Asp Bioenerg Syst* **1827**: 136–144.

Chu, D. (2017) Limited by sensing - A minimal stochastic model of the lag-phase during diauxic growth. *J Theor Biol* **414**: 137–146.

Cohn, C.A., Mueller, S., Wimmer, E., Leifer, N., Greenbaum, S., Strongin, D.R., and Schoonen, M.A. (2006) Pyrite-induced hydroxyl radical formation and its effect on nucleic acids. *Geochem Trans* **7**: 3.

Cojean, A.N.Y., Zopfi, J., Gerster, A., Frey, C., Lepori, F., and Lehmann, M.F. (2019) Direct O2 control on the partitioning between denitrification and dissimilatory nitrate reduction to ammonium in lake sediments. *Biogeosciences* **16**: 4705–4718.

Cypionka, H. (2000) Oxygen Respiration by Desulfovibrio Species. *Annu Rev Microbiol* **54**: 827–848.

Dalsgaard, T. and Bak, F. (1994) Nitrate Reduction in a Sulfate-Reducing Bacterium, Desulfovibrio desulfuricans, Isolated from Rice Paddy Soil: Sulfide Inhibition, Kinetics, and Regulation. *Appl Environ Microbiol* **60**: 291–297.

Dannenberg, S., Kroder, M., Dilling, W., and Cypionka, H. (1992) Oxidation of H2, organic compounds and inorganic sulfur compounds coupled to reduction of O2 or nitrate by sulfate-reducing bacteria. *Arch Microbiol* **158**: 93–99.

DeAngelis, K.M., Silver, W.L., Thompson, A.W., and Firestone, M.K. (2010) Microbial communities acclimate to recurring changes in soil redox potential status. *Environ Microbiol* **12**: 3137–3149.

Delafontaine, M.T., Flemming, B.W., and Mai, S. (2000) The Wadden Sea squeeze as a cause of decreasing sedimentary organic loading. In *Proceedings in Marine Science*. Flemming, B.W., Delafontaine, M.T., and Liebezeit, G. (eds). Elsevier, pp. 273–286.

Dias, D.M.C., Copeland, J.M., Milliken, C.L., Shi, X., Ferry, J.L., and Shaw, T.J. (2016) Production of Reactive Oxygen Species in the Rhizosphere of a Spartina-Dominated Salt Marsh Systems. *Aquat Geochem* **22**: 573–591.

Dilling, W. and Cypionka, H. (1990) Aerobic respiration in sulfate-reducing bacteria. *FEMS Microbiol Lett* **71**: 123–127.

Dolla, A., Fournier, M., and Dermoun, Z. (2006) Oxygen defense in sulfate-reducing bacteria. *Asp Prokaryotic Genome Res* **126**: 87–100.

Dowrick, D.J., Freeman, C., Lock, M.A., and Reynolds, B. (2006) Sulphate reduction and the suppression of peatland methane emissions following summer drought. *Geoderma* **132**: 384–390.

Du, H., Cao, Y., Li, Z., Li, L., and Xu, H. (2021) Formation and mechanisms of hydroxyl radicals during the oxygenation of sediments in Lake Poyang, China. *Water Res* **202**: 117442.

Du, H., Wang, H., Chi, Z., Song, N., Wang, C., and Xu, H. (2021) Burst of hydroxyl radicals in sediments derived by flooding/drought transformation process in Lake Poyang, China. *Sci Total Environ* **772**: 145059.

Ezraty, B., Gennaris, A., Barras, F., and Collet, J.-F. (2017) Oxidative stress, protein damage and repair in bacteria. *Nat Rev Microbiol* **15**: 385–396.

Fazzolari, É., Nicolardot, B., and Germon, J.C. (1998) Simultaneous effects of increasing levels of glucose and oxygen partial pressures on denitrification and dissimilatory nitrate reduction to ammonium in repacked soil cores. *Eur J Soil Biol* **34**: 47–52.

Fenchel, T.M. and Jørgensen, B.B. (1977) Detritus Food Chains of Aquatic Ecosystems: The Role of Bacteria. In *Advances in Microbial Ecology*. Alexander, M. (ed). Boston, MA: Springer US, pp. 1–58.

Fida, T.T., Voordouw, J., Ataeian, M., Kleiner, M., Okpala, G., Mand, J., and Voordouw, G. (2018) Synergy of Sodium Nitroprusside and Nitrate in Inhibiting the Activity of Sulfate Reducing Bacteria in Oil-Containing Bioreactors. *Front Microbiol* **9**:.

Flamholz, A., Noor, E., Bar-Even, A., Liebermeister, W., and Milo, R. (2013) Glycolytic strategy as a tradeoff between energy yield and protein cost. *Proc Natl Acad Sci* **110**: 10039–10044.

Frette, L., Gejlsbjerg, B., and Westermann, P. (1997) Aerobic denitrifiers isolated from an alternating activated sludge system. *FEMS Microbiol Ecol* **24**: 363–370.

Froelich, P.N., Klinkhammer, G.P., Bender, M.L., Luedtke, N.A., Heath, G.R., Cullen, D., et al. (1979) Early oxidation of organic matter in pelagic sediments of the eastern equatorial Atlantic: suboxic diagenesis. *Geochim Cosmochim Acta* **43**: 1075–1090.

Gao, H., Schreiber, F., Collins, G., Jensen, M.M., Kostka, J.E., Lavik, G., et al. (2010) Aerobic denitrification in permeable Wadden Sea sediments. *ISME J* **4**: 417–426.

Garrido-Ramírez, E.G., Theng, B.K.G., and Mora, M.L. (2010) Clays and oxide minerals as catalysts and nanocatalysts in Fenton-like reactions — A review. *Appl Clay Sci* **47**: 182–192.

Geisel, N. (2011) Constitutive versus Responsive Gene Expression Strategies for Growth in Changing Environments. *PLOS ONE* **6**: e27033.

Gieg, L.M., Jack, T.R., and Foght, J.M. (2011) Biological souring and mitigation in oil reservoirs. *Appl Microbiol Biotechnol* **92**: 263–282.
Gligorovski, S., Strekowski, R., Barbati, S., and Vione, D. (2015) Environmental Implications of Hydroxyl Radicals (•OH). *Chem Rev* **115**: 13051–13092.
Goldstone, J.V. and Voelker, B.M. (2000) Chemistry of Superoxide Radical in Seawater: CDOM Associated Sink of Superoxide in Coastal Waters. *Environ Sci Technol* **34**: 1043–1048.
Greene, E.A., Hubert, C., Nemati, M., Jenneman, G.E., and Voordouw, G. (2003) Nitrite reductase activity of sulphate-reducing bacteria prevents their inhibition by nitrate-reducing, sulphide-oxidizing bacteria. *Environ Microbiol* **5**: 607–617.
Grigoryan, A.A., Cornish, S.L., Buziak, B., Lin, S., Cavallaro, A., Arensdorf, J.J., and Voordouw, G. (2008) Competitive Oxidation of Volatile Fatty Acids by Sulfate- and Nitrate-Reducing Bacteria from an Oil Field in Argentina. *Appl Environ Microbiol* **74**: 4324–4335.
Grimbergen, A.J., Siebring, J., Solopova, A., and Kuipers, O.P. (2015) Microbial bet-hedging: the power of being different. *Environ Microbiol • Extrem* **25**: 67–72.
de Groot, D.H., Tjalma, A.J., Bruggeman, F.J., and van Nimwegen, E. (2023) Effective bet-hedging through growth rate dependent stability. *Proc Natl Acad Sci* **120**: e2211091120.
Hansel, C.M. and Diaz, J.M. (2021) Production of Extracellular Reactive Oxygen Species by Marine Biota. *Annu Rev Mar Sci* **13**: 177–200.
Haveman, S.A., Greene, E.A., Stilwell, C.P., Voordouw, J.K., and Voordouw, G. (2004) Physiological and Gene Expression Analysis of Inhibition of Desulfovibrio vulgaris Hildenborough by Nitrite. *J Bacteriol* **186**: 7944–7950.
Haveman, S.A., Greene, E.A., and Voordouw, G. (2005) Gene expression analysis of the mechanism of inhibition of Desulfovibrio vulgaris Hildenborough by nitrate-reducing, sulfide-oxidizing bacteria. *Environ Microbiol* **7**: 1461–1465.
Heukelekian, H. (1943) Effect of the Addition of Sodium Nitrate to Sewage on Hydrogen Sulfide Production and B.O.D. Reduction. *Sew Works J* **15**: 255–261.
Hitzman, D.O. and Sperl, G.T. (1994) A New Microbial Technology for Enhanced Oil Recovery and Sulfide Prevention and Reduction., p. SPE-27752-MS.
Hubert, C., Nemati, M., Jenneman, G., and Voordouw, G. (2003) Containment of Biogenic Sulfide Production in Continuous Up-Flow Packed-Bed Bioreactors with Nitrate or Nitrite. *Biotechnol Prog* **19**: 338–345.
Huettel, M., Berg, P., and Kostka, J.E. (2014) Benthic Exchange and Biogeochemical Cycling in Permeable Sediments. *Annu Rev Mar Sci* **6**: 23–51.
Imlay, J.A. (2019) Where in the world do bacteria experience oxidative stress? *Environ Microbiol* **21**: 521–530.
Jakobsen, R. and Postma, D. (1999) Redox zoning, rates of sulfate reduction and interactions with Fe-reduction and methanogenesis in a shallow sandy aquifer, Rømø, Denmark. *Geochim Cosmochim Acta* **63**: 137–151.
Jenneman, G.E., McInerney, M.J., and Knapp, R.M. (1986) Effect of Nitrate on Biogenic Sulfide Production. *Appl Environ Microbiol* **51**: 1205–1211.
de Jong, I.G., Haccou, P., and Kuipers, O.P. (2011) Bet hedging or not? A guide to proper classification of microbial survival strategies. *BioEssays* **33**: 215–223.
Jørgensen, B.B. (1994) Sulfate reduction and thiosulfate transformations in a cyanobacterial mat during a diel oxygen cycle. *FEMS Microbiol Ecol* **13**: 303–312.
Jørgensen, B.B., Findlay, A.J., and Pellerin, A. (2019) The Biogeochemical Sulfur Cycle of Marine Sediments. *Front Microbiol* **10**:.

Kater, B.J., Dubbeldam, M., and Postma, J.F. (2006) Ammonium Toxicity at High pH in a Marine Bioassay Using Corophium volutator. *Arch Environ Contam Toxicol* **51**: 347–351.
Khademian, M. and Imlay, J.A. (2017) Escherichia coli cytochrome c peroxidase is a respiratory oxidase that enables the use of hydrogen peroxide as a terminal electron acceptor. *Proc Natl Acad Sci* **114**: E6922–E6931.
Knorr, K.-H., Lischeid, G., and Blodau, C. (2009) Dynamics of redox processes in a minerotrophic fen exposed to a water table manipulation. *Geoderma* **153**: 379–392.
Korte, H.L., Fels, S.R., Christensen, G.A., Price, M.N., Kuehl, J.V., Zane, G.M., et al. (2014) Genetic basis for nitrate resistance in Desulfovibrio strains. *Front Microbiol* **5**:.
Kraft, B., Tegetmeyer, H.E., Sharma, R., Klotz, M.G., Ferdelman, T.G., Hettich, R.L., et al. (2014) The environmental controls that govern the end product of bacterial nitrate respiration. *Science* **345**: 676–679.
Krekeler, D. and Cypionka, H. (1995) The preferred electron acceptor of Desulfovibrio desulfuricans CSN. *FEMS Microbiol Ecol* **17**: 271–277.
Krekeler, D., Teske, A., and Cypionka, H. (1998) Strategies of sulfate-reducing bacteria to escape oxygen stress in a cyanobacterial mat. *FEMS Microbiol Ecol* **25**: 89–96.
Kussell, E. and Leibler, S. (2005) Phenotypic Diversity, Population Growth, and Information in Fluctuating Environments. *Science* **309**: 2075–2078.
Lagage, V. and Uphoff, S. (2020) Pulses and delays, anticipation and memory: seeing bacterial stress responses from a single-cell perspective. *FEMS Microbiol Rev* **44**: 565–571.
Lin, E.C.C. and Iuchi, S. (1991) Regulation of gene espression in fermentative and respiratory systems in Escherichia coli and related bacteria. *Annu Rev Genet* **25**: 361–387.
Ling, C., Liu, X., Li, M., Wang, X., Shi, Y., Qi, J., et al. (2021) Sulphur vacancy derived anaerobic hydroxyl radical generation at the pyrite-water interface: Pollutants removal and pyrite self-oxidation behavior. *Appl Catal B Environ* **290**: 120051.
Litchman, E., Edwards, K.F., and Klausmeier, C.A. (2015) Microbial resource utilization traits and trade-offs: implications for community structure, functioning, and biogeochemical impacts at present and in the future. *Front Microbiol* **6**:.
Lloyd, D., Boddy, L., and Davies, K.J.P. (1987) Persistence of bacterial denitrification capacity under aerobic conditions: The rule rather than the exception. *FEMS Microbiol Ecol* **3**: 185–190.
Londry, K.L. and Suflita, J.M. (1999) Use of nitrate to control sulfide generation by sulfate-reducing bacteria associated with oily waste. *J Ind Microbiol Biotechnol* **22**: 582–589.
Lorenzen, J.P., Kröger, A., and Unden, G. (1993) Regulation of anaerobic respiratory pathways in Wolinella succinogenes by the presence of electron acceptors. *Arch Microbiol* **159**: 477–483.
Lovley, D.R. and Goodwin, S. (1988) Hydrogen concentrations as an indicator of the predominant terminal electron-accepting reactions in aquatic sediments. *Geochim Cosmochim Acta* **52**: 2993–3003.
Lovley, D.R. and Phillips, E.J.P. (1987) Competitive Mechanisms for Inhibition of Sulfate Reduction and Methane Production in the Zone of Ferric Iron Reduction in Sediments. *Appl Environ Microbiol* **53**: 2636–2641.
Lycus, P., Soriano-Laguna, M.J., Kjos, M., Richardson, D.J., Gates, A.J., Milligan, D.A., et al. (2018) A bet-hedging strategy for denitrifying bacteria curtails their release of N2O. *Proc Natl Acad Sci* **115**: 11820–11825.

Ma, S., Tong, M., Yuan, S., and Liu, H. (2019) Responses of the Microbial Community Structure in Fe(II)-Bearing Sediments to Oxygenation: The Role of Reactive Oxygen Species. *ACS Earth Space Chem* **3**: 738–747.

Madigan, M.T., Martinko, J.M., Bender, K.S., Buckley, D.H., and Stahl, D.A. (2015) Microbial Metabolism. In *Brock Biology of Microorganisms*. Pearson.

Mahlert, F., Bauer, C., Jaun, B., Thauer, R.K., and Duin, E.C. (2002) The nickel enzyme methyl-coenzyme M reductase from methanogenic archaea: In vitro induction of the nickel-based MCR-ox EPR signals from MCR-red2. *JBIC J Biol Inorg Chem* **7**: 500–513.

Mai, S. and Bartholomä, A. (2000) The missing mud flats of the Wadden Sea: a reconstruction of sediments and accommodation space lost in the wake of land reclamation. In *Proceedings in Marine Science*. Flemming, B.W., Delafontaine, M.T., and Liebezeit, G. (eds). Elsevier, pp. 257–272.

Maktabifard, M., Zaborowska, E., and Makinia, J. (2018) Achieving energy neutrality in wastewater treatment plants through energy savings and enhancing renewable energy production. *Rev Environ Sci Biotechnol* **17**: 655–689.

Mao, J., Blanchard, A.E., and Lu, T. (2015) Slow and Steady Wins the Race: A Bacterial Exploitative Competition Strategy in Fluctuating Environments. *ACS Synth Biol* **4**: 240–248.

Marchant, H.K., Ahmerkamp, S., Lavik, G., Tegetmeyer, H.E., Graf, J., Klatt, J.M., et al. (2017) Denitrifying community in coastal sediments performs aerobic and anaerobic respiration simultaneously. *ISME J* **11**: 1799–1812.

Marchant, H.K., Lavik, G., Holtappels, M., and Kuypers, M.M.M. (2014) The Fate of Nitrate in Intertidal Permeable Sediments. *PLOS ONE* **9**: e104517.

Marietou, A. (2016) Nitrate reduction in sulfate-reducing bacteria. *FEMS Microbiol Lett* **363**: fnw155.

Marietou, A., Griffiths, L., and Cole, J. (2009) Preferential Reduction of the Thermodynamically Less Favorable Electron Acceptor, Sulfate, by a Nitrate-Reducing Strain of the Sulfate-Reducing Bacterium Desulfovibrio desulfuricans 27774. *J Bacteriol* **191**: 882–889.

Martins, B.M. and Locke, J.C. (2015) Microbial individuality: how single-cell heterogeneity enables population level strategies. *Cell Regul* **24**: 104–112.

McKinney, R.E. and Conway, R.A. (1957) Chemical Oxygen in Biological Waste Treatment. *Sew Ind Wastes* **29**: 1097–1106.

Mclnerney, M.J., Bhupathiraju, V.K., and Sublette, K.L. (1992) Evaluation of a microbial method to reduce hydrogen sulfide levels in a porous rock biofilm. *J Ind Microbiol* **11**: 53–58.

Merz, E., Dick, G.J., de Beer, D., Grim, S., Hübener, T., Littmann, S., et al. (2021) Nitrate respiration and diel migration patterns of diatoms are linked in sediments underneath a microbial mat. *Environ Microbiol* **23**: 1422–1435.

Mishra, S. and Imlay, J. (2012) Why do bacteria use so many enzymes to scavenge hydrogen peroxide? *Catalases Hydrog Peroxide Metab* **525**: 145–160.

Mitchell, G.J., Jones, J.G., and Cole, J.A. (1986) Distribution and regulation of nitrate and nitrite reduction by Desulfovibrio and Desulfotomaculum species. *Arch Microbiol* **144**: 35–40.

Mitchell, P. (1961) Coupling of Phosphorylation to Electron and Hydrogen Transfer by a Chemi-Osmotic type of Mechanism. *Nature* **191**: 144–148.

Montgomery, A.D., Mclnerney, M.J., and Sublette, K.L. (1990) Microbial control of the production of hydrogen sulfide by sulfate-reducing bacteria. *Biotechnol Bioeng* **35**: 533–539.

Morawska, L.P., Hernandez-Valdes, J.A., and Kuipers, O.P. (2022) Diversity of bet-hedging strategies in microbial communities—Recent cases and insights. *WIREs Mech Dis* **14**: e1544.

Morley, N. and Baggs, E.M. (2010) Carbon and oxygen controls on N2O and N2 production during nitrate reduction. *Soil Biol Biochem* **42**: 1864–1871.

Morris, J.J., Rose, A.L., and Lu, Z. (2022) Reactive oxygen species in the world ocean and their impacts on marine ecosystems. *Redox Biol* **52**: 102285.

Murphy, S.A., Meng, S., Solomon, B.M., Dias, D.M.C., Shaw, T.J., and Ferry, J.L. (2016) Hydrous Ferric Oxides in Sediment Catalyze Formation of Reactive Oxygen Species during Sulfide Oxidation. *Front Mar Sci* **3**:.

Nelson, D.L. and Cox, M.M. (2013) Enzymes. In *Lehninger Principles of Biochemistry*. W. H. Freeman and Company, pp. 189–242.

New, A.M., Cerulus, B., Govers, S.K., Perez-Samper, G., Zhu, B., Boogmans, S., et al. (2014) Different Levels of Catabolite Repression Optimize Growth in Stable and Variable Environments. *PLOS Biol* **12**: e1001764.

Page, S.E., Logan, J.R., Cory, R.M., and McNeill, K. (2014) Evidence for dissolved organic matter as the primary source and sink of photochemically produced hydroxyl radical in arctic surface waters. *Environ Sci Process Impacts* **16**: 807–822.

Page, S.E., Sander, M., Arnold, W.A., and McNeill, K. (2012) Hydroxyl Radical Formation upon Oxidation of Reduced Humic Acids by Oxygen in the Dark. *Environ Sci Technol* **46**: 1590–1597.

Pandey, C.B., Kumar, U., Kaviraj, M., Minick, K.J., Mishra, A.K., and Singh, J.S. (2020) DNRA: A short-circuit in biological N-cycling to conserve nitrogen in terrestrial ecosystems. *Sci Total Environ* **738**: 139710.

Patureau, D., Zumstein, E., Delgenes, J.P., and Moletta, R. (2000) Aerobic Denitrifiers Isolated from Diverse Natural and Managed Ecosystems. *Microb Ecol* **39**: 145–152.

Peiffer, S., Kappler, A., Haderlein, S.B., Schmidt, C., Byrne, J.M., Kleindienst, S., et al. (2021) A biogeochemical–hydrological framework for the role of redox-active compounds in aquatic systems. *Nat Geosci* **14**: 264–272.

Philippi, T. and Seger, J. (1989) Hedging one's evolutionary bets, revisited. *Trends Ecol Evol* **4**: 41–44.

Pomowski, A., Zumft, W.G., Kroneck, P.M.H., and Einsle, O. (2011) N2O binding at a [4Cu:2S] copper–sulphur cluster in nitrous oxide reductase. *Nature* **477**: 234–237.

Porubsky, W.P., Weston, N.B., and Joye, S.B. (2009) Benthic metabolism and the fate of dissolved inorganic nitrogen in intertidal sediments. *Estuar Coast Shelf Sci* **83**: 392–402.

Postma, D. and Jakobsen, R. (1996) Redox zonation: Equilibrium constraints on the Fe(III)/SO4-reduction interface. *Geochim Cosmochim Acta* **60**: 3169–3175.

Rajeev, L., Chen, A., Kazakov, A.E., Luning, E.G., Zane, G.M., Novichkov, P.S., et al. (2015) Regulation of Nitrite Stress Response in Desulfovibrio vulgaris Hildenborough, a Model Sulfate-Reducing Bacterium. *J Bacteriol* **197**: 3400–3408.

Reise, K. (2005) Coast of change: habitat loss and transformations in the Wadden Sea. *Helgol Mar Res* **59**: 9–21.

Richards, F.A., Cline, J.D., Broenkow, W.W., and Atkinson, L.P. (1965) Some consequences of the decomposition of organic matter in Lake Nitinat, an anoxic fjord. *Limnol Oceanogr* **10**: R185–R201.

Roberts, K.L., Kessler, A.J., Grace, M.R., and Cook, P.L.M. (2014) Increased rates of dissimilatory nitrate reduction to ammonium (DNRA) under oxic conditions in a periodically hypoxic estuary. *Geochim Cosmochim Acta* **133**: 313–324.

Robertson, E.K., Roberts, K.L., Burdorf, L.D.W., Cook, P., and Thamdrup, B. (2016) Dissimilatory nitrate reduction to ammonium coupled to Fe(II) oxidation in sediments of a periodically hypoxic estuary. *Limnol Oceanogr* **61**: 365–381.

Robertson, E.K. and Thamdrup, B. (2017) The fate of nitrogen is linked to iron(II) availability in a freshwater lake sediment. *Geochim Cosmochim Acta* **205**: 84–99.

Roller, B.R. and Schmidt, T.M. (2015) The physiology and ecological implications of efficient growth. *ISME J* **9**: 1481–1487.

Rose, A. (2012) The Influence of Extracellular Superoxide on Iron Redox Chemistry and Bioavailability to Aquatic Microorganisms. *Front Microbiol* **3**:.

Saragosti, E., Tchernov, D., Katsir, A., and Shaked, Y. (2010) Extracellular Production and Degradation of Superoxide in the Coral Stylophora pistillata and Cultured Symbiodinium. *PLOS ONE* **5**: e12508.

Sass, A.M., Eschemann, A., Kühl, M., Thar, R., Sass, H., and Cypionka, H. (2002) Growth and chemosensory behavior of sulfate-reducing bacteria in oxygen–sulfide gradients. *FEMS Microbiol Ecol* **40**: 47–54.

Sass, H., Cypionka, H., and Babenzien, H.-D. (1997) Vertical distribution of sulfate-reducing bacteria at the oxic-anoxic interface in sediments of the oligotrophic Lake Stechlin. *FEMS Microbiol Ecol* **22**: 245–255.

Schreiber, F. and Ackermann, M. (2020) Environmental drivers of metabolic heterogeneity in clonal microbial populations. *Energy Biotechnol ● Environ Biotechnol* **62**: 202–211.

Schreiber, F., Littmann, S., Lavik, G., Escrig, S., Meibom, A., Kuypers, M.M.M., and Ackermann, M. (2016) Phenotypic heterogeneity driven by nutrient limitation promotes growth in fluctuating environments. *Nat Microbiol* **1**: 16055.

Schwermer, C.U., Ferdelman, T.G., Stief, P., Gieseke, A., Rezakhani, N., Van Rijn, J., et al. (2010) Effect of nitrate on sulfur transformations in sulfidogenic sludge of a marine aquaculture biofilter. *FEMS Microbiol Ecol* **72**: 476–484.

Seager, S., Schrenk, M., and Bains, W. (2012) An Astrophysical View of Earth-Based Metabolic Biosignature Gases. *Astrobiology* **12**: 61–82.

Seitz, H.-J. and Cypionka, H. (1986) Chemolithotrophic growth of Desulfovibrio desulfuricans with hydrogen coupled to ammonification of nitrate or nitrite. *Arch Microbiol* **146**: 63–67.

Sessions, A.L., Doughty, D.M., Welander, P.V., Summons, R.E., and Newman, D.K. (2009) The Continuing Puzzle of the Great Oxidation Event. *Curr Biol* **19**: R567–R574.

Shade, A., Peter, H., Allison, S., Baho, D., Berga, M., Buergmann, H., et al. (2012) Fundamentals of Microbial Community Resistance and Resilience. *Front Microbiol* **3**:.

Sørensen, J. (1987) Nitrate reduction in marine sediment: Pathways and interactions with iron and sulfur cycling. *Geomicrobiol J* **5**: 401–421.

Stoeva, M.K. and Coates, J.D. (2019) Specific inhibitors of respiratory sulfate reduction: towards a mechanistic understanding. *Microbiology* **165**: 254–269.

Sutherland, K.M., Wankel, S.D., and Hansel, C.M. (2020) Dark biological superoxide production as a significant flux and sink of marine dissolved oxygen. *Proc Natl Acad Sci* **117**: 3433–3439.

Thattai, M. and van Oudenaarden, A. (2004) Stochastic Gene Expression in Fluctuating Environments. *Genetics* **167**: 523–530.

Tiedje, J.M., Sexstone, A.J., Myrold, D.D., and Robinson, J.A. (1983) Denitrification: ecological niches, competition and survival. *Antonie Van Leeuwenhoek* **48**: 569–583.
Tong, M., Yuan, S., Ma, S., Jin, M., Liu, D., Cheng, D., et al. (2016) Production of Abundant Hydroxyl Radicals from Oxygenation of Subsurface Sediments. *Environ Sci Technol* **50**: 214–221.
Tong, M., Zhao, Y., Sun, Q., Li, P., Liu, H., and Yuan, S. (2022) Fe(II) oxygenation inhibits bacterial Mn(II) oxidation by P. putida MnB1 in groundwater under O2-perturbed conditions. *J Hazard Mater* **435**: 128972.
Trebuch, L.M., Oyserman, B.O., Janssen, M., Wijffels, R.H., Vet, L.E.M., and Fernandes, T.V. (2020) Impact of hydraulic retention time on community assembly and function of photogranules for wastewater treatment. *Water Res* **173**: 115506.
Trusiak, A., Treibergs, L.A., Kling, G.W., and Cory, R.M. (2018) The role of iron and reactive oxygen species in the production of CO2 in arctic soil waters. *Geochim Cosmochim Acta* **224**: 80–95.
Unden, G. and Bongaerts, J. (1997) Alternative respiratory pathways of Escherichia coli: energetics and transcriptional regulation in response to electron acceptors. *Biochim Biophys Acta BBA - Bioenerg* **1320**: 217–234.
Vuono, D.C., Read, R.W., Hemp, J., Sullivan, B.W., Arnone, J.A., Neveux, I., et al. (2019) Resource Concentration Modulates the Fate of Dissimilated Nitrogen in a Dual-Pathway Actinobacterium. *Front Microbiol* **10**:.
Wolfe, B.M., Lui, S.M., and Cowan, J.A. (1994) Desulfoviridin, a multimeric-dissimilatory sulfite reductase from Desulfovibrio vulgaris (Hildenborough) Purification, characterization, kinetics and EPR studies. *Eur J Biochem* **223**: 79–89.
Wolff, W.J. (1992) The End of a Tradition: 1000 Years of Embankment and Reclamation of Wetlands in the Netherlands. *Ambio* **21**: 287–291.
Xue, B. and Leibler, S. (2016) Evolutionary learning of adaptation to varying environments through a transgenerational feedback. *Proc Natl Acad Sci* **113**: 11266–11271.
Yoon, S., Cruz-García, C., Sanford, R., Ritalahti, K.M., and Löffler, F.E. (2015) Denitrification versus respiratory ammonification: environmental controls of two competing dissimilatory NO3−/NO2− reduction pathways in Shewanella loihica strain PV-4. *ISME J* **9**: 1093–1104.
Yoon, S., Sanford, R.A., and Löffler, F.E. (2015) Nitrite Control over Dissimilatory Nitrate/Nitrite Reduction Pathways in Shewanella loihica Strain PV-4. *Appl Environ Microbiol* **81**: 3510–3517.
Yu, G.-H. and Kuzyakov, Y. (2021) Fenton chemistry and reactive oxygen species in soil: Abiotic mechanisms of biotic processes, controls and consequences for carbon and nutrient cycling. *Earth-Sci Rev* **214**: 103525.
Zhang, T., Hansel, C.M., Voelker, B.M., and Lamborg, C.H. (2016) Extensive Dark Biological Production of Reactive Oxygen Species in Brackish and Freshwater Ponds. *Environ Sci Technol* **50**: 2983–2993.
Zhang, Y., Tong, M., Yuan, S., Qian, A., and Liu, H. (2020) Interplay between iron species transformation and hydroxyl radicals production in soils and sediments during anoxic-oxic cycles. *Geoderma* **370**: 114351.
Zhao, G., Tan, M., Wu, B., Zheng, X., Xiong, R., Chen, B., et al. (2023) Redox Oscillations Activate Thermodynamically Stable Iron Minerals for Enhanced Reactive Oxygen Species Production. *Environ Sci Technol* **57**: 8628–8637.

Zhao, G., Wu, B., Zheng, X., Chen, B., Kappler, A., and Chu, C. (2022) Tide-Triggered Production of Reactive Oxygen Species in Coastal Soils. *Environ Sci Technol* **56**: 11888–11896.

Zhou, Z., Henkel, S., Kasten, S., and Holtappels, M. (2023) The iron "redox battery" in sandy sediments: Its impact on organic matter remineralization and phosphorus cycling. *Sci Total Environ* **865**: 161168.

Zimmermann, M., Escrig, S., Lavik, G., Kuypers, M.M.M., Meibom, A., Ackermann, M., and Schreiber, F. (2018) Substrate and electron donor limitation induce phenotypic heterogeneity in different metabolic activities in a green sulphur bacterium. *Environ Microbiol Rep* **10**: 179–183.

Manuscript 1:

Simultaneous sulfate and nitrate reduction in coastal sediments

O. M. Bourceau[1], T. Ferdelman[1], G. Lavik[1], M. Mussmann[2], M. M. M. Kuypers[1] and H. K. Marchant[1,3]

Published in **ISME Communications**

doi: https://doi.org/10.1038/s43705-023-00222-y
The supplementary information is available in the online version of this article.

[1]Max Planck Institute for Marine Microbiology, Celsiusstraße 1, 28359 Bremen, Germany. [2]University of Vienna, Department of Microbiology and Ecosystem Science, Division of Microbial Ecology, Djerassiplatz 1, A-1030 Vienna, Austria. [3]University of Bremen, Center for Marine Environmental Sciences, MARUM, 28359 Bremen, Germany.

ISME

www.nature.com/ismecomms

ARTICLE OPEN

Simultaneous sulfate and nitrate reduction in coastal sediments

O. M. Bourceau[1], T. Ferdelman[1], G. Lavik[1], M. Mussmann[2], M. M. M. Kuypers[1] and H. K. Marchant[1,3]✉

© The Author(s) 2023

The oscillating redox conditions that characterize coastal sandy sediments foster microbial communities capable of respiring oxygen and nitrate simultaneously, thereby increasing the potential for organic matter remineralization, nitrogen (N)-loss and emissions of the greenhouse gas nitrous oxide. It is unknown to what extent these conditions also lead to overlaps between dissimilatory nitrate and sulfate respiration. Here, we show that sulfate and nitrate respiration co-occur in the surface sediments of an intertidal sand flat. Furthermore, we found strong correlations between dissimilatory nitrite reduction to ammonium (DNRA) and sulfate reduction rates. Until now, the nitrogen and sulfur cycles were assumed to be mainly linked in marine sediments by the activity of nitrate-reducing sulfide oxidisers. However, transcriptomic analyses revealed that the functional marker gene for DNRA (nrfA) was more associated with microorganisms known to reduce sulfate rather than oxidise sulfide. Our results suggest that when nitrate is supplied to the sediment community upon tidal inundation, part of the sulfate reducing community may switch respiratory strategy to DNRA. Therefore increases in sulfate reduction rate in-situ may result in enhanced DNRA and reduced denitrification rates. Intriguingly, the shift from denitrification to DNRA did not influence the amount of N_2O produced by the denitrifying community. Our results imply that microorganisms classically considered as sulfate reducers control the potential for DNRA within coastal sediments when redox conditions oscillate and therefore retain ammonium that would otherwise be removed by denitrification, exacerbating eutrophication.

ISME Communications; https://doi.org/10.1038/s43705-023-00222-y

INTRODUCTION

The permeable sandy sediments that fringe coastlines act as highly effective biocatalytic filters that remineralize organic carbon, and remove fixed nitrogen through denitrification [1–5]. The microbial communities that catalyze biogeochemical transformations in permeable sediments are subjected to frequent oscillations in electron acceptor supply, wherein the depth to which oxygen and nitrate penetrate the sediment can change in minutes [6–10]. These oscillations are due to changes in porewater advection resulting from changing tidal currents, waves, the shape of sandbed surfaces, and bio-turbation and bio-irrigation [4, 11, 12]. On longer time scales high currents and storm events mobilize sandy sediments, redistributing sand grains and their attached microorganisms between sediment layers [13–17].

Many of the microorganisms within permeable sediments appear to be adapted to the oscillating oxic and anoxic conditions [18]. Such adaptations include metabolic specialization of organisms involved in the process of denitrification, which leads to the removal of nitrate but also substantial nitrous oxide emissions [19, 20]. Furthermore, rapid shifts in redox conditions and electron acceptor availability result in microorganisms simultaneously using terminal oxidases and N-reductases. This leads to the co-occurrence of denitrification and aerobic respiration processes, which are typically spatially or temporally separated in diffusion limited sediments [10, 18, 19]. Potentially, sulfate reduction and nitrate reduction may also occur simultaneously in surface sediments where nitrate is intermittently supplied [21], or even sulfate reduction and oxygen respiration. However, the potential interactions between simultaneous sulfate reduction and pathways of nitrate reduction in permeable sediments remain unexplored.

Typically, microorganisms in marine sediments employ different electron acceptors over depth, largely in accordance with their decreasing energy yield, which often leads to an apparent spatial separation of sulfate reduction from nitrate reduction [22–24]. This separation is likely maintained by competitive exclusion, wherein N-reducers outcompete sulfate reducers because they conserve more energy per electron donated [24–27]. Furthermore, nitrite accumulation, which has been observed to occur due to metabolic specialization in sands [20], can also competitively inhibit sulfite reductase, an enzyme crucial for sulfate reduction [28, 29]. Nevertheless, sulfate reduction and denitrification can be linked via microbial activity [22]. For example, microbes can bridge the distance between sulfidic and nitrate-rich sediment by either migration [30] or electrogenic pili and perform sulfide oxidation coupled to nitrate reduction [31, 32]. When nitrate reduction is coupled to complete sulfide oxidation, sulfate reduction can therefore be underestimated [33–36].

Several lines of evidence suggest that sulfate reduction in intertidal permeable sediments should be tolerant of nitrate. Sulfate reducers are present and highly active in the upper layers of sediment, even though this area is frequently exposed to both nitrate and oxygen [6, 37–40]. A recent study has shown that

[1]Max Planck Institute for Marine Microbiology, Celsiusstraße 1, 28359 Bremen, Germany. [2]University of Vienna, Department of Microbiology and Ecosystem Science, Division of Microbial Ecology, Djerassiplatz 1, A-1030 Vienna, Austria. [3]University of Bremen, Center for Marine Environmental Sciences, MARUM, 28359 Bremen, Germany.
✉email: hmarchan@mpi-bremen.de

Received: 11 November 2022 Revised: 30 January 2023 Accepted: 9 February 2023
Published online: 08 March 2023

sulfate reducing bacteria have higher acetate assimilation rates in the uppermost sediment layer than in deeper sediment layers [41]. Furthermore, in chemostat enrichments of intertidal permeable sediments, sulfide produced from sulfate reducers fueled denitrifier and ammonifier populations [42, 43]. Together, these studies suggest that sulfate reducers in permeable intertidal sediments can coexist with denitrifying microorganisms and could be adapted to, rather than inhibited by, frequent exposure to nitrate and even oxygen.

The co-occurrence of nitrate and sulfate respiration has the potential to impact N-removal pathways. For example, the presence of sulfide has previously been predicted to lead to higher nitrous oxide emissions during denitrification [44], and might enhance emissions of this potent greenhouse gas from permeable sediments. The occurrence of sulfate reduction might also alter the balance between denitrification and dissimilatory reduction of nitrate/nitrite to ammonium (DNRA), a process which retains fixed N in coastal systems rather than removing it. For example, the oxidation of sulfide produced by sulfate reduction has recently been linked to the DNRA community rather than the denitrifying community in coastal salt marsh sediments [45]. The link between sulfate and nitrate respiration could also be more direct, as many organisms that are traditionally thought of as sulfate reducing bacteria also have the potential to reduce nitrite to ammonium. Of these, some have been shown to switch to canonical DNRA when nitrate becomes available and use the pathway to support growth [46, 47], while others continue to preferentially reduce sulfate in the presence of oxidized N-compounds [48–50]. The reduction of nitrite to ammonia can be also catalyzed by sulphite reductase itself, although this conversion likely has no physiological benefit [28, 29]. Organisms such as *Desulfovibrio vulgaris* can prevent this competitive inhibition of sulphite reductase via constitutive expression of periplasmic cytochrome c nitrite reductase (Nrf) to remove the nitrite, although there are contrasting reports as to whether this is also linked to energy generation [51, 52].

In this study we hypothesised that the dynamic conditions typical for intertidal permeable sediments lead to simultaneous nitrate and sulfate respiration, analogous to previous observations of simultaneous aerobic and anaerobic respiration [18]. Furthermore, we investigated whether the co-occurrence of nitrate and sulfate respiration impacts the balance of denitrification, DNRA and N_2O production and thereby the functioning of sands as biocatalytic filters. To test this, nitrate and sulfate reduction rates were determined simultaneously in freshly collected sediments from the upper two cm of the Janssand intertidal sand flat in the North Sea. Subsequently, flow-through cores comprised of the same sediments were used to gain mechanistic insights into how oscillations in NO_3^- availability typically caused by tidal currents or storm events impact the balance of denitrification, DNRA, N_2O production and sulfate reduction. We found strong correlations between DNRA and sulfate reduction rates, indicating a close link between the two cycles. To gain further insights into the potential metabolism of the microorganisms responsible for this link, we examined the phylogenetic affiliations of transcripts associated with nrfA, the key marker gene for DNRA.

RESULTS AND DISCUSSION

Sediment conditioning

Spatial and temporal overlaps between denitrification, DNRA, and sulfate reduction in permeable coastal sediments were investigated using both fresh surface sediment and surface sediment conditioned over five days to different electron acceptor supply. Sediment was conditioned immediately after collection in October 2018 using different nitrate regimes designed to mimic the variability that occurs in different sediment horizons *in situ*.

On the tidal flat, oxygen and nitrate can penetrate to depths of 5–10 cm at high tide, but are quickly consumed when the tide recedes, whereupon they are only present in the upper mm [6, 53]. On longer time scales, sediment redistribution can bury the microorganisms that are attached to sand grains deeper into the sand flat, or, bring sand grains from deeper, more stably anoxic depths to the surface (Fig. 1A) [13, 14]. To mimic this variability in electron acceptor availability, two flow-through sediment cores were supplied with nitrate for 6 h, followed by a period of 6 h with no nitrate, similar to the upper layer of the sand flat (Fig. 1A). In one of these cores, flow was maintained constantly in order to remove metabolic products such as sulfide and Fe II (Variable Redox / Product Elimination), while in the other core, flow was stopped and metabolic products could accumulate (Variable Redox / Product Accumulation) (Fig. 1B). To mimic the conditions

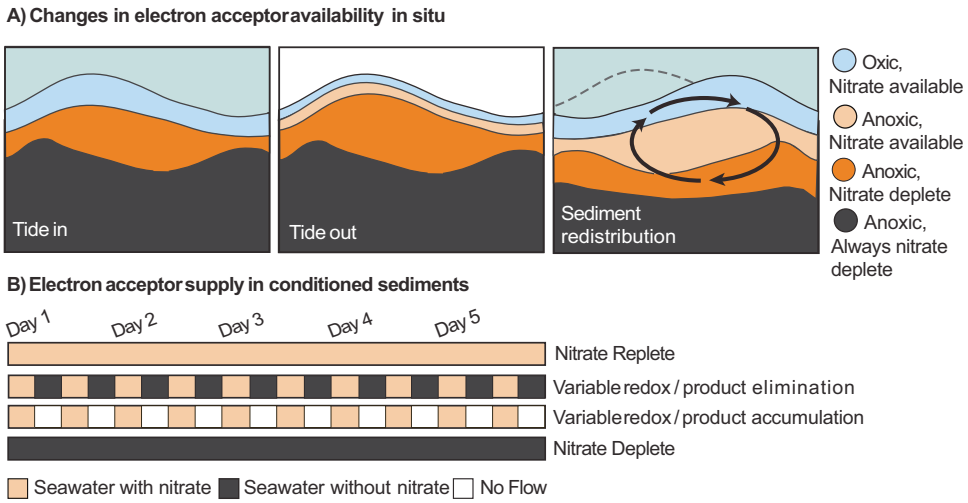

Fig. 1 Exposure of the microbial community to variable NO_3^- conditions in intertidal sand flats. A Changes in electron availability in situ. Schematic of the changes that occur on hourly to daily time scales on intertidal sand flats. When the tide is in, advection can transport O_2 and NO_3^- to depths of up to 5–10 cm. When the tide goes out, both are rapidly consumed and are only present in the upper mm to cm. When bottom currents become strong enough, or when wave action is high, the rippled sediment structures start to migrate, redistributing sand and exposing deeper sediments which have been NO_3^- deplete for longer time periods. **B** Electron acceptor supply in the conditioned sediments: In addition to carrying out rate measurements on freshly collected sediments, sediments were exposed to different conditions over five days in flow-through reactors supplied with anoxic water.

in the uppermost and deeper layers of the sediment, a third core was constantly supplied with nitrate-rich seawater (Nitrate Replete), while a fourth was constantly supplied with nitrate free seawater (Nitrate Deplete). All cores were kept anoxic throughout the conditioning period to isolate the effect of nitrate variations from those caused by oxygen.

During the five day conditioning period, the nitrate provided to the cores was consumed, indicating that nitrate reduction was likely occurring, or alternatively had been stored by the sediment diatom community [54]. Free sulfide was not detected in porewater at the outlet of any of the four cores, however substantial concentrations of dissolved Fe II were measured (Supplementary Fig. 2). Fe II release combined with rapid formation of black spots and gray sediment (indicative of iron sulfide formation) in cores receiving no nitrate (Supplementary Fig. 1), suggested the occurrence of substantial sulfate reduction in the cores [55].

At the end of the conditioning period, sediment from the center of the cores was sub-sampled in an anaerobic hood and 2 cm^3 of sediment was placed into multiple 12 cm^3 glass vials which were filled to the top with anoxic, filtered seawater before capping to create slurries. Rates of both sulfate reduction and nitrate consumption were then determined in the slurries in incubations amended with ^{35}S sulfate tracer and no nitrate (Unamended incubations), or ^{35}S sulfate and ^{15}N-NO_3^- (NO_3^- Amended incubations). Nitrate reduction was determined in slurries receiving ^{15}N-NO_3^- but no ^{35}S tracer. Throughout the incubation period the slurries were gently mixed by placing the glass vials in a roller tank to avoid the formation of nitrate-depleted microniches.

Ubiquitous sulfate reduction

Sulfate reduction occurred in all of the freshly collected and conditioned sediments when they were incubated without NO_3^- (Unamended incubations) (Fig. 2, Supplementary Tables 1–3). Sulfate reduction rates in conditioned sediments (0.9–11.5 nmol cm^{-3} sed hr^{-1}) varied substantially between cores, but overlapped with the range observed in freshly collected sediments (1.6–3.0 nmol cm^{-3} sed hr^{-1}) and those measured previously in the upper two cm of the sand flat (0.42–16 nmol cm^{-3} h^{-1}) [37, 56]. The rate of sulfate reduction in the sediment in the Variable Redox/ Product Elimination condition (1.8–3.7 nmol cm^{-3} sed hr^{-1}) was most similar to that of the fresh sediment, indicating that this regime most closely simulated the surface sediments at the tidal flat. The occurrence of sulfate reduction in the surface layer of the sand flat, and in all of the conditioned sediments, including those that had been exposed to high NO_3^- concentrations for five days (250–150 µM NO_3^- in the variable cores) strongly indicates that sulfate reducers at the sandflat are acclimated to the recurring presence of NO_3^- and sulfate reduction is therefore ubiquitous in these sediments. This is consistent with the observation of high acetate uptake by sulfate reducers in the surface sediment [41], and with the continued transcription of sulfate reduction genes in chemostats containing Janssand sediments after 100 days of continuous but low NO_3^- exposure [42].

Nevertheless, the substantial differences in sulfate reduction rates between cores incubated with different NO_3^- availabilities indicate that nitrate exposure does have some control over net sulfate reduction. Rates were 5 times higher in the Nitrate Deplete core (which had received no NO_3^- for 5 days) than in the Nitrate Replete core (which had been constantly supplied with NO_3^- for 5 days) (Fig. 2). Compared to the in situ rates, sulfate reduction rates were lower in the Nitrate Replete core, and vice versa, were higher in the Nitrate Deplete core. In contrast, in the Variable Redox conditioned sediments, NO_3^- availability could not be clearly linked to the changes sulfate reduction rates. Although both Variable Redox sediments were exposed to similar nitrate regimes during the conditioning period, sulfate reduction rates were threefold higher in the flow-through core which had a stagnant period of 6 h (Variable Redox / Product Accumulation) in comparison to the reactor with constant flow (Variable Redox / Product Elimination).

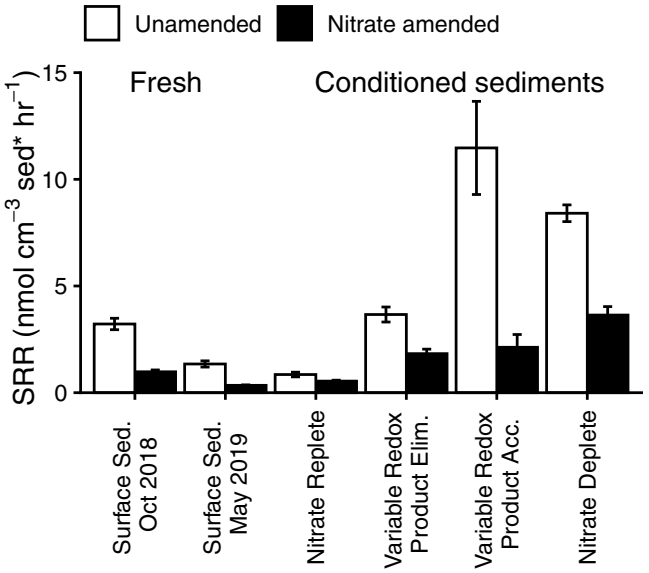

Fig. 2 Sulfate reduction rates: Sulfate reduction rates (SRR) from sediments amended with NO_3^- (black bars) or without NO_3^- (white bars) in nmol cm^{-3} sed. hr^{-1}. Sulfate reduction began immediately in all incubations, and rates are calculated from the period of time where rates were linear. See Supplementary Tables 1+2 for associated statistics. All rates had an adjusted R^2 of at least 0.85, except for the Variable Redox / Product Accumulation condition, which had an R^2 of 0.56 when amended with NO_3^-, and 0.75 without NO_3^-. All error bars represent standard error. The conditioned sediment incubations were carried out in October 2018.

Co-occurrence of sulfate reduction with nitrate reduction

In the slurry incubations amended with 50–60 µM NO_3^-, sulfate and NO_3^- reduction proceeded simultaneously in both the freshly collected and conditioned sediments (Fig. 3, Supplementary Fig. 5). In combination with the persistent sulfate reduction in NO_3^- conditioned sediment (where no NO_3^- was added during the incubation itself), these results suggest that the dynamic conditions at the sand flat select for a background level of constitutive sulfate reduction in anoxic permeable Janssand sediments, even in the presence a more thermodynamically favorable electron acceptor (NO_3^-). These results bear many similarities to the occurrence of denitrification in the presence of oxygen, previously observed in these sediments [10, 18].

Sulfate reduction always occurred in the presence of nitrate, albeit at ~20–60% of the rate observed in the unamended slurries (Fig. 2). There are at least three mechanisms that can explain this apparent decrease in sulfate reduction rates in the presence of NO_3^-; (1) competitive inhibition of sulfite reductase by NO_2^- [29], (2) sulfate reducing bacteria switching their metabolism to DNRA [46, 47] and (3) complete sulfide oxidation to sulfate coupled to NO_3^- reduction [57, 58]. Reported thresholds at which NO_2^- completely inhibits sulfate reduction and/or growth by sulfate reducing bacteria vary greatly (0.04 mM – 10 mM), but are generally above the concentrations observed during our incubations, where NO_2^- concentrations peaked at 35 µM (Supplementary Figs. 3, 4) [27, 59, 60]. While purified dissimilatory sulphite reductase has a high affinity (although low turnover) for NO_2^- ($K_m = 38$ µM; $k_{cat} = 0.038$ mol s^{-1} mol^{-1} haem) [29] there was no obvious link between an accumulation of NO_2^- and decreased sulfate reduction in the incubations (Supplementary Figs. 3–5). Therefore we suggest that the reoxidation of sulfide by sulfide oxidisers (sometimes referred

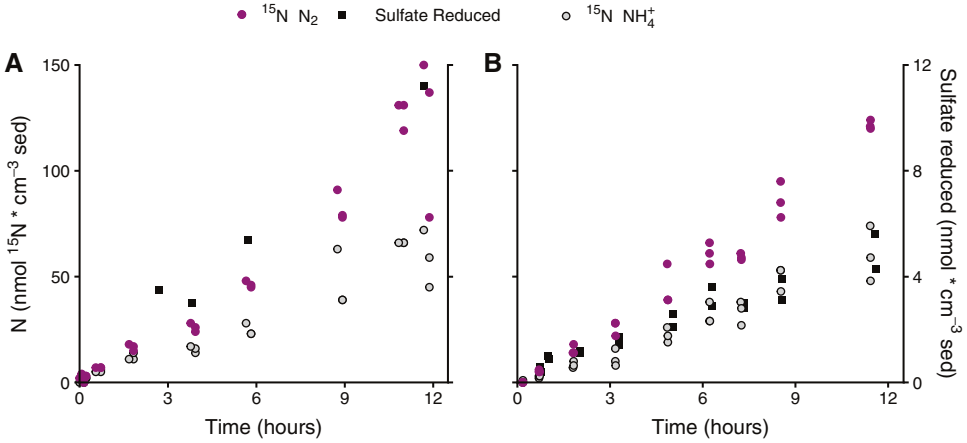

Fig. 3 Concurrent NO_3^- and sulfate reduction in freshly collected surface sediments: $^{15}NH_4^+$ (light gray circles) and ^{15}N-N_2 production (purples circles) and the total sulfate reduced (black squares) are plotted for parallel nitrate amended incubations of surface sediment collected in October 2018 (**A**) and May 2019 (**B**). Each point represents a measurement from a separate incubation. Note the different scale bars.

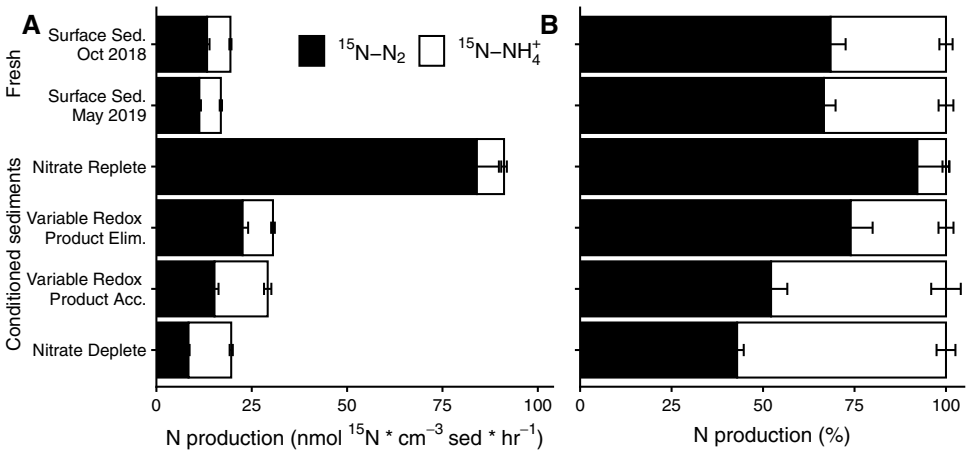

Fig. 4 NO_3^- reduction: A Rates of N_2 (black) and NH_4^+ production (white) in nmol ^{15}N cm^{-3} sed. in the four conditioned sediments and two freshly collected surface sediments. All error bars represent standard error of rates. All rates were fit to points where N_2 production was approximately linear, and all rates have an R^2 of at least 0.86 (see Supplementary Tables 1, 2 for associated statistic). **B** Normalized data from panel A showing the ^{15}N-NO_3^- converted to NH_4^+ or N_2 as a percentage of the total rate of ^{15}N-NO_3^- conversion to either N_2 or NH_4^+. Error bars represent propagated standard error. The conditioned sediment incubations were carried out in October 2018.

to as cryptic sulfur cycling), or sulfate reducers switching their metabolism to DNRA are more likely explanations for the apparent decrease in sulfate reduction with NO_3^- addition. However, it should be noted that sulfate reduction samples were processed using the Cr-II reduction method (Roy et al., 2014), which captures both produced sulfide and sulfur intermediate oxidation state compounds (e.g., pyrite, elemental S, thiosulfate, sulfite). As such re-oxidation of sulfide to sulfur intermediates would be included in the sulfate reduction rate determinations, but not any ^{35}S-labeled sulfide that was rapidly and completely oxidized back to sulfate.

Changing ratios of denitrification:DNRA in the presence of sulfate reduction

During the course of the incubations ^{15}N-NO_3^- was reduced to both ^{15}N-N_2 and ^{15}N-NH_4^+, indicating that when nitrate was present there was the potential for both denitrification and DNRA to occur within the sediment (Fig. 4A). However the ratio of N_2: NH_4^+ production differed substantially between sediments after they had been conditioned (Fig. 4B). For example, in the Nitrate Replete condition, denitrification was the dominant process and ^{15}N- N_2 production was 12 times higher than ^{15}N- NH_4^+ production (Fig. 4). This was much higher than the ratio observed in the freshly collected surface sediments, where, as is typical for these sediments, denitrification was around twice as high as DNRA [54, 61]. Denitrification was also around twice as high as DNRA in the Variable Redox / Product Elimination sediment, while in the Variable Redox / Product Accumulation sediment, denitrification and DNRA rates were similar. Within the Nitrate Deplete core, DNRA was marginally higher than denitrification.

Different factors seem to have driven the changes in ratio in the different conditions, for example, in the Nitrate Replete condition, denitrification rates were far higher than those normally measured in the freshly collected sediments, while DNRA rates showed little change. This suggests that constantly anoxic, nitrate replete conditions allow the denitrification community to thrive in permeable sands. More interestingly, the relative contributions of DNRA and denitrification consistently varied with respect to sulfate reduction rates in the incubations (Fig. 5A, B), with the proportion of DNRA positively and strongly correlating with increased sulfate reduction rates (Fig. 5C). This suggests that sulfate reduction might exert an important influence on N-respiration when the processes co-occur.

Linking microorganisms capable of DNRA to sulfur cycling

The correlation between denitrification to DNRA ratio and sulfate reduction was largely driven by increases in the DNRA rate (Fig. 5),

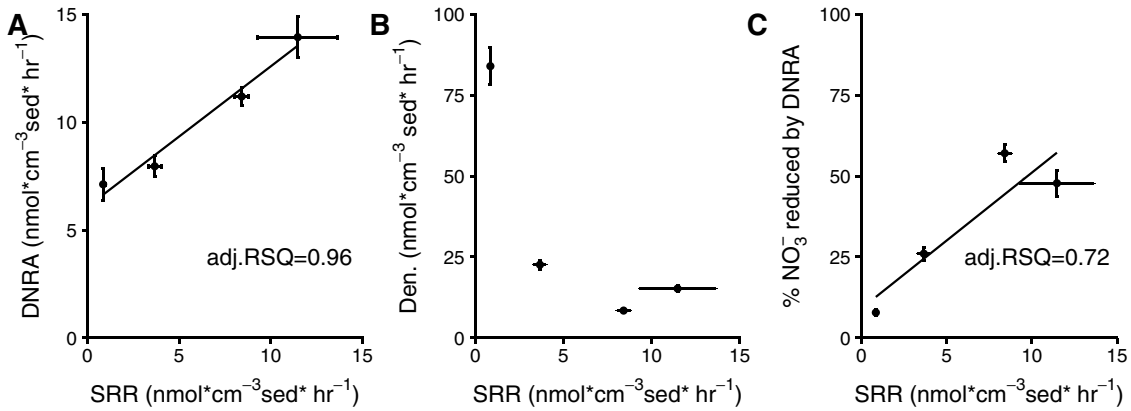

Fig. 5 Correlations between sulfate reduction rates and nitrate reduction: A The rate of DNRA plotted against the sulfate reduction rate in the absence of nitrate. **B** The rate of denitrification (formation of $^{15}N\text{-}N_2$) plotted against the sulfate reduction rate in the absence of nitrate. Vertical bars represent standard error and horizontal bars are the propagated standard errors of sulfate reduction rates. **C** The rate of $^{15}NH_4^+$ production (DNRA) as a percentage of the total production of reduced N (i.e. $^{15}N\text{-}N_2 + {}^{15}NH_4^+$) plotted against the rate of sulfate reduction (SRR) that was determined in parallel incubations in the absence of nitrate. Horizontal bars represent standard error while vertical bars represent propagated standard error. These incubations were carried out in October 2018.

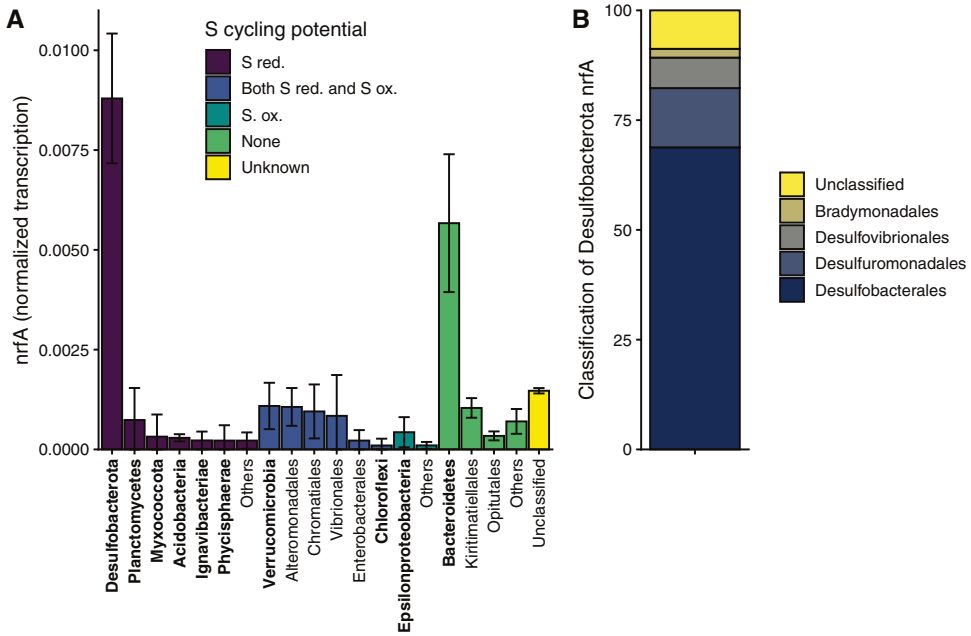

Fig. 6 Transcription of nrfA, a key marker gene for DNRA in surface sediments at the sampling site A assignment of nrfA transcripts to phylum (bold), or order level. The colors indicate the potential of these classes to carry out sulfur metabolism as identified from literature surveys. Transcript abundance was normalized by gene length and against the total abundance of rpoB in the metatranscriptome. **B** Assignment of Desulfobacterota nrfA transcripts to order level, as a percentage of total nrfA transcripts assigned to Desulfobacterota. In both panels averages are shown from three individual metatranscriptomes and error bars are standard deviation. These samples were sequenced in 2015.

rather than decreases in the denitrification rate (Fig. 5C), the latter of which was similar in the Variable and the Nitrate deplete conditions (Fig. 4B). In fact, DNRA rates in the Nitrate Deplete condition were more than double those measured in the freshly collected sediment, which suggests that the constantly anoxic, nitrate deplete conditions supported microorganisms capable of switching quickly to DNRA upon nitrate addition. Furthermore, the decrease in sulfate reduction rate that we observed upon addition of nitrate was also strongly correlated to the DNRA rate (Supplementary Fig. 6). These results suggest that DNRA could be linked to the re-oxidation of reduced compounds formed during sulfate reduction (i.e. Fe or H_2S), or alternatively, that a portion of the sulfate reducing community may have switched to DNRA in the presence of nitrate. However, the complete re-oxidation of sulfide back to sulfate is notoriously hard to quantify experimentally in marine sediments [62], therefore we switched to an –omic approach to gain insights into the potential links between DNRA and sulfur cycling within these sediments.

We examined the phylogenetic affiliations of nrfA transcripts (the key marker gene for DNRA) in three sediment layers at the sampling site (0–1 cm, 2–4 cm and 7–10 cm). On average, 90% of the identified nrfA transcripts could be taxonomically assigned to class level (Fig. 6). Transcript assignments were similar in all sediment layers, although relative levels of nrfA transcription were higher in the two deeper sediment layers (Supplementary Fig. 7). Around half of the transcripts were assigned to orders within the Desulfobacterota phylum (recently reclassified from the Deltaproteobacteria; see ref. [63]) which are associated with sulfate

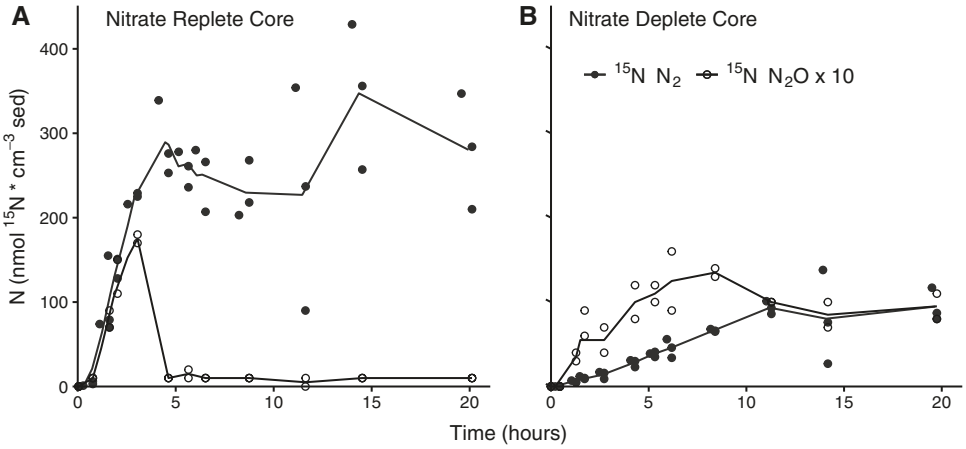

Fig. 7 N_2O and N_2 production The production of N_2 (black circles) and N_2O (open circles, values multiplied by 10) in the Nitrate Replete core (**A**) and Nitrate Deplete core (**B**) over the entire incubation time in nmol ^{15}N cm^{-3} sediment. Lines connect the average value at each timepoint. Each point represents a measurement from a separate incubation. These incubations were carried out in October 2018.

reduction; mainly Desulfobacterales, followed by Desulfuromonadales and Desulfovibrionales (Fig. 6B). In contrast, there were very few nrfA transcripts assigned to classes containing sulfide oxidizers, such as the Chromatiales and Woeseiaceae, which are common in these sediments [64, 65]. Most other nrfA transcripts were taxonomically assigned to a class that is rarely associated with dissimilatory sulfur metabolism; the Bacteroidetes and specifically, the families Bacteroidia and Flavobacteriia (Supplementary Fig. 7 and Supplementary Tables 4, 5), which are generally facultative anaerobes and fermenters.

The transcription of nrfA therefore suggests that DNRA in the sediment is largely carried out either by facultative anaerobes/fermenters and organisms that are classically considered to be sulfate reducers. Taken together our results indicate that the correlation between sulfate reduction and DNRA in the sediment is driven by sulfate reducing microorganisms switching between sulfate reduction and DNRA. This observation shows that the nitrogen and sulfur cycle in sediments can be linked by the direct activity of bacteria that switch electron acceptors, rather than, as is typically assumed, sulfide oxidation coupled to NO_3^- reduction.

Nitrous oxide production remained similar regardless of N-reduction pathway

The accumulation of sulfide during S-cycling has also been suggested to impact N-cycling via the inhibition of nitrous oxide reductase, thereby decreasing N_2 production and increasing N_2O production [44, 66]. In contrast, there was only a weak negative correlation between sulfate reduction rate and N_2 production rates in this study, and the correlation was mainly driven by the very high denitrification rate in the nitrate replete condition (Fig. 6). Changes in N_2 production rate were not compensated for by large increases in N_2O production, which represented only a few percent of total gaseous N production (i.e. $N_2O + N_2$) (Supplementary Table 6). Net N_2O production occurred in all of the sediments in the first hours of the incubations, followed by net consumption as nitrate became limiting, as is typically observed in these sediments (Fig. 7, Supplementary Figs. 3, 4, 8, 9). Intriguingly, the net N_2O production at the start of the incubations was similar regardless of the overall denitrification rate. This led to a substantial increase in the N_2O:N_2 production ratio at the start of the incubations in which denitrification rates were low and DNRA and sulfate reduction rates were high. Furthermore, there was a slower net reduction of N_2O when NO_3^- became limiting in these incubations. It is possible that the production of sulfide partially inhibited N_2O reductase (although it should be noted that this would not have been a major driver of the denitrification:DNRA ratio). Alternatively, the production of Fe(II) in the incubations with higher sulfate reduction rates could have led to enhanced production of N_2O by abiotic reactions [67]. Regardless of the mechanism, our results suggest that the release of the greenhouse gas N_2O would not be reduced by a shift from denitrification to DNRA, despite the fact that DNRA itself does not release any N_2O.

Environmental implications of overlaps between sulfate reduction, DNRA and denitrification

Here we show that in coastal permeable sediments sulfate reduction occurs in nitrate replete sediments, where it overlaps with the processes of denitrification and DNRA, thereby increasing the volume of sediment in which sulfate reduction can occur. Nevertheless, sulfate reduction rates measured in freshly collected surface sediments were approximately 10–20% of the rate of N-reduction. This implies that while sulfate reducers seem to be tolerant to nitrate in the sediment, they only contribute to a minor proportion of total carbon turnover in the surface layer (0–2 cm), as has been noted for other permeable intertidal sediments [8].

Furthermore, we found that a substantial proportion of DNRA in the sediment appears to be performed by organisms considered to be classical sulfate reducers. The ability of these microorganisms to respire and even grow via nitrate reduction has long been recognized and interestingly has also been associated with a high tolerance to oxygen exposure [48, 49, 68]. However, the reduction of nitrate as respiration strategy by sulfate reducers in marine sediments has rarely been observed; likely because sulfate reduction is generally considered to occur only in stable, nitrate deplete, anoxic environments. In contrast, organisms that would typically be classed as sulfate reducers, appear to be key members of the microbial community in permeable sediments where there are rapid fluctuations between fully oxic and nitrate replete conditions and anoxic and nitrate deplete conditions (Fig. 8). As a consequence, sulfate and nitrate reduction do not only co-occur in the sediment, but are directly linked within the *Desulforbacterota*. This implies that the size and activity of the sulfate reducing community controls the potential for DNRA within these sediments (Fig. 8). This could also explain the enhanced DNRA activity and increased ammonium fluxes to the water column that have been observed in sediments underlying hypoxic water columns [69]. This contrasts with the common view that the ratio of electron donor to nitrate/nitrite is the major factor driving the balance between DNRA and denitrification [70–72]. As DNRA retains fixed nitrogen within ecosystems as ammonium, rather than removing it like denitrification, our results indicate that the presence of active sulfate reducing communities can influence eutrophication.

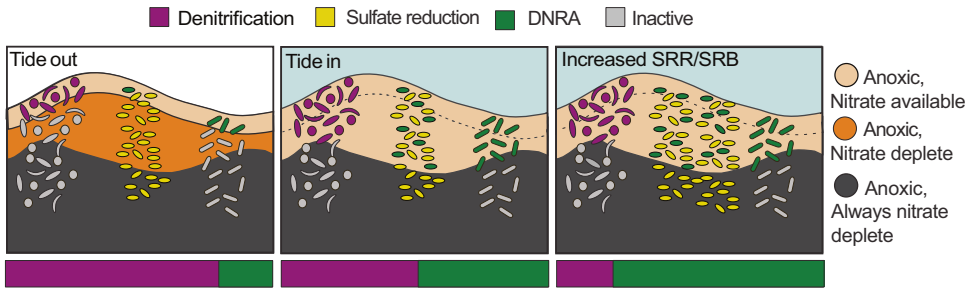

Fig. 8 Influence of changing boundary conditions on process rates Schematic outlining the changes in microbial activity over a tidal cycle (left and middle panels) and in a case where sulfate reducing bacteria become more abundant (right panel). When the tide is out, only the upper surface of the sediment has nitrate, and nitrogen reduction is dominated by denitrification. When the tide is in, nitrate reaches deeper into the surface and correspondingly to more sulfate reducers, which switch their metabolism to DNRA. This results in a more even denitrification:DNRA ratio. In sediments with more sulfate reducers, it is expected that DNRA rates would also increase as some sulfate reducers perform DNRA. For simplicity, oxygen dynamics are neglected.

METHODS

Sampling site

Sediments were collected from the Janssand sand flat, a sandy intertidal area that lies in the back barrier region of the island of Spiekeroog, in the Wadden Sea, North West Germany i.e. between the island and the mainland, detailed site descriptions are available in [6, 56, 73]. The flat has a semidiurnal tidal cycle, whereby it is inundated with water for 5–6 h during high tide and exposed for 6–7 h during low tide [6, 73]. The upper flat has a mean grain size of 176 µm, a porosity of 0.35 and a permeability of approximately 7.2 * 10^{-12} m^2 [6, 56]. When the sand flat is inundated with seawater, the interaction of bottom water currents with rippled sediment topography lead to variable advection of seawater into the sediment and O_2 penetration depths vary between 1 and 5 cm [7, 10, 53]. During low tide O_2 and NO_3^- within the porewater are quickly depleted and O_2 penetration depths drop to <1 cm [10, 54].

Fresh sediment incubations

PVC core liners (I.D. 3.5 cm) were used to collect three vertical cores from the upper sand flat of Janssand during low tide on two occasions (October 17, 2018 and May 22, 2019) and transported to the lab (~2 h). In October surface water was approximately 14 °C, and in May 11 °C.

Cores were transferred to an anaerobic chamber and the upper pale (oxidized) layer (0–3 cm) was separated from a dark (reduced) layer (7–10 cm) (Supplementary Fig. 1). The upper layer was well mixed before 2 cm^3 aliquots of sediment was transferred into 12 mL glass vials with septa (LabCo, Manchester), hereafter referred to as "Exetainers", that were filled with filtered anoxic seawater collected October 10, 2018 (NO_3^- + NO_2^- - < 2 µM) creating sediment slurries. Exetainers were capped headspace free and removed from the anaerobic chamber whereupon they were assigned to one of three treatment groups (Supplementary Fig. 1). 38 Exetainers per core received 60 µM ^{15}N-labeled NO_3^- (corresponding to ~300 nmol/cm^3 sediment), 24 received 60 µM ^{15}N-labeled NO_3^- and 250 kBq of ^{35}S-labeled sulfate, 24 received only 250 kBq of ^{35}S-labeled sulfate. Filled Exetainers were placed in roller tanks on a roller table. The roller table speed was set in order to gently invert the Exetainers every 44 seconds along their longitudinal axis to ensure that the slurries remained homogenous. Visual observations confirmed that this constantly mixed the sediment with the seawater in the vials.

Slurries were weighed and killed in duplicates at 12 selected time points with the aim of including timepoints before and after NO_3^- depletion. Slurries without added ^{35}S (i.e. those with only ^{15}N) were killed by injecting 100 µL 30% w/v zinc chloride and 200 µL saturated mercury chloride so that they were suitable for later ^{15}N gas analysis. Slurries with added ^{35}S were killed by first removing 1.8 mL sample water that was directly pipetted into 200 µL 20% w/v zinc acetate (total radioactivity samples) and stored at 4 °C, and the remaining sediment and water was decanted directly into 50 mL falcon tubes pre-filled with 7 mL 30% zinc acetate (TRIS samples) and frozen at −20 °C.

Conditioned sediment incubations

Sediment from the upper 2 cm of the sand and approximately 70 L of surface seawater (~13 °C, NO_2^- + NO_3^- - < 2 µM) was collected on October 10, 2018 during low tide and transported to the lab (~2 h). The seawater was filtered (polyethersulfone filters, .2 µm pore size) and stored in the dark at 4 °C for use in flow-through cores and incubations.

Core set up. The surface sand was homogenized and filled into four cylindrical acrylic cores with a 9 cm inner diameter following [5]. The radial groves surrounding a center port in the base of the cores was protected with 500 µm nylon mesh (Hydra-BIOS, Germany) to facilitate plug flow. Cores were filled gently with sand to 23–27 cm while immersed in freshly collected seawater to avoid trapping air bubbles. Filled cores were capped and then connected to a peristaltic pump at the base using viton tubing (Supplementary Fig. 1).

Cores were assigned to 1 of 4 conditions (Table 1) and filtered seawater previously deoxygenated by bubbling with N_2 (and subsequently kept under a N_2 headspace) was pumped into the bottom of the core according to the four conditioning regimes for five days. The core intended to mimic surface sediment, the Nitrate Replete condition, received a constant supply of NO_3^--rich water, while the core intended to mimic deep sediment, the Nitrate Deplete condition received a constant supply of NO_3^--poor seawater (Fig. 1). Two additional cores were intended to mimic portions of sediment with variable NO_3^- availability. In the first, the Variable Redox / Product Elimination condition, water flow was constant, bringing NO_3^- rich water for 6 h followed by NO_3^- poor water for 6 h. In the second, the Variable Redox / Product Accumulation condition, NO_3^- rich water was provided for 6 h and then the water was allowed to stagnate in the core for 6 h. Seawater for NO_3^- amended cores was provided with 200 µM NO_3^- for the first two days and thereafter 400 µM to ensure NO_3^- availability throughout the testing zone (4–10 cm from the inlet; see Supplementary Table 7). Seawater was provided at a rate of ~50 mL per hour during pumping and therefore had a residence time of ~11 h in the cores with constant water flow (Nitrate Replete, Nitrate Deplete and Variable Redox / Product Elimination conditions). The influence and availability of O_2 was minimal, as inlet water had been degassed by N_2 bubbling. Sulfide and Fe II were determined using methylene blue [74, 75].

Conditioned sediment ^{15}N & ^{35}S incubations. After 5 days pre-conditioning, NO_3^- and sulfate reduction rates were determined for sediment from each core. Each core was placed in an anaerobic chamber under an N_2 atmosphere and sediment was sampled from 4 to 10 cm above the core base and homogenized. Sediment was then transferred to Exetainers (Labco, Manchester) to create slurries whereupon labeling with ^{15}N-NO_3^-, ^{35}S-sulfate and subsequent sampling was carried out identically to the fresh sediment incubations. ^{35}S-sulfate labeled samples from T0-T2 in the Nitrate Replete and Nitrate Deplete conditions, and T0 in the variably conditioned sediments were not weighed before they were decanted into zinc acetate, therefore the average sediment mass from other samples in their respective treatments was used for rate calculations.

Sulfur and nitrogen rate determinations

Determination of sulfate reduction rates. Sulfate reduction rates were determined according to Roy et al. [76]. Briefly, the zinc-preserved ^{35}S samples were treated with a cold chromium acid distillation to extract the total reduced inorganic sulfur content (TRIS) containing ^{35}S. Total ^{35}S radioactivity in the supernatant, and TRIS ^{35}S radioactivity was determined

Table 1. Conditioning regimes.

Core	Nitrate amendment	Flow
Surface Sediment Proxy	+	Constant
Variable Redox + Product Build-up	+	6 h on, 6 h off
Variable Redox + Product Removal	+	6 h on
	–	6 h on
Deep Sediment Proxy	–	Constant

Flow through cores made up of the top 2 cm of the sand flat were conditioned with different water and nitrate regimes. Two cores had changing water provision and two had constant. The Variable Redox + Product Removal switched water sources every six hours, from one with nitrate to one without nitrate.

for each individual exetainer on a liquid scintillation counter (Tri-Carb 4910 TR Liquid Scintillation Analyzer, Perkin Elmer) using Ultima-Gold scintillation fluid (Perkin-Elmer). The total amount of sulfate reduced per sample was calculated with Eq. (1) adapted from [76]. Rates were determined by plotting the total sulfate reduced over time and applying linear fits. In the October fresh sediment incubations, an inconsistent amount of tracer was injected into the exetainers, so only those exetainers containing more than 20 kBq ^{35}S at measurement were included.

$$SO_4^{2-}\,reduced\left(\frac{\mu mol}{cm^3}\right) = \frac{Decays\ per\ minute_{TRIS}}{Decays\ per\ minute_{Total}} * 1.04 * \left[SO_4^{2-}\right] \quad (1)$$

Sulfate concentrations $\left(\left[SO_4^{2-}\right]\right)$ in the exetainer incubations were determined by ion chromatography (Metrohm 9300 Compact IC Flex with in-line zinc-trapping column), and the average value (calculated without outliers from dilution error) for each time series was used for subsequent rate calculations.

Nitrogen measurements. A 2 mL helium headspace was created in the Exetainers (Labco, Manchester) to which ^{15}N had been added. The liquid that was removed during this procedure was then used for NOx and $^{15}NH_4^+$ measurement.

NOx measurement. The NOx concentration of water was determined photometrically (Infinite M200 Pro, Tecan) using a version of the Griess reaction modified to sequentially determine NO_3^- and NO_2^- at low concentrations in small volumes [77, 78].

^{15}N- N_2 measurement. ^{15}N-N_2 concentrations were measured with a GC-IRMS (Isoprime PrecisION, Elementar). In total, 100 µL gas subsampled from the headspace of the Exetainers was injected directly into the GC-IRMS to determine the relative abundance of 29 and 30 N_2. A standard curve of ambient air injections was then used to calculate gas concentrations according to [79]. Values were corrected for gas dissolved in water removed during headspacing. The sum of ^{15}N-N_2 production at each time point was calculated as ($^{29}N_2 + (2 * {}^{30}N_2)$).

^{15}N N_2O measurement. After ^{15}N-N_2 measurement, the Exetainers were spiked with 60 µL N_2O and allowed to equilibrate overnight. Samples were measured as above, but injecting 250 µL gas, detecting $^{45}N_2O$ and $^{46}N_2O$, and with an N_2O standard curve. Values were corrected for N_2O solubility and for gas dissolved in water removed during headspacing. In October N_2O was only measured in two exetainers per time point, while in May three exetainers were measured per timepoint.

^{15}N-ammonium measurement. ^{15}N-ammonium production was determined after oxidation to N_2 according to [80, 81]. ^{15}N-N_2 in the headspace was then measured as above. ^{15}N- NH_4^+ standards were converted concurrently to ensure that conversion efficiency was always > 95%.

Rate calculation. Linear regression was performed on the data in order to calculate rates (Supplementary Table 1–3).

Metatranscriptomics

Metatranscriptomics was performed on nine samples collected in July 2015 previously described in ref. [38]. Briefly, sediment was sampled at late low tide from the Janssand sand flat using three sediment cores. Cores were immediately sliced into 3 layers (0–1 cm, 2–4 cm and 6–8 cm) according to sediment color (brownish, brown to gray and gray to black), which is representative of the oxidized/sulfide free upper sediment zone, the sulfide transition zone and the reduced sulfidic zone. Sediment was transferred into 50 ml tubes within 20 s and immediately stored on dry ice or at −80 C until further processing. Total RNA was extracted after treatment with DNA-ase, purification and bacterial rRNA depletion before construction of RNA TrueSEQ libraries. These were sequenced paired end on an Illumina HiSeq platform (see ref. [38] for further details).

Transcripts of nrfA and rpoB were identified in the metatranscriptomes using the ROCker-approach detailed in Marchant et al. (2018). ROCker models were built according to ref. [82] using using a collection of curated protein sequences and in the case of nrfA, closely related outgroup protein sequences (downloaded from http://enve-omics.ce.gatech.edu/rocker/models). For comparison between metatranscriptomes, nrfA transcript read numbers were normalized against rpoB transcript read numbers and the corresponding size of each gene before calculating an average for each of the three replicate sediment layers. The taxonomic identity of the transcripts was inferred using Kaiju [83] (Genbank nr_euk database downloaded on 04. Aug. 2020) and samples were grouped to at least class level where possible. The capacity of organisms contained within each class to utilize S-compounds as either an electron donor or acceptor was then assigned based on literature searches (see in particular refs. [84] and [85]). For the Deltaproteobacteria and Bacteroidetes (which were the classes to which most of the nrfA transcripts were assigned) taxonomy was inferred to family level, before S-utilization capacity was assigned.

DATA AVAILABILITY

The nine metatranscriptomes described in the manuscript available on NCBI under BioProject ID PRJNA924993.

REFERENCES

1. Boudreau BP, Huettel M, Forster S, Jahnke RA, McLachlan A, Middelburg JJ, et al. Permeable marine sediments: Overturning an old paradigm. Eos, Trans Am Geophys Union. 2001;82:133–6.
2. Cook PL, Wenzhöfer F, Rysgaard S, Galaktionov OS, Meysman FJ, Eyre BD, et al. Quantification of denitrification in permeable sediments: Insights from a two-dimensional simulation analysis and experimental data. Limnol Oceanogr Methods. 2006;4:294–307.
3. Evrard V, Glud RN, Cook PL. The kinetics of denitrification in permeable sediments. Biogeochemistry. 2013;113:563–72.
4. Huettel M, Berg P, Kostka JE. Benthic exchange and biogeochemical cycling in permeable sediments. Ann Rev Marine Sci. 2014;6:23–51.
5. Rao AMF, McCarthy MJ, Gardner WS, Jahnke RA. Respiration and denitrification in permeable continental shelf deposits on the South Atlantic Bight: Rates of carbon and nitrogen cycling from sediment column experiments. Continental Shelf Res. 2007;27:1801–19.
6. Billerbeck M, Werner U, Polerecky L, Walpersdorf E, de Beer D, Huettel M Surficial and deep pore water circulation governs spatial and temporal scales of nutrient recycling in intertidal sand flat sediment. Marine Ecol Progr Series. 2006;326:61–76.
7. Jansen S, Walpersdorf E, Werner U, Billerbeck M, Böttcher ME, de Beer D. Functioning of intertidal flats inferred from temporal and spatial dynamics of O2, H2S and pH in their surface sediment. Ocean Dyn. 2009;59:317–32.
8. de Beer D, Wenzhöfer F, Ferdelman TG, Boehme SE, Huettel M, van Beusekom JEE, et al. Transport and mineralization rates in North Sea sandy intertidal sediments, Sylt-Rømø Basin, Wadden Sea. Limnol Oceanogr. 2005;50:113–27.
9. Gao H, Matyka M, Liu B, Khalili A, Kostka JE, Collins G, et al. Intensive and extensive nitrogen loss from intertidal permeable sediments of the Wadden Sea. Limnol Oceanogr. 2012;57:185–98.
10. Gao H, Schreiber F, Collins G, Jensen MM, Kostka JE, Lavik G, et al. Aerobic denitrification in permeable Wadden Sea sediments. ISME J. 2009;4:417.
11. Elliott AH, Brooks NH. Transfer of nonsorbing solutes to a streambed with bed forms: Theory. Water Resour Res. 1997;33:123–36.
12. Precht E, Huettel M. Advective pore-water exchange driven by surface gravity waves and its ecological implications. Limnol Oceanogr. 2003;48:1674–84.

13. Ahmerkamp S, Marchant HK, Peng C, Probandt D, Littmann S, Kuypers MM, et al. The effect of sediment grain properties and porewater flow on microbial abundance and respiration in permeable sediments. Sci Rep. 2020;10:1–12.
14. Ahmerkamp S, Winter C, Krämer K, Beer DD, Janssen F, Friedrich J, et al. Regulation of benthic oxygen fluxes in permeable sediments of the coastal ocean. Limnol Oceanogr. 2017;62:1935–54.
15. Cardenas MB, Wilson JL Dunes, turbulent eddies, and interfacial exchange with permeable sediments. Water Resour Res. 2007;43:W08412.
16. Santos IR, Eyre BD, Huettel M. The driving forces of porewater and groundwater flow in permeable coastal sediments: a review. Estuarine, Coastal Shelf Sci. 2012;98:1–15.
17. Probandt D, Eickhorst T, Ellrott A, Amann R, Knittel K. Microbial life on a sand grain: from bulk sediment to single grains. ISME J. 2018;12:623–33.
18. Marchant HK, Ahmerkamp S, Lavik G, Tegetmeyer HE, Graf J, Klatt JM, et al. Denitrifying community in coastal sediments performs aerobic and anaerobic respiration simultaneously. ISME J. 2017;11:1799.
19. Marchant HK, Holtappels M, Lavik G, Ahmerkamp S, Winter C, Kuypers MMM. Coupled nitrification–denitrification leads to extensive N loss in subtidal permeable sediments. Limnol Oceanogr. 2016;61:1033–48.
20. Marchant HK, Tegetmeyer HE, Ahmerkamp S, Holtappels M, Lavik G, Graf J, et al. Metabolic specialization of denitrifiers in permeable sediments controls N2O emissions. Environ Microbiol. 2018;20:4486–502.
21. Laverman AM, Pallud C, Abell J, Van, Cappellen P. Comparative survey of potential nitrate and sulfate reduction rates in aquatic sediments. Geochimica et Cosmochimica Acta. 2012;77:474–88.
22. Fenchel T, Jørgensen B. Detritus food chains of aquatic ecosystems: the role of bacteria. Adv Microb Ecol. 1977;1:1–58.
23. Canfield DE, Kristensen E, Thamdrup B Aquatic Geomicrobiology: Elsevier Science; 2005.
24. Froelich PN, Klinkhammer G, Bender ML, Luedtke N, Heath GR, Cullen D, et al. Early oxidation of organic matter in pelagic sediments of the eastern equatorial Atlantic: suboxic diagenesis. Geochimica et cosmochimica Acta. 1979;43:1075–90.
25. Eckford RE, Fedorak PM. Chemical and microbiological changes in laboratory incubations of nitrate amendment "sour" produced waters from three western Canadian oil fields. J Ind Microbiol Biotechnol. 2002;29:243–54.
26. Grigoryan AA, Cornish SL, Buziak B, Lin S, Cavallaro A, Arensdorf JJ, et al. Competitive oxidation of volatile fatty acids by sulfate- and nitrate-reducing bacteria from an oil field in Argentina. Appl Environ Microbiol. 2008;74:4324.
27. Hubert C, Nemati M, Jenneman G, Voordouw G. Containment of biogenic sulfide production in continuous up-flow packed-bed bioreactors with nitrate or nitrite. Biotechnol Progr. 2003;19:338–45.
28. Greene EA, Hubert C, Nemati M, Jenneman GE, Voordouw G. Nitrite reductase activity of sulphate-reducing bacteria prevents their inhibition by nitrate-reducing, sulphide-oxidizing bacteria. Environ Microbiol. 2003;5:607–17.
29. Wolfe BM, Lui SM, Cowan JA. Desulfoviridin, a multimeric-dissimilatory sulfite reductase from Desulfovibrio vulgaris (Hildenborough) Purification, characterization, kinetics and EPR studies. Eur J Biochem. 1994;223:79–89.
30. Fossing H, Gallardo VA, Jørgensen BB, Hüttel M, Nielsen LP, Schulz H, et al. Concentration and transport of nitrate by the mat-forming sulphur bacterium Thioploca. Nature. 1995;374:713–15.
31. Jørgensen BB. Big sulfur bacteria. ISME J. 2010;4:1083.
32. Marzocchi U, Trojan D, Larsen S, Louise Meyer R, Peter Revsbech N, Schramm A, et al. Electric coupling between distant nitrate reduction and sulfide oxidation in marine sediment. ISME J. 2014;8:1682.
33. Londry KL, Suflita JM. Use of nitrate to control sulfide generation by sulfate-reducing bacteria associated with oily waste. J Ind Microbiol Biotechnol. 1999;22:582–9.
34. McInerney MJ, Bhupathiraju VK, Sublette KL. Evaluation of a microbial method to reduce hydrogen sulfide levels in a porous rock biofilm. J Ind Microbiol. 1992;11:53–8.
35. Schwermer CU, Ferdelman TG, Stief P, Gieseke A, Rezakhani N, Van Rijn J, et al. Effect of nitrate on sulfur transformations in sulfidogenic sludge of a marine aquaculture biofilter. FEMS Microbiol Ecol. 2010;72:476–84.
36. Thamdrup B, Fossing H, Jørgensen BB. Manganese, iron and sulfur cycling in a coastal marine sediment, Aarhus Bay, Denmark. Geochimica et Cosmochimica Acta. 1994;58:5115–29.
37. Al-Raei AM, Bosselmann K, Böttcher ME, Hespenheide B, Tauber F. Seasonal dynamics of microbial sulfate reduction in temperate intertidal surface sediments: controls by temperature and organic matter. Ocean Dyn. 2009;59:351–70.
38. Dyksma S, Pjevac P, Ovanesov K, Mussmann M. Evidence for H2 consumption by uncultured Desulfobacterales in coastal sediments. Environ Microbiol. 2018;20:450–61.
39. Musat N, Werner U, Knittel K, Kolb S, Dodenhof T, van Beusekom JEE, et al. Microbial community structure of sandy intertidal sediments in the North Sea, Sylt-Rømø Basin, Wadden Sea. Syst Appl Microbiol. 2006;29:333–48.
40. Mußmann M, Ishii K, Rabus R, Amann R. Diversity and vertical distribution of cultured and uncultured Deltaproteobacteria in an intertidal mud flat of the Wadden Sea. Environ Microbiol. 2005;7:405–18.
41. Dyksma S, Lenk S, Sawicka JE, Mußmann M. Uncultured gammaproteobacteria and desulfobacteraceae account for major acetate assimilation in a coastal marine sediment. Front Microbiol. 2018;9:3124
42. Chen J, Hanke A, Tegetmeyer HE, Kattelmann I, Sharma R, Hamann E, et al. Impacts of chemical gradients on microbial community structure. ISME J. 2017;11:920.
43. Saad S, Bhatnagar S, Tegetmeyer HE, Geelhoed JS, Strous M, Ruff SE. Transient exposure to oxygen or nitrate reveals ecophysiology of fermentative and sulfate-reducing benthic microbial populations. Environ Microbiol. 2017;19:4866–81.
44. Brunet RC, Garcia-Gil LJ. Sulfide-induced dissimilatory nitrate reduction to ammonia in anaerobic freshwater sediments. FEMS Microbiol Ecol. 1996;21:131–8.
45. Murphy AE, Bulseco AN, Ackerman R, Vineis JH, Bowen JL. Sulphide addition favours respiratory ammonification (DNRA) over complete denitrification and alters the active microbial community in salt marsh sediments. Environ Microbiol. 2020;22:2124–39.
46. Krekeler D, Cypionka H. The preferred electron acceptor of Desulfovibrio desulfuricans CSN. FEMS Microbiol Ecol. 1995;17:271–7.
47. Seitz H-J, Cypionka H. Chemolithotrophic growth of Desulfovibrio desulfuricans with hydrogen coupled to ammonification of nitrate or nitrite. Arch Microbiol. 1986;146:63–7.
48. Dalsgaard T, Bak F. Nitrate reduction in a sulfate-reducing bacterium, Desulfovibrio desulfuricans, isolated from rice paddy soil: sulfide inhibition, kinetics, and regulation. Appl Environ Microbiol. 1994;60:291–7.
49. Marietou A. Nitrate reduction in sulfate-reducing bacteria. FEMS Microbiol Lett. 2016;363:fnw155.
50. Marietou A, Griffiths L, Cole J. Preferential reduction of the thermodynamically less favorable electron acceptor, sulfate, by a nitrate-reducing strain of the sulfate-reducing bacterium Desulfovibrio desulfuricans 27774. J Bacteriol. 2009;191:882–889.
51. Korte HL, Saini A, Trotter VV, Butland GP, Arkin AP, Wall JD. Independence of nitrate and nitrite inhibition of Desulfovibrio vulgaris Hildenborough and use of nitrite as a substrate for growth. Environ Sci Technol. 2015;49:924–931.
52. Pereira IA, LeGall J, Xavier AV, Teixeira M. Characterization of a heme c nitrite reductase from a non-ammonifying microorganism, Desulfovibrio vulgaris Hildenborough. Biochimica et Biophysica Acta (BBA)-Protein Struct Mol Enzymol. 2000;1481:119–130.
53. Werner U, Billerbeck M, Polerecky L, Franke U, Huettel M, van Beusekom JEE, et al. Spatial and temporal patterns of mineralization rates and oxygen distribution in a permeable intertidal sand flat (Sylt, Germany). Limnol Oceanogr. 2006;51:2549–63.
54. Marchant HK, Lavik G, Holtappels M, Kuypers MMM. The fate of nitrate in intertidal permeable sediments. PLOS ONE. 2014;9:e104517.
55. Canfield DE. Reactive iron in marine sediments. Geochimica et cosmochimica acta. 1989;53:619–632.
56. Billerbeck M, Werner U, Bosselmann K, Walpersdorf E, Huettel M. Nutrient release from an exposed intertidal sand flat. Marine Ecol Progr Series. 2006;316:35–51.
57. Canfield DE, Stewart FJ, Thamdrup B, De Brabandere L, Dalsgaard T, Delong EF, et al. A cryptic sulfur cycle in oxygen-minimum–zone waters off the Chilean Coast. Science. 2010;330:1375.
58. Jørgensen BB, Findlay AJ, Pellerin A. The biogeochemical sulfur cycle of marine sediments. Front Microbiol. 2019;10:849.
59. Nemati M, Mazutinec TJ, Jenneman GE, Voordouw G. Control of biogenic H2S production with nitrite and molybdate. J Ind Microbiol Biotechnol. 2001;26:350–355.
60. Haveman SA, Greene EA, Stilwell CP, Voordouw JK, Voordouw G. Physiological and Gene Expression Analysis of Inhibition of Desulfovibrio vulgaris Hildenborough by Nitrite. J Bacteriol. 2004;186:7944–7950.
61. Behrendt A, de Beer D, Stief P. Vertical activity distribution of dissimilatory nitrate reduction in coastal marine sediments. Biogeosciences. 2013;10:7509–23.
62. Findlay AJ, Pellerin A, Laufer K, Jørgensen BB. Quantification of sulphide oxidation rates in marine sediment. Geochimica et Cosmochimica Acta. 2020;280:441–52.
63. Waite DW, Chuvochina M, Pelikan C, Parks DH, Yilmaz P, Wagner M, et al. Proposal to reclassify the proteobacterial classes Deltaproteobacteria and Oligoflexia, and the phylum Thermodesulfobacteria into four phyla reflecting major functional capabilities. Int J Syst Evolut Microbiol. 2020;70:5972–6016.
64. Dyksma S, Bischof K, Fuchs BM, Hoffmann K, Meier D, Meyerdierks A, et al. Ubiquitous Gammaproteobacteria dominate dark carbon fixation in coastal sediments. ISME J. 2016;10:1939–1953.
65. Lenk S, Arnds J, Zerjatke K, Musat N, Amann R, Mußmann M. Novel groups of Gammaproteobacteria catalyse sulfur oxidation and carbon fixation in a coastal, intertidal sediment. Environ Microbiol. 2011;13:758–774.

66. An S, Gardner W S. Dissimilatory nitrate reduction to ammonium (DNRA) as a nitrogen link, versus denitrification as a sink in a shallow estuary (Laguna Madre/Baffin Bay, Texas). Marine Ecol Progr Series. 2002;237:41–50.
67. Wankel SD, Ziebis W, Buchwald C, Charoenpong C, de Beer D, Dentinger J, et al. Evidence for fungal and chemodenitrification based N2O flux from nitrogen impacted coastal sediments. Nat Commun. 2017;8:15595.
68. Moura I, Bursakov S, Costa C, Moura JJ. Nitrate and nitrite utilization in sulfate-reducing bacteria. Anaerobe. 1997;3:279–290.
69. Song G, Liu S, Zhang J, Zhu Z, Zhang G, Marchant HK, et al. Response of benthic nitrogen cycling to estuarine hypoxia. Limnol Oceanogr. 2021;66:652–66.
70. Tiedje JM, Sexstone AJ, Myrold DD, Robinson JA. Denitrification: ecological niches, competition and survival. Antonie van Leeuwenhoek. 1983;48:569–583.
71. Strohm TO, Griffin B, Zumft WG, Schink B. Growth yields in bacterial denitrification and nitrate ammonification. Appl Environ Microbiol. 2007;73:1420–1424.
72. Rütting T, Boeckx P, Müller C, Klemedtsson L. Assessment of the importance of dissimilatory nitrate reduction to ammonium for the terrestrial nitrogen cycle. Biogeosciences. 2011;8:1779–91.
73. Røy H, Lee JS, Jansen S, de Beer D. Tide-driven deep pore-water flow in intertidal sand flats. Limnol Oceanogr. 2008;53:1521–30.
74. Cline JD. Spectrophotometric determination of hydrogen sulfide in natural waters 1. Limnol Oceanogr. 1969;14:454–458.
75. Viollier E, Inglett P, Hunter K, Roychoudhury A, Van, Cappellen P. The ferrozine method revisited: Fe (II)/Fe (III) determination in natural waters. Appl Geochem. 2000;15:785–90.
76. Røy H, Weber HS, Tarpgaard IH, Ferdelman TG, Jørgensen BB. Determination of dissimilatory sulfate reduction rates in marine sediment via radioactive 35S tracer. Limnol Oceanogr Methods. 2014;12:196–211.
77. García-Robledo E, Corzo A, Papaspyrou S. A fast and direct spectrophotometric method for the sequential determination of nitrate and nitrite at low concentrations in small volumes. Marine Chem. 2014;162:30–36.
78. Miranda KM, Espey MG, Wink DA. A rapid, simple spectrophotometric method for simultaneous detection of nitrate and nitrite. Nitric Oxide. 2001;5:62–71.
79. Holtappels M, Lavik G, Jensen MM, Kuypers MMM Chapter ten - 15N-Labeling Experiments to Dissect the Contributions of Heterotrophic Denitrification and Anammox to Nitrogen Removal in the OMZ Waters of the Ocean. In: Klotz MG, editor. Methods in Enzymology. 486: Academic Press; 2011. p. 223-251.
80. Preisler A, De Beer D, Lichtschlag A, Lavik G, Boetius A, Jørgensen BB. Biological and chemical sulfide oxidation in a Beggiatoa inhabited marine sediment.ISME J. 2007;1:341–353.
81. Warembourg FR 5 - Nitrogen fixation in soil and plant systems. In: Knowles R, Blackburn TH, editors. Nitrogen Isotope Techniques. San Diego: Academic Press; 1993. p. 127-156.
82. Orellana LH, Rodriguez-R LM, Konstantinidis KT. ROCker: accurate detection and quantification of target genes in short-read metagenomic data sets by modeling sliding-window bitscores. Nucleic Acids Res. 2016;45:e14–e14.
83. Menzel P, Ng KL, Krogh A. Fast and sensitive taxonomic classification for metagenomics with Kaiju. Nat Commun. 2016;7:11257.
84. Anantharaman K, Hausmann B, Jungbluth SP, Kantor RS, Lavy A, Warren LA, et al. Expanded diversity of microbial groups that shape the dissimilatory sulfur cycle. ISME J. 2018;12:1715–28.
85. Watanabe T, Kojima H, Fukui M. Identity of major sulfur-cycle prokaryotes in freshwater lake ecosystems revealed by a comprehensive phylogenetic study of the dissimilatory adenylylsulfate reductase. Sci Rep. 2016;6:36262.

ACKNOWLEDGEMENTS

We would like to thank Kirsten Imhoff and Swantje Lillienthal for assistance with sulfate reduction measurements and Gabi Klockgether for assistance with IRMS measurements.

AUTHOR CONTRIBUTIONS

OMB and HKM designed research, carried out experiments and analysed data. TF assisted with design of the sulfate reduction measurements and analysis. MM provided metatranscriptomics data. OMB, HKM, TF, MM, GL and MMMK wrote the manuscript.

FUNDING

This research was funded by the Max Planck Society and HKM was funded by the DFG Cluster of Excellence "The Ocean Floor – Earth's Uncharted Interface" at MARUM, University of Bremen (EXC-2077). Open Access funding enabled and organized by Projekt DEAL.

COMPETING INTERESTS

The authors declare no competing interests.

ADDITIONAL INFORMATION

Supplementary information The online version contains supplementary material available at https://doi.org/10.1038/s43705-023-00222-y.

Correspondence and requests for materials should be addressed to H. K. Marchant.

Reprints and permission information is available at http://www.nature.com/reprints

Publisher's note Springer Nature remains neutral with regard to jurisdictional claims in published maps and institutional affiliations.

Open Access This article is licensed under a Creative Commons Attribution 4.0 International License, which permits use, sharing, adaptation, distribution and reproduction in any medium or format, as long as you give appropriate credit to the original author(s) and the source, provide a link to the Creative Commons license, and indicate if changes were made. The images or other third party material in this article are included in the article's Creative Commons license, unless indicated otherwise in a credit line to the material. If material is not included in the article's Creative Commons license and your intended use is not permitted by statutory regulation or exceeds the permitted use, you will need to obtain permission directly from the copyright holder. To view a copy of this license, visit http://creativecommons.org/licenses/by/4.0/.

© The Author(s) 2023

Manuscript 2:

Reactive oxygen species affect the potential for mineralization processes in permeable intertidal flats

Marit R. van Erk[1,3,5], **Olivia M. Bourceau**[1,5], Chyrene Moncada[1], Subhajit Basu[1,4], Colleen M. Hansel[2] & Dirk de Beer[1]

Published in **Nature Communications**
doi: https://doi.org/10.1038/s41467-023-35818-4
The supplemental information is available in the online version of this article.

[1]Max Planck Institute for Marine Microbiology, Bremen, Germany. [2]Department of Marine Chemistry and Geochemistry, Woods Hole Oceanographic Institution, Woods Hole, MA, USA. [3]Present address: Department of Microbiology, Radboud University, The Netherlands. [4]Present address: School of Health Sciences and Technology (SoHST), University of Petroleum and Energy Studies (UPES), Dehradun, Uttarakhand 248007, India. [5]**These authors contributed equally: Marit R. van Erk, Olivia M. Bourceau**.

nature communications

Article

https://doi.org/10.1038/s41467-023-35818-4

Reactive oxygen species affect the potential for mineralization processes in permeable intertidal flats

Received: 10 December 2021

Accepted: 3 January 2023

Published online: 20 February 2023

Check for updates

Marit R. van Erk[1,3,5] ✉, Olivia M. Bourceau[1,5] ✉, Chyrene Moncada[1], Subhajit Basu[1,4], Colleen M. Hansel[2] & Dirk de Beer[1]

Intertidal permeable sediments are crucial sites of organic matter remineralization. These sediments likely have a large capacity to produce reactive oxygen species (ROS) because of shifting oxic-anoxic interfaces and intense iron-sulfur cycling. Here, we show that high concentrations of the ROS hydrogen peroxide are present in intertidal sediments using microsensors, and chemiluminescent analysis on extracted porewater. We furthermore investigate the effect of ROS on potential rates of microbial degradation processes in intertidal surface sediments after transient oxygenation, using slurries that transitioned from oxic to anoxic conditions. Enzymatic removal of ROS strongly increases rates of aerobic respiration, sulfate reduction and hydrogen accumulation. We conclude that ROS are formed in sediments, and subsequently moderate microbial mineralization process rates. Although sulfate reduction is completely inhibited in the oxic period, it resumes immediately upon anoxia. This study demonstrates the strong effects of ROS and transient oxygenation on the biogeochemistry of intertidal sediments.

Reactive oxygen species (ROS) are short-lived oxygen-containing intermediates with lifetimes of seconds to hours, including superoxide, hydrogen peroxide and hydroxyl radicals. They are formed by a variety of photochemical, abiotic, and biotic processes[1]. Biotic formation occurs both intracellularly and extracellularly as a byproduct of metabolic and other physiological mechanisms[2]. In addition to photochemical pathways, a number of light-independent abiotic processes can lead to ROS formation, including oxidation of sulfide and ferrous iron (Fe^{2+})[3,4], as well as anaerobic reactions with pyrite[5]. Intracellular ROS can damage cell components such as DNA, proteins, and lipids via a range of oxidative processes[6], and thus be detrimental to microorganisms at elevated levels. However, both intracellular and extracellular ROS also have beneficial roles, including pathogen resistance[7], nutrient acquisition[8], microbial growth[9], and as signaling molecules[10]. As such, ROS levels are strictly controlled by degrading enzymes[2], such as superoxide dismutase, which converts superoxide to hydrogen peroxide, and catalase, which converts hydrogen peroxide to oxygen and water. Electron donor-driven mechanisms also actively degrade ROS, such as through reactions with metals and organic material[11].

Despite the large potential of ROS to influence microbial processes, the distribution of ROS, including hydrogen peroxide, in marine sediment is understudied. To date, only a few studies have investigated hydrogen peroxide concentrations in sediments[12], and most of these focused on the potential of sediments to generate hydrogen peroxide upon oxygenation or sulfide exposure[3]. Studies of anoxic soils and aquifer sediments have shown great potential for the generation of ROS upon reoxygenation and have also shown that ROS directly impacts CO_2 evolution[13–17]. As hydrogen peroxide has also been demonstrated to have both stimulatory and inhibitory effects on microorganisms[6,7,10], it may greatly affect carbon cycling in marine sediments.

[1]Max Planck Institute for Marine Microbiology, Bremen, Germany. [2]Department of Marine Chemistry and Geochemistry, Woods Hole Oceanographic Institution, Woods Hole, MA, USA. [3]Present address: Department of Earth Sciences, Utrecht University, Utrecht, The Netherlands. [4]Present address: School of Health Sciences and Technology (SoHST), University of Petroleum and Energy Studies (UPES), Dehradun, Uttarakhand 248007, India. [5]These authors contributed equally: Marit R. van Erk, Olivia M. Bourceau. ✉e-mail: merk@mpi-bremen.de; obourcea@mpi-bremen.de

Particularly during disturbance events and at oxic–anoxic interfaces, which happen frequently in intertidal permeable sediments, elevated ROS levels are expected[12,16–20]. The depth to which oxygen penetrates into intertidal permeable sediment varies according to tides, currents, storms, and bioturbation[21]. The oxic zone can shift between several mm to several cm deep multiple times a day[22]. Nevertheless, anaerobes in the upper sediment maintain high rates of sulfate reduction, dissimilatory nitrate reduction, fermentation, and other anaerobic processes[23–25]. The high rates of carbon and nitrogen remineralization make these sediments biocatalytic filters[21,26], essential for the functioning of shallow water ecosystems. Consequently, ROS may play an unappreciated role in the biogeochemistry of dynamic coastal sediments.

This work supports our hypothesis that high levels of ROS develop in intertidal permeable sediments and that ROS have the potential to control biomineralization rates. Both a newly developed Fe^{2+}-resistant hydrogen peroxide microsensor and a chemiluminescence method detect significant concentrations of hydrogen peroxide in intact sediment cores and extracted porewater from the intertidal sandflat Janssand in the German Wadden Sea. Potential biogeochemical process rates in slurries of these sediments amended with ROS-removing enzymes confirm that ROS can affect microbial respiration. Potential rates of oxygen consumption, sulfate reduction, and H_2 and dissolved Fe^{2+} accumulation are all increased by the removal of ROS. This impact is despite the varied recovery time after oxygenation, with sulfate reduction resuming immediately but Fe^{2+} accumulation taking more than 12 h. The distribution and impact of ROS in these extremely dynamic environments deserve further attention, as ROS may well be important in coastal carbon cycling.

Results and discussion

Hydrogen peroxide in intertidal sediments

We determined porewater hydrogen peroxide concentrations in sandy surface sediments from the intertidal sandflat Janssand (53°44'25.51"N, 7°41'28.63"E)[27–29], a sandflat in the German Wadden Sea. Hydrogen peroxide concentrations were determined using two independent methods: microsensing in a sediment core, and a chemiluminescence technique applied to porewater that was extracted from either a parallel sediment core, or directly from the flat. Microprofiles of hydrogen peroxide, which were measured with a newly developed microsensor, show the presence of hydrogen peroxide (Fig. 1a, b and Supplementary Fig. 1a–c). The microsensors that were used contained ferrozine in their electrolyte, and were therefore not sensitive to Fe^{2+} (Supplementary Fig. 2), which is abundant in these sediments (Supplementary Fig. 3). Steady-state hydrogen peroxide levels were elevated in comparison to many environmental systems[13,14,17,30], reaching concentrations >50 μM. Maximum hydrogen peroxide production, determined from the microprofiles, was 1×10^{-4} mol m^{-3} s^{-1} (Supplementary Fig. 4), which is much higher than in tidal pools, soil waters, aquifers, and brackish and freshwater ponds[13,14,18,31].

The presence of hydrogen peroxide was confirmed using a chemiluminescence technique. Hydrogen peroxide was measured in porewater extracted from a sediment core not used for microsensor measurements, and in porewater extracted on the sandflat. Porewater extracted on the sandflat was directly fixed with ferrozine in the extraction syringe to prevent reaction with iron before analysis. Absolute concentrations determined by chemiluminescence (Supplementary Fig. 5a, b) differ from those in microprofiles, which may be explained by sampling artefacts and loss during storage between sampling and analysis. As the samples measured using chemiluminescence were not fixed with acid, loss of hydrogen peroxide may have occurred between sampling and analysis a few hours later. Nevertheless, both methods detected large quantities of hydrogen peroxide.

At steady state, the standing stock of hydrogen peroxide represents a balance between production and consumption processes. Injection of oxygenated seawater at 3 and 4 cm depth led to a transient peak of hydrogen peroxide (Fig. 2a, b and Supplementary Fig. 6a). Processes responsible for hydrogen peroxide in deeper, anoxic sediments may be related to cycling of dissolved Fe^{2+}, iron oxides, and pyrite[3–5]. The sediments were iron-rich, with concentrations of 9.7 ± 1.8 and 2.3 ± 0.6 μmol g^{-1} sed in surface sediments (0–2 cm depth) in May and July 2020, and 4.0 ± 0.3 μmol g^{-1} sed in deep sediment (10–14 cm depth) in July 2020 (Supplementary Table 1), and Fe^{2+} was present in the porewater (Supplementary Fig. 3). Despite persistent hydrogen peroxide levels at some depths, the sediment had a high capacity to rapidly degrade hydrogen peroxide. Additions of hydrogen peroxide resulted in rapid consumption at 3 and 4 cm depth (Fig. 2c and Supplementary Fig. 6b, c), as the transient peaks of hydrogen peroxide lasted for only less than a minute. Injections of hydrogen peroxide near an oxygen sensor at the same depths resulted in large transient oxygen peaks (Fig. 2c and Supplementary Fig. 6d). The underlying mechanisms responsible for the hydrogen peroxide-induced burst in oxygen are currently unresolved, but may include rapid catalytic activity by catalase within and outside the cell. We conclude that the ROS concentration in these sediments is delicately balanced between production and consumption.

Impact of reactive oxygen species on respiration

To test if the ROS in porewater can affect respiration, we used constantly mixed sediment slurries with several different amendments of ROS-removing enzymes catalase and superoxide dismutase, both together and alone. Some sediments were amended with an inert (i.e., non-ROS degrading protein, bovine serum albumin (BSA)). BSA served as a protein control, to rule out any non-catalytic effects of protein in the catalase and superoxide dismutase amendments. The effect of the amendments on aerobic respiration and sulfate reduction, the most

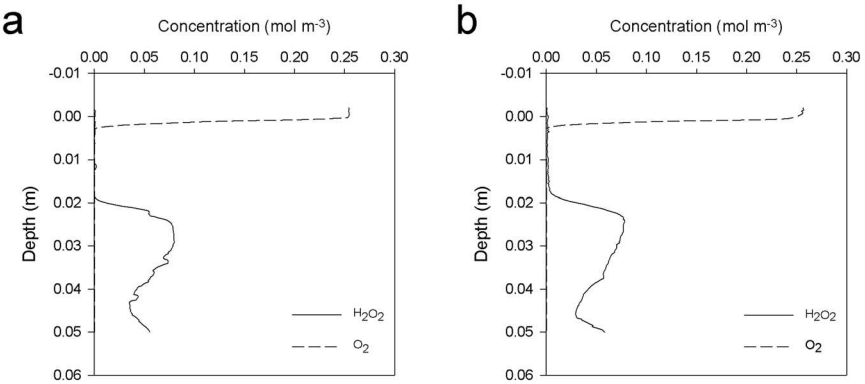

Fig. 1 | Steady-state microprofiles of hydrogen peroxide and oxygen. a Microprofiles (H_2O_2; solid line, O_2; dashed line) measured at 17:00. **b** Same measurements repeated at 20:30.

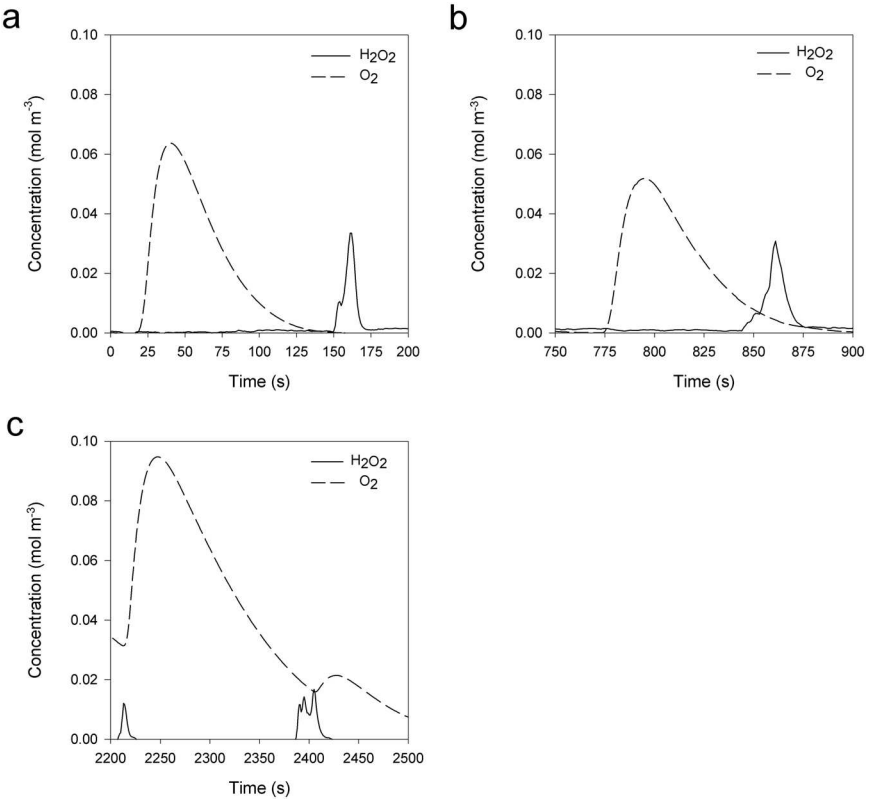

Fig. 2 | Dynamics of hydrogen peroxide (H_2O_2; solid line) and oxygen (O_2; dashed line) in a sediment core. Hydrogen peroxide and oxygen microsensors were at a constant position (4 cm depth). **a**, **b** Hydrogen peroxide and oxygen concentrations after injection of oxygenated seawater, **c** hydrogen peroxide and oxygen concentrations after injection of hydrogen peroxide.

relevant processes for coastal carbon turnover[32], and on hydrogen and Fe^{2+} accumulation was assessed by using oxygen microsensing, a $^{35}S\text{-}SO_4^{2-}$ radiotracer technique, gas chromatography, and spectrophotometry, respectively. In all cases, the slurries were initially oxic and became anoxic within the first hours of incubation.

While slurries do not completely mimic the natural heterogeneity and complexity of sediment environments, they have the advantage of more uniform environmental conditions than intact sediment cores, thus allowing for measurements along a time series[33]. Since we were interested in respiration rates over an oxic–anoxic transition, and in the effects of transient ROS exposure, it was important to be able to precisely determine the oxic–anoxic shift. All rates presented here are potential conversion rates rather than environmental rates, although measured rates are within previously reported ranges for intertidal flat sediments[25,34].

Removal of hydrogen peroxide and superoxide via additions of catalase and superoxide dismutase, respectively, substantially increased the rates of oxygen consumption, sulfate reduction, and Fe^{2+} and hydrogen accumulation (Fig. 3). This effect was not simply due to the addition of protein as a carbon or nitrogen substrate, as incubations with a comparable amount of BSA, did not stimulate these biogeochemical process rates. Superoxide dismutase and catalase both enzymatically produce oxygen as follows (reactions 1 and 2, respectively):

$$2O_2^{\bullet-} + 2H^+ \rightarrow H_2O_2 + O_2 \quad (1)$$

$$2H_2O_2 \rightarrow 2H_2O + O_2 \quad (2)$$

Despite this enzymatic production/recycling of oxygen, oxygen consumption was approximately four times faster in incubations containing both catalase and superoxide dismutase, showing ROS affects aerobic respiration in these sediments (Fig. 3a).

Sulfate reduction, for which rates were calculated for the anoxic period of the incubations, was faster in the presence of a combination of catalase and superoxide dismutase (Fig. 3b). The effect of ROS removal on carbon turnover rates was calculated using rates for untreated slurries and slurries amended with the combination of catalase and superoxide dismutase, using aerobic respiration (stoichiometry oxygen:carbon of 138:106) and sulfate reduction rates (stoichiometry sulfate:carbon of 1:2). Removal of ROS by catalase and superoxide dismutase led to a 4-times increase in biotic carbon turnover by aerobic respiration and sulfate reduction (Supplementary Table 2). We found no evidence that superoxide dismutase could alone affect respiration processes. This does not necessarily mean that superoxide does not impact the rate of sulfate reduction. In the absence of catalase, a positive effect of removing superoxide on the resident sulfate-reducing community may be masked by the negative effect of increasing hydrogen peroxide (reaction 1). Furthermore, superoxide dismutase is inhibited by hydrogen peroxide, which may have also masked any effect of superoxide[35]. Nevertheless, our data indicates that the addition of catalase, rather than superoxide dismutase, seems to be the driver for the increase of process rates after ROS removal.

Hydrogen and Fe^{2+} accumulation rates were much higher in the presence of catalase alone and with combined catalase and superoxide dismutase (Fig. 3c, d). Fe^{2+} accumulation could not be explained by the release of Fe^{2+} from catalase, as the release of the 4 Fe atoms from the active site of each catalase molecule would only lead to a concentration of 0.5 μM. Net accumulation of Fe^{2+}, as shown in Fig. 3d, only

https://doi.org/10.1038/s41467-023-35818-4

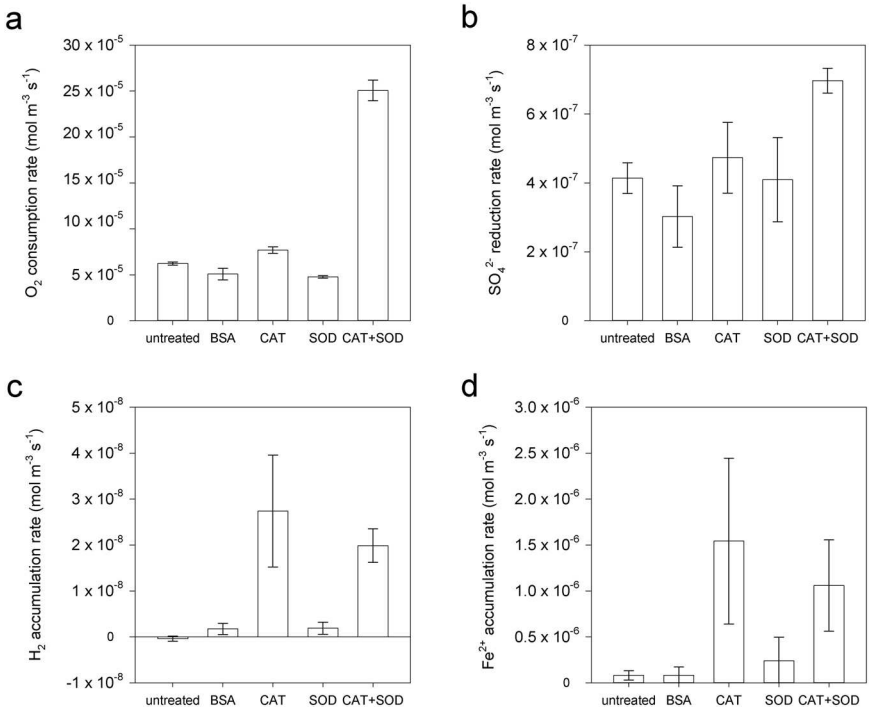

Fig. 3 | The influence of reactive oxygen species (ROS) on respiration rates. Respiration rates in untreated slurries and slurries treated with bovine serum albumin (BSA), and with ROS-removing enzymes catalase (CAT), superoxide dismutase (SOD), and a combination of CAT and SOD (CAT + SOD), from sediments collected on June 15, 2020. **a** Oxygen (O_2) consumption, **b** sulfate (SO_4^{2-}) reduction, **c** hydrogen (H_2) accumulation, **d** ferrous iron (Fe^{2+}) accumulation. Sulfate reduction, hydrogen accumulation, and Fe^{2+} accumulation rates were calculated for the anoxic period of the incubation. Error bars represent the standard error of the slope.

occurred under anoxic conditions. Any oxygen produced by the activity of catalase and superoxide dismutase under these anoxic conditions will directly be used for the reoxidation of reduced compounds such as Fe^{2+} or sulfide. Production of oxygen by enzyme activity is thus likely slower than the production of reduced compounds. In situ, hydrogen concentrations were low (0.03 ± 0.01 nmol cm^{-3} sed (9.8 ± 3.9 nmol L^{-1} porewater) in July 2020 and 0.04 ± 0.01 nmol cm^{-3} sed (13.1 ± 2.1 nmol L^{-1} porewater) in March 2021), without trends with depth (Supplementary Table 3). Hydrogen in sediments can derive from fermentation, via H_2S reacting with iron sulfide (Wächterhäuser reaction)[36,37], or N_2 fixation. Given the generally low-to-undetectable levels of dissolved sulfide in these sediments (Supplementary Table 4), we attribute most hydrogen production in our incubations to fermentation. Our results reconcile with previous observations that catalase additions significantly increase the rate of fermentation in cultures[38,39], but reveals a previously unknown constraint of ROS on fermentation in marine sediments.

Marine sediments are characterized by a tight balance between hydrogen production by fermentation and consumption by sulfate reduction[40]. To test if hydrogenotrophic sulfate reduction was active in these sediments, and if the presence of ROS could affect the tight balance, we amended slurries with sodium molybdate, a selective inhibitor of sulfate reduction. The ensuing hydrogen evolution (Supplementary Fig. 7) confirmed that hydrogenotrophic sulfate reduction occurred in these sediments. However, hydrogen fuels only a minor proportion of the sulfate reduction, as the highest hydrogen accumulation rate (with molybdate addition) was 20 times lower than the sulfate reduction rates (Supplementary Fig. 8). The addition of catalase alone and combined catalase and superoxide dismutase nevertheless disrupted the tight balance between hydrogen production by fermentation and consumption by sulfate reduction common in marine sediments[40] such that hydrogen accumulated.

Anaerobic respiration after transient oxygenation

Oxygen and ROS sensitivity are expected to be closely linked, as much of the damage oxygen does to anaerobes is mediated by ROS[41]. Anaerobes are often regarded as extremely sensitive to oxygen, with their respiration taking several hours to recover from oxygenation. In their active state, reduced enzymes with iron cofactors that are involved in sulfate reduction become irreversibly damaged by oxygen, and release intracellular ROS, which can lead to cell death[6,42]. In an environment that frequently switches between oxic and anoxic conditions, such a degree of sensitivity would strongly suppress overall anaerobic respiration. Indeed, oxygen-tolerant anaerobic respiration has increasingly been measured in diverse environments[43–47]. We therefore investigated if there was a lag in the onset of anaerobic respiration after transient oxygenation in constantly mixed sediment slurries that were allowed to become anoxic.

An environment that fluctuates multiple times per day between oxic and anoxic conditions, such as surface intertidal sediments, exerts a strong selective pressure for sulfate reducers capable of coping with oxygen. However, the strong selective pressure for sulfate reducers to be able to withstand oxygen appears not to have selected for sulfate reducers capable of respiring in the presence of oxygen, as has been found in cyanobacterial mats[48]. Instead, though sulfate reducers were unable to perform sulfate reduction under oxic conditions, they performed sulfate reduction directly upon anoxia (Fig. 4a and Supplementary Fig. 9). While undetectable in the oxic period of incubations, sulfate reduction resumed instantly after oxygen depletion in both surface sediment normally subject to daily reoxygenation (0–2 cm depth) and deeper permanently anoxic sediment (10–14 cm depth) (Fig. 4a and Supplementary Fig. 9). Rapid sulfide oxidation to sulfate could not explain the absence of sulfate reduction during the oxic period, as it was also not detected by the silver wire method (Fig. 4b). That is the method of choice for detecting aerobic sulfate reduction since sulfide binds instantly and irreversibly to silver[49]. Incomplete

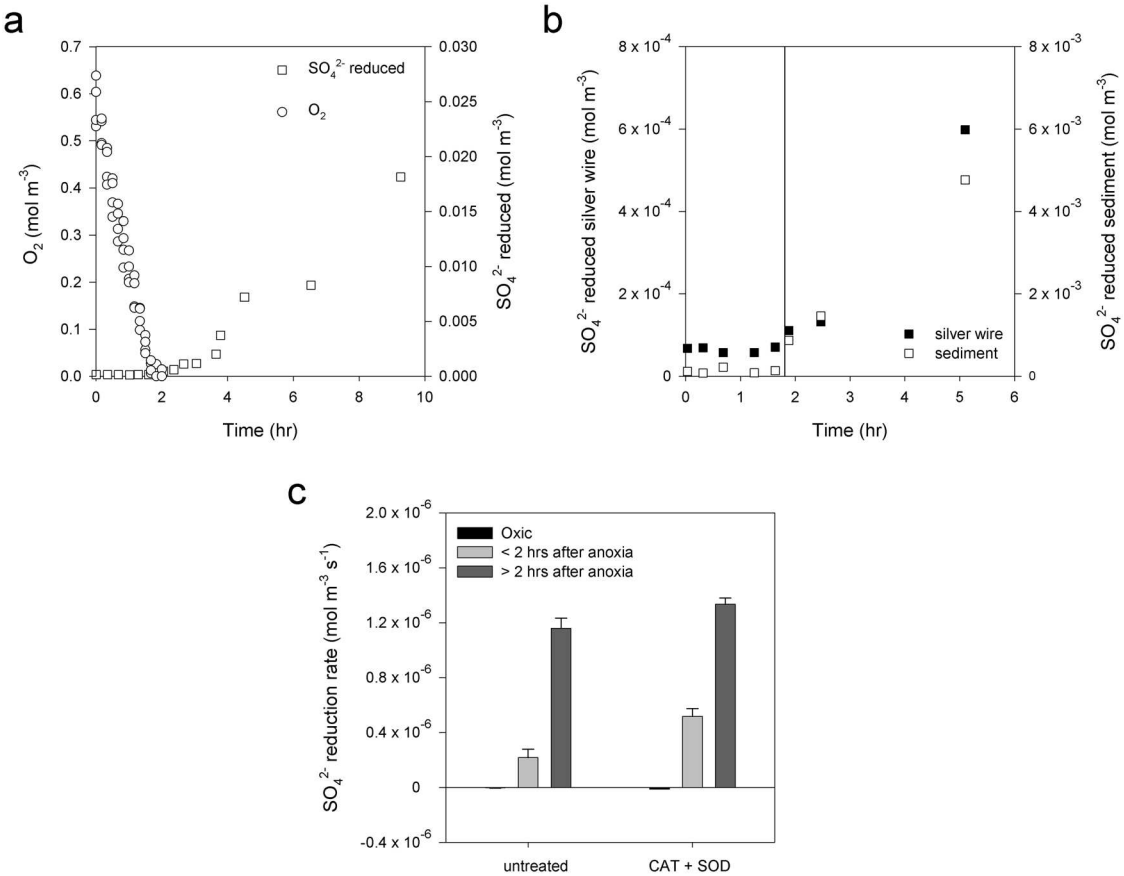

Fig. 4 | Influence of oxygen (O_2) on respiration. a Oxygen concentrations (open circles) and sulfate (SO_4^{2-}) reduced (open squares) in mol m^{-3} sed in slurries over an oxic-anoxic transition. Slurries were from sediment collected on May 25, 2020. Oxygen concentrations are shown for four Exetainers, resampled over the course of the incubation. **b** Radiolabeled sulfate reduced bound to a silver wire (closed squares), or to the sediment in the same incubation vial (open squares) in incubations including a silver wire over an oxic-anoxic transition. For all sulfate reduction measurements, each point corresponds to a separate incubation vial. The vertical line represents the transition to anoxic conditions. **c** Sulfate reduction rates in sediment slurries from May 25, 2020 during three different periods of incubation. Slurries were untreated or amended with a combination of catalase (CAT) and superoxide dismutase (SOD). Black bars represent the sulfate reduction rate in the oxic period of the incubation, light gray bars represent the sulfate reduction rate between the start and 2 h after the start of anoxia, dark gray bars the sulfate reduction rate between 2 h after the start of anoxia and the end of the incubation (20–22.5 h). Error bars represent the standard error of the slope.

sulfide reoxidation to intermediate sulfur oxidation states, e.g., via reactions with iron oxides, would also have been detected by the radiochemical reduction method used[50]. Sulfate reduction rates in slurries treated with a combination of catalase and superoxide dismutase were higher mainly directly upon anoxia (Fig. 4c), suggesting that recovery of sulfate reducers was faster when ROS were removed. Thus, while sulfate reduction was controlled by oxygen, the sulfate reducers were not killed, but instead inactive. The rapid recovery upon anoxia suggests that microbes are robust to ROS, while our incubations suggest that ROS reduce respiration. Microbes may have substantial ROS defenses that allow rapid respiration after anoxia, but are not sufficient to overcome all ROS inhibition. Similarly, ROS has been shown to be responsible for bacterial inactivation and changes in microbial community structures in Fe(II)-containing sediments from a more stable river-groundwater system[51].

Changes in hydrogen levels were minor in the first 24 h of incubation, with levels remaining below 1 nmol cm^{-3} sed (Supplementary Fig. 10). Neither Fe^{2+} (Supplementary Fig. 11) nor methane (Supplementary Table 5) accumulated immediately after anoxia. Fe^{2+} accumulation started after more than 10 h, while methane concentrations stayed constant below 2 nmol cm^{-3} sed during the first 24 h. While this lag period could indicate that fermenters, iron reducers, and methanogens are more sensitive to oxygenation than sulfate reducers, these communities are regularly exposed to oxygen, so under selection pressure, are probably adapted to oxygen exposure. Rather than anaerobic processes being stalled for so long, hydrogen, reduced iron, and methane are likely rapidly re-oxidized by pools of electron acceptors, such as Fe(III) and manganese(III,IV)[52], until these pools are exhausted[53]. Sulfide was also scavenged by these pools of oxidants as concentrations were very low (Supplementary Table 6), despite the occurrence of sulfate reduction.

Impact of ROS on mineralization in intertidal sediments

Here, we show that removal of extracellular ROS within intertidal permeable sediments substantially boosts the potential rates of oxygen consumption, sulfate reduction, and Fe^{2+} and hydrogen accumulation. Aerobic respiration and sulfate reduction together are responsible for most of the mineralization in coastal sediments[32], so factors limiting these processes have the potential to directly impact the effectiveness of sands as biocatalytic filters (Fig. 5). We propose that ROS reduce biotic mineralization either through abiotically changing the availability of organic carbon, such as the direct degradation of organic molecules by ROS[13], or due to biotic effects such as through direct oxidative stress[6]. While this study points to the importance of ROS in marine sediment biogeochemistry, the extent of the impact of ROS requires in situ measurements of these compounds over space and time. Yet, there is only very limited data on the potential for ROS formation in marine sediments and their in situ distribution[3,12], limiting our understanding of the importance of ROS in sediment biogeochemistry.

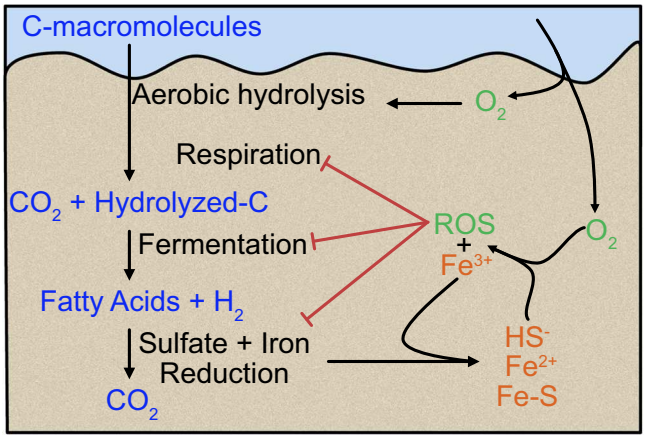

Fig. 5 | Flow diagram of the proposed effects of reactive oxygen species (ROS) in intertidal sands. Arrows represent transport and production processes. Red lines represent limiting effects. Organic material in the form of macromolecules is transported into the sediments. Hydrolysis and fermentation convert these molecules into e.g., fatty acids and hydrogen, which are substrates for sulfate and iron reducers. Also, oxygen (O_2) is transported into the sediments, where it can come in contact with reduced sulfur and iron, resulting in, among others, ferric iron (Fe^{3+}) and ROS. ROS influence biotic reactions with organic material. Sulfate- and iron reduction are limited either indirectly via fermentation, or directly, which is not further assessed in this study.

Methods

Sampling

Sediments were collected in the German Wadden Sea from the back-barrier area behind the island of Spiekeroog, on the intertidal sandflat Janssand (53°44'25.51"N, 7°41'28.63"E)[27–29]. The flat is subjected to advective flushing according to the tides, which are semi-diurnal and have a tidal range of ~2 m. The flat is inundated at high tide and exposed for ~6 h around low tide. Samples were collected from the upper, sandy part of the flat during low tide on five occasions over three seasons, May 25th, June 15th, July 28th, October 8th, 2020, and March 18th, 2021. The upper part of the flat has a porosity of 0.33, a mean grain size of 176 μm, and a permeability of ~7.2×10^{-12} m^2 (see refs. [27,28]). Sediment was scraped from the upper 2 cm, transferred into a canister and covered with seawater. Deeper sediments and depth profiles were collected with core liners. Seawater was collected adjacent to the flat. On March 18, 2021, porewater samples were sampled in situ for Fe^{2+} and hydrogen peroxide measurements using Rhizons (Rhizosphere Research Products, The Netherlands). Sediment cores were sampled using core liners for oxygen and hydrogen peroxide measurements.

Incubation set up

All incubations were carried out in 6-mL gas-tight vials, hereafter called Exetainers (Labco, UK) that were filled without headspace, with 2 cm^3 sediment and 4 mL seawater. During incubation, all Exetainers were placed in light-impermeable roller tanks and inverted every 30 s, to allow thorough slurry mixing. All incubations, except for incubations in October 2020, were started on the same day as the sediment was sampled. In October 2020, sediment and seawater were stored at 4 °C for six days before incubations started. Incubations were conducted at room temperature. Exetainers were filled on a lab bench after sediment was thoroughly mixed, and seawater was shaken to bring to equilibrium with the air. For all measurements except oxygen, Exetainers were destructively sampled, so each timepoint represents a separate individual Exetainer.

Depending on the experiment, incubations were untreated, or amended with 28 mmol L^{-1} sodium molybdate, 1500 U mL^{-1} catalase, 217 U mL^{-1} superoxide dismutase, a combination of 217 U mL^{-1} superoxide dismutase and 1500 U mL^{-1} catalase, or 0.5 mg mL^{-1} bovine serum albumin (BSA). The BSA treatment served as a control for the enzyme treatment, to allow the separation of the effects of enzymatic activity from the effect of added protein. Separate Exetainers were used to measure sulfate reduction, hydrogen accumulation, and methane accumulation, depending on the experiment. When total sulfate and dissolved iron and sulfide were measured, these were measured from the supernatant of the hydrogen Exetainers.

Oxygen consumption measurements

Oxygen concentrations were measured repeatedly from a series of 3–4 Exetainers which were quickly opened at regular intervals to allow insertion of a Clark-type oxygen microsensor produced in-house[54]. When this process introduced a bubble to the Exetainer headspace, the Exetainer was discarded. Oxygen microsensors were calibrated against air-saturated seawater and anoxic sodium ascorbate.

One linear trend line per treatment was plotted through the individual measurements of the Exetainers, and its intersection with an oxygen concentration of zero μM was calculated, which was defined as the transition between oxic and anoxic conditions. For each trend line, the standard error of the slope was calculated.

Sulfate reduction rate measurements

Sulfate reduction was determined according to ref. [50]. In all, 250 kBq of $^{35}S\text{-}SO_4^{2-}$ were added to each Exetainer used for sulfate reduction measurements. Incubations were stopped by transferring the entire content of the Exetainers to 6 mL 20% (w/v) ZnAc and then stored at −20 °C until distillation. Reduced sulfur was distilled from samples using a cold acid-chromium distillation within 2 months. All bioactive extracellular sulfur, except for sulfate, should be captured in this fraction. Radioactivity in the distilled sulfur fraction was determined with a scintillation counter (Perkin-Elmer Tri-Carb 4910 TR; using Ultima-Gold Scintillation cocktail). Sulfate reduction rates were calculated by plotting a linear trend line through the individual measurements of the anoxic period, and for each trend line, the standard error of the slope was calculated. For incubations conducted in May 2020, sulfate reduction in untreated slurries and slurries treated with a combination of catalase and superoxide dismutase were calculated for different periods of the incubation (oxic, <2 h after anoxia, and >2 h after anoxia).

In July 2020, sulfate reduction was also determined as above with the inclusion of a silver wire twice the length of the Exetainer, to increase sensitivity to oxic sulfate reduction[49]. Exetainers were sampled as above, with a higher resolution during the oxic period. The silver wire was then rinsed twice in 50 mM sodium sulfate, then radioactivity was determined using a scintillation counter.

Hydrogen measurements

At each timepoint during the incubation, a 2-mL headspace was created in an Exetainer using nitrogen gas by removing 2-mL supernatant. The Exetainer was shaken vigorously for 2 min to allow for headspace equilibration, then 1 mL of the headspace was injected into a gas chromatograph (Peak Performer RCP 910-Series, Peak Laboratories, USA) using a gas- and pressure-tight syringe. The gas chromatograph was calibrated against a 100 ppm hydrogen standard (Air Products, Germany). Hydrogen accumulation rates were calculated by plotting a linear trend line through the individual points, and for each trend line, the standard error of the slope was calculated.

Dissolved iron, sulfide, and sulfate measurements

The supernatant that was replaced by N_2 during headspacing from the Exetainers for hydrogen determination was used to measure dissolved iron, sulfide, and sulfate. Immediately after removing the supernatant using a syringe, the syringe was connected to a 0.2-μm PTFE filter. The first 0.5 mL from the syringe was transferred directly into 0.1 mL 5% (w/

v) ZnAc for subsequent sulfide and/or sulfate analysis. In all, 1 mL from the remaining volume was added directly to 0.1 mL ferrozine for subsequent dissolved iron measurements. Dissolved iron was measured spectrophotometrically. Porewater samples collected using Rhizons were fixed with ferrozine (for Fe^{2+}; March 2021) and ZnAc (for sulfide; May 2020) and transferred to cuvettes and measured using spectrophotometric methods. Sulfide was measured spectrophotometrically using the methylene blue method[55], and dissolved iron using the ferrozine method[56]. Sulfate was measured using an ion chromatograph (Metrohm 920 Compact IC Flex, Metrohm AG, Switzerland) with a zinc trap, calibrated against a standard curve of a sulfate standard.

Methane measurements

Slurries in Exetainers in July 2020 used for methane analysis were fixed using 200 μL saturated $ZnCl_2$ solution, and stored upside-down until analysis. A headspace of 2 mL was created using helium gas, and 500 μL headspace was injected in a gas chromatograph using a gas- and pressure-tight syringe. The gas chromatograph was calibrated against a 100 ppm methane standard (Air Liquide, Germany).

Solid-phase iron extraction

Solid-phase iron was extracted from sediments in May and July 2020. Samples of ~100–500 mg taken from the sediment surface (0–2 cm depth), or from a depth of 10–14 cm in a freshly sliced core, were quickly transferred to 0.5 M HCl and allowed to react for 0.5 h. The extract was then immediately filtered through 0.2 μm PTFE syringe filters and analyzed spectrophotometrically using the ferrozine method[56].

Hydrogen peroxide sensor

The sensor consisted of an etched 50 μm-thick platinum anode plated with platinum chloride (8% $PtCl_4$ in MilliQ water), an etched 100 μm-thick platinum guard, and a thick platinum reference. The anode, guard, and reference were mounted in a glass casing, with the sensing anode at a distance of ca 50 μm from the tip. The tip diameter of the outer capillary had a diameter of 25–30 μm and a tip opening of 10 μm. Before mounting the electrodes, the tip of the outer capillary was sealed by a thin polyurethane membrane (D6)[57]. The membrane was dissolved in tetrahydrofuran (50 mg mL^{-1}) and applied by shortly immersing the capillary in the solution that is kept in the tip of a Pasteur pipette and left to cure overnight. The membrane was applied under microscopic guidance. The membrane separated the electrolyte from the seawater but was permeable for hydrogen peroxide. After mounting the electrodes in the casing, the sensor was filled with electrolyte, a borate/potassium chloride buffer (50 mM borate, 3 M potassium chloride and 500 μM ferrozine), with pH 9. Sensor performance is described in the Supplementary Information.

The sensor was connected to a picoammeter and polarized at +700 mV until a stable current was obtained, which happened normally within an hour. The medium in which the sensor was used was connected to an external reference electrode. The sensors were calibrated before use in a stirred beaker with filtered seawater to which aliquots of stabilized 3% hydrogen peroxide were added.

Hydrogen peroxide microsensor measurements

Steady-state hydrogen peroxide microprofiles were measured using the new hydrogen peroxide microsensor (see Hydrogen peroxide sensor, Supplementary Information, Supplementary Table 7, and Supplementary Figs. 12 and 13) in a sediment core collected March 18, 2021. Parallel oxygen microprofiles were measured using an oxygen microsensor as described in ref. [54]. The interface between the overlying water column and sediment was set at depth zero. The water column was continuously stirred to ensure a well-mixed column and a constant boundary layer. The oxygen microsensor was 2-point calibrated (air and 1 M Na-ascorbate pH 11). The hydrogen peroxide microsensor was calibrated by incremental addition of a 3% hydrogen peroxide solution to seawater. Microprofiles were measured using a motor-equipped micromanipulator, controlled by a laptop on which also the data were acquired.

Production of hydrogen peroxide was calculated using the steady-state depth profile. Fluxes were calculated by multiplying the effective molecular diffusion coefficient ($D_{eff} = 1.18 \times 10^{-8}$ m^2 s^{-1}) with the concentration gradient, where $D_{eff} = D_0(1.13 \times 10^{-9}$ m^2 $s^{-1}) \times porosity^{-2}$. Conversion (production or consumption) was then calculated using the change in flux over depth.

The dynamics of hydrogen peroxide and oxygen were assessed by the addition of oxygen-saturated seawater and hydrogen peroxide solution to sediment in parallel cores. A needle connected to a syringe filled with the seawater, or seawater containing hydrogen peroxide, was slowly inserted into the sediment. Care was taken that injection occurred close to the sensors. Concentrations of hydrogen peroxide and oxygen were measured over time, while keeping the sensors at constant depth (3 or 4 cm).

Hydrogen peroxide chemiluminescent measurements

Hydrogen peroxide concentrations from sediment porewater were determined in a FeLume system[58,59], essentially a circular flowcell with a photomultiplier placed directly on top to detect the photons from a chemiluminescent reaction in the flowcell. The flowcell and detector combination were placed in a black box to protect against light interference. Hydrogen peroxide is proportional to the number of photons produced by the chemiluminescent reaction with 10-methyl-9-(p-formylphenyl)-acridinium carboxylate trifluoromethanesulfonate (AE) under alkaline conditions[58,59]. The analysis was carried out in a flow-injection mode. Reagent solutions were prepared in 18.2 MΩ-cm MilliQ water with analytical-grade reagents. A pH 3 phosphate buffer with freshly 2 μM AE reagent served as the sample carrier solution. A 6-way injector valve with 50 μL sample loop was used to inject the samples and standards in the carrier stream. Both carrier stream and a 0.1 M sodium carbonate solution (pH 11.3) were pumped using a peristaltic pump (Gilson Minipuls 3) at flow rates of 2 mL min^{-1} into the flowcell. Directly upon mixing the carrier flow and the alkaline buffer the chemiluminescent reaction started.

Catalase (10 U mL^{-1}) was added to AE and carbonate reagents to remove background hydrogen peroxide. The reagents with added catalase were left for a couple of hours which helped to obtain a stable baseline for the assay. For calibration, standard solutions (0.5–50 μM) of hydrogen peroxide were prepared in aged 0.22 μm-filtered seawater collected from the sampling area. Following extraction, porewater samples were immediately injected into the running FeLume. The response time to obtain a chemiluminescent peak was ~15 s after the injection. Standards were injected periodically during the assays, to check for drift. Hydrogen peroxide standards with added catalase (100 U mL^{-1}) were also injected to confirm the disappearance of the signal during the assay.

Porewaters contain high concentrations of Fe^{2+} (Supplementary. Fig. 3). Oxidation of Fe^{2+} during sampling and analysis can lead to hydrogen peroxide generation. To prevent such interference by Fe^{2+}, we added ~200 μM ferrozine to the sampling syringe while drawing 2–3 mL of porewater using Rhizons (Rhizosphere Research Products, The Netherlands). Ferrozine was also added to the reagents and standards at similar concentrations to prevent any bias. Ferrozine does not have any effect on the hydrogen peroxide concentrations[58].

Hydrogen distributions

In July 2020 and March 2021, cores were taken from the upper flat using core liners with 1 cm ports drilled into the side every 2 cm. On the sandflat (or in the harbor in March 2021), 12 mL Exetainers were

filled with 10 mL 35% (w/v) NaCl solution (6 mL Exetainers with 4 mL 35% (w/v) NaCl solution in March 2021), in a modification of the procedure outlined in ref. [60]. 2 cm^3 of sediment were removed from the cores every 2 cm via the ports using cut-off syringes and transferred into the Exetainers. Exetainers were capped without headspace. Four Exetainers served as controls and were filled with 35% (w/v) NaCl solution to account for any hydrogen produced during transport. Immediately upon returning to the home laboratory in Bremen (~3 h later) 2 mL of the water phase of each Exetainer was replaced with nitrogen gas. After equilibration, headspace hydrogen concentrations were measured using a gas chromatograph (see hydrogen measurements). The hydrogen present in the control Exetainers was subtracted from the amounts in the Exetainers with sediment added, after correcting for the slightly increased water volume in the control Exetainers.

Carbon turnover

Carbon turnover rates for untreated slurries and slurries treated with a combination of catalase and superoxide dismutase were used to assess the influence of ROS on carbon turnover in the sediments. Carbon turnover was calculated using the aerobic respiration and sulfate reduction rates for slurries from sediment collected in June 2020. Linear trend lines were plotted through the individual oxygen measurements and reduced sulfate measurements for untreated slurries, and slurries treated with a combination of catalase and superoxide dismutase. For sulfate reduction rates, only the anoxic period of the incubations was used. A stoichiometry of sulfate:carbon of 1:2, and of oxygen:carbon of 138:106 was used to convert these rates to carbon turnover rates. As sulfate reduction is the dominant anaerobic pathway in coastal marine sediments, summed carbon turnover rates derived from aerobic respiration and sulfate reduction are a reliable estimation of the total carbon turnover rate via biotic respiration.

Data availability

Data that support the findings of this study are available within the paper and its supplementary files. Source data are provided with this paper and are available in PANGAEA at https://doi.org/10.1594/PANGAEA.955443.

References

1. Hansel, C. M. & Diaz, J. M. Production of extracellular reactive oxygen species by marine biota. *Annu. Rev. Mar. Sci.* **13**, 177–200 (2021).
2. Fridovich, I. Oxygen toxicity: a radical explanation. *J. Exp. Biol.* **201**, 1203–1209 (1998).
3. Murphy, S. A. et al. Hydrous ferric oxides in sediment catalyze formation of reactive oxygen species during sulfide oxidation. *Front. Mar. Sci.* **3**, 227 (2016).
4. Burns, J. M., Craig, P. S., Shaw, T. J. & Ferry, J. L. Multivariate examination of Fe(II)/Fe(III) cycling and consequent hydroxyl radical generation. *Environ. Sci. Technol.* **44**, 7226–7231 (2010).
5. Borda, M. J., Elsetinow, A. R., Schoonen, M. A. & Strongin, D. R. Pyrite-induced hydrogen peroxide formation as a driving force in the evolution of photosynthetic organisms on an Early Earth. *Astrobiology* **1**, 283–288 (2001).
6. Imlay, J. A. The molecular mechanisms and physiological consequences of oxidative stress: lessons from a model bacterium. *Nat. Rev. Microbiol.* **11**, 443–454 (2013).
7. Armoza-Zvuloni, R., Schneider, A. & Shaked, Y. Rapid hydrogen peroxide release during coral-bacteria interactions. *Front. Mar. Sci.* **3**, 124 (2016).
8. Rose, A. L., Salmon, T. P., Lukondeh, T., Neilan, B. A. & Waite, T. D. Use of superoxide as an electron shuttle for iron acquisition by the marine cyanobacterium *Lyngbya majuscula*. *Environ. Sci. Technol.* **39**, 3708–3715 (2005).
9. Hansel, C. M., Diaz, J. M. & Plummer, S. Tight regulation of extracellular superoxide points to its vital role in the physiology of the globally relevant *Roseobacter* clade. *mBio* **10**, e02668–18 (2019).
10. Aguirre, J., Ríos-Momberg, M., Hewitt, D. & Hansberg, W. Reactive oxygen species and development in microbial eukaryotes. *Trends Microbiol.* **13**, 111–118 (2005).
11. Zinser, E. R. The microbial contribution to reactive oxygen species dynamics in marine ecosystems. *Environ. Microbiol. Rep.* **10**, 412–427 (2018).
12. Dias, D. M. C. et al. Production of reactive oxygen species in the rhizosphere of a *Spartina*-dominated salt marsh systems. *Aquat. Geochem.* **22**, 573–591 (2016).
13. Trusiak, A., Treibergs, L. A., Kling, G. W. & Cory, R. M. The role of iron and reactive oxygen species in the production of CO_2 in arctic soil waters. *Geochim. Cosmochim. Acta* **224**, 80–95 (2018).
14. Zhang, N. et al. Water table fluctuations regulate hydrogen peroxide production and distribution in unconfined aquifers. *Environ. Sci. Technol.* **54**, 4942–4951 (2020).
15. Hall, S. J. & Silver, W. L. Iron oxidation stimulates organic matter decomposition in humid tropical forest soils. *Glob. Change Biol.* **19**, 2804–2813 (2013).
16. Zhao, G. et al. Tide-triggered production of reactive oxygen species in coastal soils. *Environ. Sci. Technol.* **56**, 11888–11896 (2022).
17. Yuan, X. et al. Production of hydrogen peroxide in groundwater at Rifle, Colorado. *Environ. Sci. Technol.* **51**, 7881–7891 (2017).
18. Zhang, T., Hansel, C. M., Voelker, B. M. & Lamborg, C. H. Extensive dark biological production of reactive oxygen species in brackish and freshwater ponds. *Environ. Sci. Technol.* **50**, 2983–2993 (2016).
19. Imlay, J. A. Where in the world do bacteria experience oxidative stress? *Environ. Microbiol.* **21**, 521–530 (2019).
20. Abele, D., Großpietsch, H. & Pörtner, H. O. Temporal fluctuations and spatial gradients of environmental P_{O2}, temperature, H_2O_2 and H_2S in its intertidal habitat trigger enzymatic antioxidant protection in the capitellid worm *Heteromastus filiformis*. *Mar. Ecol. Prog. Ser.* **163**, 179–191 (1998).
21. Huettel, M., Berg, P. & Kostka, J. E. Benthic exchange and biogeochemical cycling in permeable sediments. *Annu. Rev. Mar. Sci.* **6**, 23–51 (2014).
22. Jansen, S. et al. Functioning of intertidal flats inferred from temporal and spatial dynamics of O_2, H_2S and pH in their surface sediment. *Ocean Dyn.* **59**, 317–332 (2009).
23. Kessler, A. J. et al. Bacterial fermentation and respiration processes are uncoupled in anoxic permeable sediments. *Nat. Microbiol.* **4**, 1014–1023 (2019).
24. Marchant, H. K., Lavik, G., Holtappels, M. & Kuypers, M. M. M. The fate of nitrate in intertidal permeable sediments. *PLoS ONE* **9**, e104517 (2014).
25. Al-Raei, A. M., Bosselmann, K., Böttcher, M. E., Hespenheide, B. & Tauber, F. Seasonal dynamics of microbial sulfate reduction in temperate intertidal surface sediments: controls by temperature and organic matter. *Ocean Dyn.* **59**, 351–370 (2009).
26. de Beer, D. et al. Transport and mineralization rates in North Sea sandy intertidal sediments, Sylt-Rømø Basin, Wadden Sea. *Limnol. Oceanogr.* **50**, 113–127 (2005).
27. Billerbeck, M., Werner, U., Bosselmann, K., Walpersdorf, E. & Huettel, M. Nutrient release from an exposed intertidal sand flat. *Mar. Ecol. Prog. Ser.* **316**, 35–51 (2006).
28. Billerbeck, M. et al. Surficial and deep pore water circulation governs spatial and temporal scales of nutrient recycling in intertidal sand flat sediment. *Mar. Ecol. Prog. Ser.* **326**, 61–76 (2006).

29. Røy, H., Lee, J. S., Jansen, S. & de Beer, D. Tide-driven deep pore-water flow in intertidal sand flats. *Limnol. Oceanogr.* **53**, 1521–1530 (2008).
30. Hopwood, M. J., Rapp, I., Schlosser, C. & Achterberg, E. P. Hydrogen peroxide in deep waters from the Mediterranean Sea, South Atlantic and South Pacific Oceans. *Sci. Rep.* **7**, 43436 (2017).
31. Abele-Oeschger, D., Tüg, H. & Röttgers, R. Dynamics of UV-driven hydrogen peroxide formation on an intertidal sandflat. *Limnol. Oceanogr.* **42**, 1406–1415 (1997).
32. Jørgensen, B. B. Mineralization of organic matter in the sea bed—the role of sulphate reduction. *Nature* **296**, 643–645 (1982).
33. Vandieken, V. & Thamdrup, B. Identification of acetate-oxidizing bacteria in a coastal marine surface sediment by RNA-stable isotope probing in anoxic slurries and intact cores. *FEMS Microbiol. Ecol.* **84**, 373–386 (2013).
34. Werner, U. et al. Organic matter degradation processes in permeable sediments—methodological approaches. *Ber. Forschungszentrum Terramare* **12**, 122–125 (2003).
35. Hodgson, E. K. & Fridovich, I. Interaction of bovine erythrocyte superoxide dismutase with hydrogen peroxide. *Inactivation Enzym. Biochem.* **14**, 5294–5299 (1975).
36. Rickard, D. & Luther, G. W. III Kinetics of pyrite formation by the H_2S oxidation of iron (II) monosulfide in aqueous solutions between 25 and 125 °C: the mechanism. *Geochim. Cosmochim. Acta* **61**, 135–147 (1997).
37. Thiel, J., Byrne, J. M., Kappler, A., Schink, B. & Pester, M. Pyrite formation from FeS and H_2S is mediated through microbial redox activity. *Proc. Natl Acad. Sci. USA* **116**, 6897–6902 (2019).
38. Gilliland, S. E. & Speck, M. L. Biological response of lactic streptococci and lactobacilli to catalase. *Appl. Microbiol.* **17**, 797–800 (1969).
39. Collins, E. B. & Aramaki, K. Production of hydrogen peroxide by *Lactobacillus acidophilus*. *J. Dairy Sci.* **63**, 353–357 (1980).
40. Finke, N. & Jørgensen, B. B. Response of fermentation and sulfate reduction to experimental temperature changes in temperate and Arctic marine sediments. *ISME J.* **2**, 815–829 (2008).
41. Imlay, J. A. How oxygen damages microbes: oxygen tolerance and obligate anaerobiosis. *Adv. Microb. Physiol.* **46**, 111–153 (2002).
42. Rabus, R., Hansen, T.A., Widdel, F. Dissimilatory Sulfate- and Sulfur-Reducing Prokaryotes. In: *The Prokaryotes* (eds Rosenberg, E., DeLong, E.F., Lory, S., Stackebrandt, E. & Thompson, F.) (Springer, Berlin, Heidelberg, 2013).
43. Kato, M. T., Field, J. A. & Lettinga, G. High tolerance of methanogens in granular sludge to oxygen. *Biotechnol. Bioeng.* **42**, 1360–1366 (1993).
44. Tholen, A., Pester, M. & Brune, A. Simultaneous methanogenesis and oxygen reduction by *Methanobrevibacter cuticularis* at low oxygen fluxes. *FEMS Microbiol. Ecol.* **62**, 303–312 (2007).
45. Kjeldsen, K. U., Joulian, C. & Ingvorsen, K. Oxygen tolerance of sulfate-reducing bacteria in activated sludge. *Environ. Sci. Technol.* **38**, 2038–2043 (2004).
46. Krekeler, D., Teske, A. & Cypionka, H. Strategies of sulfate-reducing bacteria to escape oxygen stress in a cyanobacterial mat. *FEMS Microbiol. Ecol.* **25**, 89–96 (1998).
47. Marchant, H. K. et al. Denitrifying community in coastal sediments performs aerobic and anaerobic respiration simultaneously. *ISME J.* **11**, 1799–1812 (2017).
48. Visscher, P. T., Prins, R. A. & van Gemerden, H. Rates of sulfate reduction and thiosulfate consumption in a marine microbial mat. *FEMS Microbiol. Lett.* **86**, 283–293 (1992).
49. Cohen, Y. Oxygenic photosynthesis, anoxygenic photosynthesis, and sulfate reduction in cyanobacterial mats. in *Current Perspectives in Microbial Ecology* (eds Klug, M. J. & Reddy, C. A.) 435–441 (American Society for Microbiology, 1984).
50. Røy, H., Weber, H. S., Tarpgaard, I. H., Ferdelman, T. G. & Jørgensen, B. B. Determination of dissimilatory sulfate reduction rates in marine sediment via radioactive ^{35}S tracer. *Limnol. Oceanogr. Meth.* **12**, 196–211 (2014).
51. Ma, S., Tong, M., Yuan, S. & Liu, H. Responses of the microbial community structure in Fe(II)-bearing sediments to oxygenation: the role of reactive oxygen species. *ACS Earth Space Chem.* **3**, 738–747 (2019).
52. Bosselmann, K. et al. Iron-sulfur-manganese dynamics in intertidal surface sediments of the North Sea. *Ber. Forschungsz. Terramare* **12**, 32–35 (2003).
53. Fenchel, T. M. & Jørgensen, B. B. Detritus food chains of aquatic ecosystems: the role of bacteria. in *Advances* in Microbial *Ecology*, Vol. 1 (ed. Alexander, M.) 1–58 (Springer, 1977).
54. Revsbech, N. P. An oxygen microsensor with a guard cathode. *Limnol. Oceanogr.* **34**, 474–478 (1989).
55. Cline, J. D. Spectrophotometric determination of hydrogen sulfide in natural waters. *Limnol. Oceanogr.* **14**, 454–458 (1969).
56. Viollier, E., Inglett, P. W., Hunter, K., Roychoudhury, A. N. & Van Cappellen, P. The ferrozine method revisited: Fe(II)/Fe(III) determination in natural waters. *Appl. Geochem.* **15**, 785–790 (2000).
57. Tjell, A. Ø. & Almdal, K. Diffusion rate of hydrogen peroxide through water-swelled polyurethane membranes. *Sens. Bio-Sens. Res.* **21**, 35–39 (2018).
58. Cooper, W. J., Moegling, J. K., Kieber, R. J. & Kiddle, J. J. A chemiluminescence method for the analysis of H_2O_2 in natural waters. *Mar. Chem.* **70**, 191–200 (2000).
59. King, D. W. et al. Flow injection analysis of H_2O_2 in natural waters using acridinium ester chemiluminescence: method development and optimization using a kinetic model. *Anal. Chem.* **79**, 4169–4176 (2007).
60. Lin, Y.-S. et al. Towards constraining H_2 concentration in subseafloor sediment: a proposal for combined analysis by two distinct approaches. *Geochim. Cosmochim. Acta* **77**, 186–201 (2012).

Acknowledgements

We thank Gaby Eickert, Karin Hohmann, Vera Hübner, Anja Niclas, Ines Schröder and Cäcilia Wigand for their role in the development of the hydrogen peroxide sensor, sensor construction, and technical assistance. Volker Meyer is thanked for building the FeLume system and creating its software, Gunter Wegener for assistance with hydrogen measurements, Elisa Merz for help during sampling, and BTS Bootstouren Spiekeroog for transport. We thank Tim Ferdelman for fruitful discussions. We thank Anders Tjell for providing the polyurethane membrane. This study was funded by the Max Planck Society and the National Science Foundation (CMH; NSF OCE-1924236).

Author contributions

Conceptualization: M.v.E., O.B., and D.d.B.; investigation: M.v.E., O.B., C.M., S.B., and D.d.B.; methodology: M.v.E., O.B., C.H., and D.d.B.; visualization: M.v.E. and O.B.; writing—original draft: M.v.E. and O.B.; writing—review & editing: M.v.E., O.B., C.M., S.B., C.H., and D.d.B.

Funding
Open Access funding enabled and organized by Projekt DEAL.

Competing interests
The authors declare no competing interests.

Additional information
Supplementary information The online version contains supplementary material available at https://doi.org/10.1038/s41467-023-35818-4.

Correspondence and requests for materials should be addressed to Marit R. van Erk or Olivia M. Bourceau.

Peer review information *Nature Communications* thanks the anonymous reviewer(s) for their contribution to the peer review of this work. Peer reviewer reports are available.

Reprints and permissions information is available at http://www.nature.com/reprints

Publisher's note Springer Nature remains neutral with regard to jurisdictional claims in published maps and institutional affiliations.

Open Access This article is licensed under a Creative Commons Attribution 4.0 International License, which permits use, sharing, adaptation, distribution and reproduction in any medium or format, as long as you give appropriate credit to the original author(s) and the source, provide a link to the Creative Commons license, and indicate if changes were made. The images or other third party material in this article are included in the article's Creative Commons license, unless indicated otherwise in a credit line to the material. If material is not included in the article's Creative Commons license and your intended use is not permitted by statutory regulation or exceeds the permitted use, you will need to obtain permission directly from the copyright holder. To view a copy of this license, visit http://creativecommons.org/licenses/by/4.0/.

© The Author(s) 2023

Manuscript 3:

The effects of reactive oxygen species and short oxygenation on sulfate and nitrate reduction in intertidal sediments

Olivia Bourceau[1], Marit van Erk[1,2], Nina Tölke[1], Chyrene Moncada[1], Hannah Marchant[1,3], Tim Ferdelman[1], Dirk de Beer[1]

This manuscript is unpublished and contains preliminary results

[1]Max Planck Institute for Marine Microbiology, Celsiusstraße 1, 28359 Bremen, Germany.
[2]Present address: Department of Microbiology, Radboud University, The Netherlands [3]University of Bremen, Center for Marine Environmental Sciences, MARUM, 28359 Bremen, Germany.

The effects of reactive oxygen species and short oxygenation on sulfate and nitrate reduction in intertidal sediments

Olivia Bourceau, Marit van Erk, Nina Tölke, Chyrene Moncada, Tim Ferdelman, Hannah Marchant, Dirk de Beer

Abstract

We recently found that reactive oxygen species (ROS) impact the rate of mineralization processes in permeable sediments following transient oxygenation and that hydrogen peroxide accumulates in the anoxic zone. Here, we investigated whether ROS also impact sulfate reduction, denitrification, and DNRA in sediments without recent oxygen exposure. We found that ROS can affect the rate of sulfate reduction even in the absence of transient oxygen exposure, but that denitrification and DNRA were not affected. We hypothesize that this is due to a higher sensitivity of sulfate reducers to ROS. Interestingly, a transient oxygenation period sometimes increased the subsequent rate of anoxic sulfate reduction, but not of denitrification or DNRA. Further work is necessary to determine the mechanism of this effect. The complexity in responses of the investigated processes to oxygen and ROS suggest variations in pathways of organic matter degradation depending on seasons and locations on tidal flats.

Introduction

Intertidal sands are subject to frequent shifts in redox conditions, cycling between oxidizing and reducing conditions. These shifts are caused by advective exchange of porewater with overlying oxygenated seawater, which occurs more frequently in permeable sediments than in impermeable sediments. This advection is driven by tides, currents, sediment topography, and bioturbation (de Beer *et al.*, 2005; Werner *et al.*, 2006; Huettel *et al.*, 2014). These shifts in redox conditions can lead to production of reactive oxygen species (ROS), formed by the oxidation of reduced iron and organic matter by oxygen (Page *et al.*, 2013; Zhao *et al.*, 2022, 2023). Large

standing stocks of hydrogen peroxide were found in intertidal sands in the Wadden Sea (van Erk *et al.*, 2023). Curiously, hydrogen peroxide peaked in the anoxic zone, though it was expected that ROS are primarily formed under oxic and hypoxic conditions. Pyrite can anoxically react with water to form ROS which may be the source of this hydrogen peroxide (Borda *et al.*, 2001; Cohn *et al.*, 2006). In iron-rich environments, ROS are rapidly cycled between different forms, including superoxide, hydrogen peroxide, and the hydroxyl radical (Gligorovski *et al.*, 2015). Each ROS interacts with organisms differently, but their reaction often involves the production of another ROS. For example, the reaction of superoxide with [4Fe-4S] clusters in proteins will produce hydrogen peroxide, which can also react with these clusters (Imlay, 2013). Hydrogen peroxide and superoxide can directly damage enzymes through multiple mechanisms, especially those containing lots of cysteine and methionine residues or iron centers (Ezraty *et al.*, 2017; Imlay, 2019; Morris *et al.*, 2022). The hydroxyl radical can react indiscriminately with organics (Gligorovski *et al.*, 2015). Oxygenation of previously anaerobic sediments or soils results in the formation of hydroxyl radicals, which react with available carbon, producing carbon dioxide (Tong *et al.*, 2016; Trusiak *et al.*, 2018). Particularly the reaction of hydroxyl radicals with organic carbon can directly alter its bioavailability (Goldstone *et al.*, 2002; Pullin *et al.*, 2004; Waggoner *et al.*, 2015) and sorbtion to sediments (Patel *et al.*, 2021). ROS, especially superoxide, hydrogen peroxide, and nitric oxide, can also serve physiological roles in organisms, including as messengers and in defense against pathogens (Hansel and Diaz, 2021).

Recently, ROS were found to suppress the rate of sulfate reduction, aerobic respiration, and iron reduction in intertidal permeable sediments following a period of transient oxygenation (van Erk *et al.*, 2023). The direct impact of ROS on sulfate reducers in the environment is expected to be negative, as ROS can directly damage the reduced and iron-containing proteins sulfate reducers require for their metabolism (Ezraty *et al.*, 2017; Lu and Imlay, 2021; Morris *et al.*, 2022). ROS may indirectly affect sulfate reducers by altering the bioavilability of the carbon pool, for example removing good electron donors like lactate (Wang *et al.*, 2012). Sulfate reducers are

obligately anaerobic in that they generally can neither grow in the presence of oxygen, nor perform sulfate reduction (Cypionka, 2000; Dolla *et al.*, 2006). They can and do, however, survive in oxic and periodically oxygenated environments (Canfield and Des Marais, 1991; Jørgensen, 1994) by forming aggregates, migrating to lower oxygen concentrations, and respiring oxygen (Dilling and Cypionka, 1990; Dolla *et al.*, 2006). It is unclear what the impact of the large standing stocks of hydrogen peroxide found in intertidal sediments would have on sulfate reducers without oxygen exposure (van Erk *et al.*, 2023). It may be that sulfate reducers have in someway adapted to a background level of hydrogen peroxide, but only in the absence of oxygen.

Similarly to oxygen, nitrate availability varies with the extent of advective flushing, causing variations in redox conditions in surface sediment (Schutte *et al.*, 2021). Two dissimilatory processes compete for nitrate in sediments, denitrification and dissimilatory nitrate reduction to ammonium (DNRA). Denitrification removes fixed nitrogen from the ecosystem and ultimately produces dinitrogen gas, reducing nitrate stepwise via the intermediates nitrite, nitric oxide, and nitrous oxide. All these intermediates may leak out of cells and accumulate in the environment and potentially affect rates of other processes. In contrast, DNRA produces ammonia from nitrite without leaking any intermediates, retaining fixed nitrogen within an ecosystem. Many factors appear to influence which of the two nitrate reduction processes are most successful in an environment. Especially the ratio of electron donor to nitrate/nitrite, the ratio of nitrate to nitrite, and iron availability is often considered crucial (Kraft *et al.*, 2014; Roberts *et al.*, 2014; Robertson and Thamdrup, 2017). Recently, the rate of sulfate reduction in intertidal permeable sediments was also found to correlate to the rate of DNRA, possibly because these processes were performed by the same organism (Bourceau *et al.*, 2023).

In this study we investigated whether ROS affect sulfate and nitrate reduction in sediments from the Wadden Sea incubated anoxically. Using slurries of these permeable intertidal sediments, we measured sulfate reduction, denitrification, and DNRA in both anoxic incubations and over an oxic-anoxic transition, with and without the ROS-removing enzymes catalase and

superoxide dismutase. This allowed us to determine the impacts of anoxically formed ROS and of a transient oxygenation period on subsequent reduction rates. We expected that a transient oxygenation period would alter the rate of respiration processes in the following anoxic period, and that anoxically formed ROS would decrease rates of respiration.

Methods:

Sediment collection:

Sediment was collected from the upper part of the Janssand tidal flat, a long-term study site behind the island of Spiekeroog in the German Wadden Sea. The upper 2 cm of oxidized sediment was collected on 8 October 2020 (Fall), 1 September 2022 (Summer), and 30 May 2023 (Spring), deposited in a jar, and brought to the lab in Bremen (~3 h). Seawater was collected just off shore of the tidal flat, to prevent sediment from flowing in the seawater containers. Sediment and seawater was stored at 4°C until starting incubations in the laboratory.

Incubations

In October 2020, incubations were performed six days after sediment collection. In September 2022, nitrate reduction incubations were performed 1 day after sampling, and sulfate reduction incubations 4 days after sampling. In May 2023, the sulfate reduction incubations were performed 1 day after sampling, while the nitrate reduction incubations were performed 2 days after sampling. Each day, seawater was allowed to come to room temperature, and, for anoxic incubations, bubbled with N_2 through a bubble stone for at least 20 minutes. Sediment and anoxic seawater for anoxic incubations was then transferred to an anaerobic chamber. Sediment was well mixed, then 2 cm^3 aliquots were transferred to 6 mL glass vials, hereafter called Exetainers (Labco, Manchester). Catalase and superoxide dismutase were then added to the appropriate seawater bottles to a final activity of 1200 U/mL and 200 U/mL, respectively. Exetainers were then filled with seawater, and capped without bubbles using gas-tight lids. Exetainers were then amended individually with the appropriate tracers (^{35}S sulfate or ^{15}N nitrate), transferred to roller tanks and placed on roller tables. Incubations for sulfate reduction measurement were killed by pouring the entire contents of the Exetainers into 6 mL of 20% w/v zinc acetate, then freezing at -20°C. Incubations for N cycling measurement in September 2022 were stopped by injecting 200 µL saturated mercury chloride. In May 2023 incubations for N cycling were killed using 200 µL 50% w/v zinc chloride.

In October 2020, incubations were divided into 4 groups, two of which had an oxic start and two an anoxic start. Of each group of 2, 1 group received 1200 U/mL catalase (Sigma Aldrich, C40) and one did not.

On the first day of incubations in September 2022, samples were divided into 4 groups: (**Table 1**). Of each group, 2 had an anoxic start, and 2 an oxic start. Of each group of 2, 1 received a combination of 1200 U/mL catalase (Sigma Aldrich, C100) and 200 U/mL superoxide dismutase, and 1 did not. Each N cycling group had 26 individual Exetainers, each receiving ~40 µM ^{15}N nitrate, also to be spread out over 13 time points.

N cycling: all received ~40 µM ^{15}N nitrate, 26 Exetainers/group	
Oxic start	Anoxic
Oxic start + Cat/SOD	Anoxic + Cat/SOD

Table 1: Incubation groups September 2022 nitrate reduction. The treatment groups for nitrate reduction measurement the first day of incubations in September are outlined above.

In September 2022, samples were divided in 4 groups to determine rates of sulfate reduction, according to **table 2**.

Sulfate reduction: all received 100 kBq ^{35}S Sulfate	
Oxic start 13 Exetainers	Anoxic 13 Exetainers
Oxic start + Cat/SOD 13 Exetainers	Anoxic + Cat/SOD 13 Exetainers

Table 2: Incubation groups September 2022 sulfate reduction. The treatment groups for sulfate reduction measurement are outlined above.

In May 2023, the sulfate reduction groups were again divided into 4 groups. Two of the groups had an anoxic start, and two an oxic start. Of each group of two, **Table 2**) one received 1200 U/mL catalase (C100) and 200 U/mL SOD, and one did not (**Table 2**).. There were three Exetainers per sulfate reduction group, and all were killed after approximately six hours of incubation. There were an additional 6 Exetainers prepared, 3 oxically and 3 anoxically, and killed immediately after injection with radio tracer.

In May 2023, there were 4 nitrogen cycling groups, two of which received only nitrate, two of which received both nitrate and 1200 U/mL catalase and 200 U/mL SOD (**Table 3**). Of each group of two, one was started oxically and one anoxically. Exetainers were killed over 8 time points by injecting each exetainer with 200 µL of 50% w/v zinc chloride, using a second syringe to avoid overpressure.

Sulfate reduction: all received 200 kBq ^{35}S sulfate, 3 Exetainers per group		N cycling: all received ~40 µM ^{15}N nitrate	
Oxic start	Anoxic start	Oxic start	Anoxic start
Oxic start + CAT/SOD	Anoxic start + CAT/SOD	Oxic start + CAT/SOD	Anoxic start + CAT/SOD

Table 3: Incubation groups May 2023 The treatment groups for sulfate and nitrate reduction.

Sulfate reduction

100 µL of each sample was transferred to a scintillation vial with 900 µL of milliQ, for total activity measurement. The entire contents of the vials of frozen sample-zinc acetate mixture was subjected to a cold chromium-acid distillation, according to Røy et al. (Røy *et al.*, 2014). The 7 mL distilled reduced sulfur was then transferred to a scintillation vial, mixed with 14 mL UltimaGold scintillation fluid, and counted on a scintillation counter. In May 2023 the sulfate concentration was measured on an ion chromatograph by diluting seawater 1:500 (Metrohm 9300 Compact IC Flex). Reduced sulfate was calculated according to equation 1.

$$\frac{nmol\ SO_4^{2-} reduced}{h} = \frac{\frac{DPM_{TRIS}}{DPM_{Total}} * [SO_4^{2-}] * V_{SW}}{V_{sed} * h}$$

Equation 1: Sulfate reduction rates The rate of sulfate reduction was calculated by dividing the activity of the distillate by the total activity in the incubation, multiplied by the concentration of seawater and the volume of seawater in the Exetainer, divided by the volume of sediment and length of the incubation.

N cycling

Exetainers for N-cycling were headspaced with 1.5 mL helium, and the headspace was allowed to equilibrate. 200 µL of the headspace was injected into a GC-IRMS (Isoprime PrecisION, Elementar) to determine the relative abundance of $^{29}N_2$ and $^{30}N_2$, then calibrated against a series of ambient air injections according to (Holtappels *et al.*, 2011). The removed supernatant was then used to measure nitrate, nitrite, and $^{15}N\ NH_4^+$. $^{15}N\ NH_4^+$ was determined by converting all NH_4^+ to N_2 with hypobromide according to (Warembourg, 1993; Preisler *et al.*, 2007) then measuring $^{15}N\ N_2$ as above. In September 2022 samples were prepared by adding 250 µL of supernatant to 1 mL of 3.5% NaCl in milliQ within 3 mL Exetainers, then injecting with 100 µL hypobromide. Samples were well shaken and allowed to react and equilibrate for 2 days. In May 2023 500 µL supernatant were added to 3.3 mL 3.5% NaCl water within 5.9 mL Exetainers, degassed with helium, then injected with 200 µL hypobromide, then shaken and allowed to react for 3 days. 500 µL of headspace was injected into a GC-IRMS calibrated against ambient air injections. Standards of $^{15}N\ NH_4^+$ were prepared to ensure that conversion efficiency was >95%. Nitrite was measured chlorometrically at 540 nm (Infinite M200 Pro, Tecan) with acidic sulfanilnamide and N-naphthyl ethylenediamine dihydrochloride, then nitrate was measured on the same mixture after addition of vanadium chloride (Miranda *et al.*, 2001; García-Robledo *et al.*, 2014).

O_2

Oxygen was either measured using an oxygen Clark-type microsensor made in house (October 2020 and May 2023) or an oxygen light microsensor (Pyroscience, Aachen) in 4 Exetainers per condition, prepared as described above. Exetainers were quickly uncapped, measured, then recapped in less than 1 minute and returned to the roller tank. Oxygen was followed until anoxia, which occurred in less than 1 hour in all conditions in September 2022 and between 35-70 minutes in May 2023.

Rates

Rates were calculated by dividing the concentration of the target molecule by the length of the anoxic incubation period. In incubations amended with nitrate, only rates calculated from the period where $^{15}N\ N_2$ and $^{15}N\ NH_4^+$ were still being produced were used.

Results

Impact of oxygenation on sulfate reduction

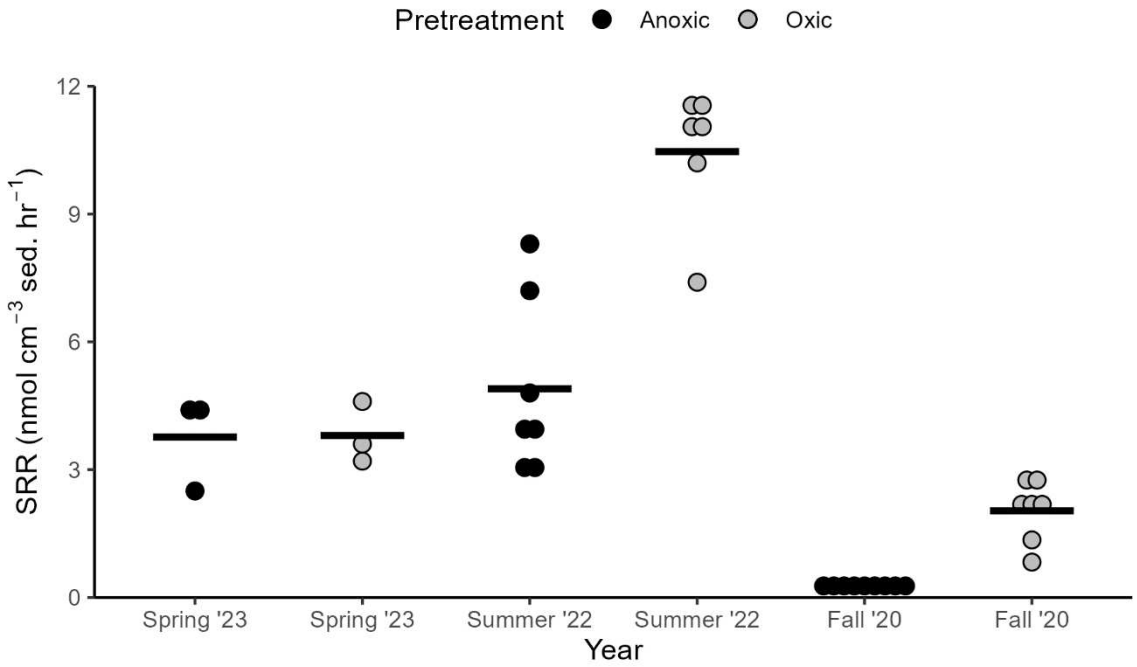

Figure 1: The impact of oxic pretreatment on sulfate reduction A) The rate of sulfate reduction in the early anoxic period is displayed for sediment collected in May 2023 (Spring), September 2022 (Summer), and October 2020 (Fall) with an anoxic (black) or oxic (grey) pretreatment. Each data point is the rate in a separate Exetainer, calculated over the anoxic incubation period, while the horizontal bars are the average rate of each group.

Starting incubations oxically resulted in 3-10x increased sulfate reduction during the following anoxic period in the fall and summer, but not in the spring (**Figure 1**). During spring, oxic pretreatments had no effect on subsequent sulfate reduction rates.

Impact of ROS on sulfate reduction

Removing ROS increased the rate of sulfate reduction in incubations started anoxically in all seasons, increasing the average rate by 30, 60, and 30% in the spring, summer, and fall, respectively (**Figure 2**).

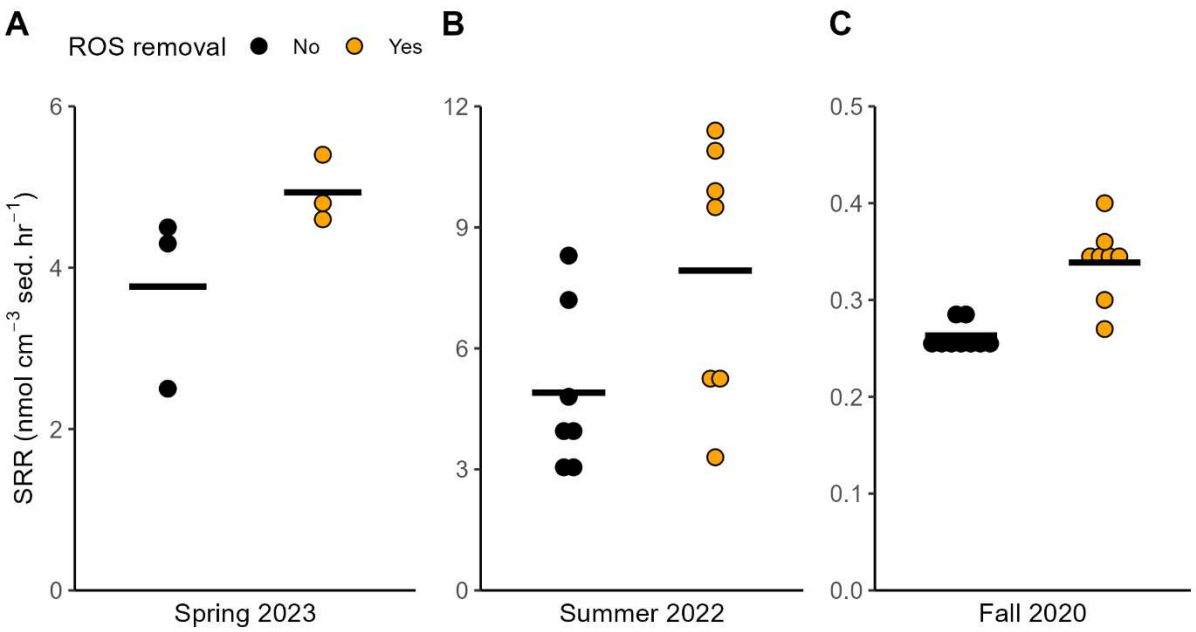

Figure 2. The impact of ROS on sulfate reduction without recent oxygen exposure The rate of sulfate reduction in incubations started anoxically and treated with (orange) or without (black) catalase and superoxide dismutase is displayed for sediment collected in May 2023 (Spring) (A) September 2022 (Summer) (B) and October 2020 (Fall) (C), Note the different scales for each season.. The data in black was also plotted in Figure 1 (also in black).

The removal of ROS increased the rates of sulfate reduction following an oxic period in fall and spring, but not summer (**Figure 3**). Average rates of sulfate reduction were increased by 30and 60% in the spring and fall, respectively.

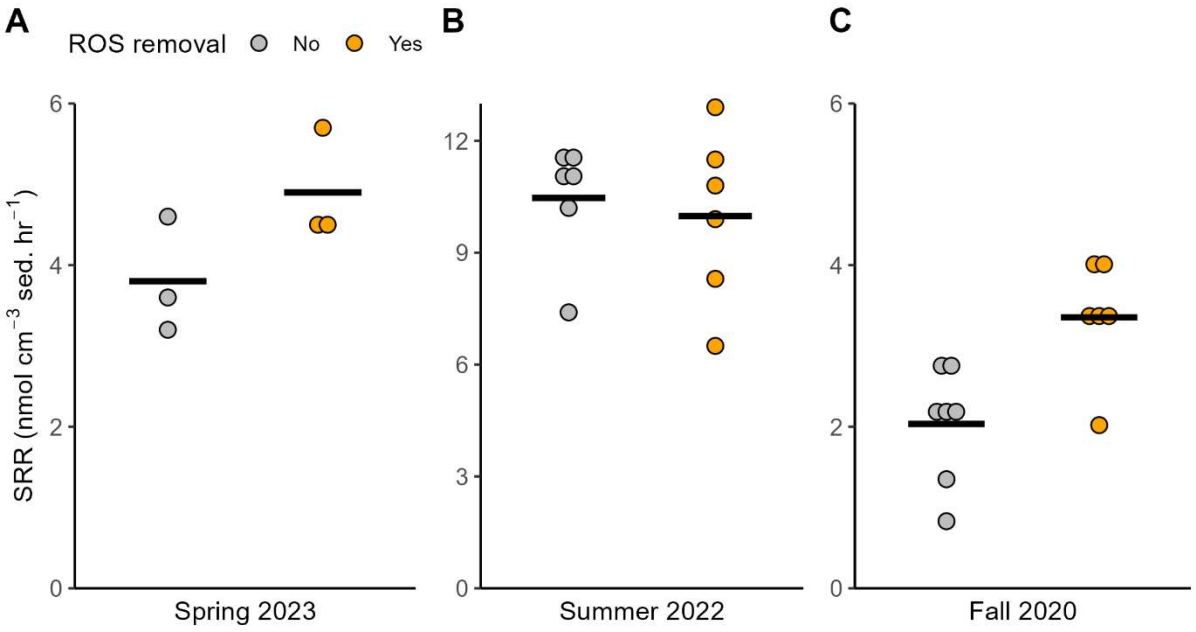

Figure 3. Impact of ROS on sulfate reduction in incubations started oxically A) The rate of sulfate reduction in in incubations started oxically and treated with (orange) or without (black) catalase and superoxide dismutase is displayed for sediment collected in in May 2023 (Spring) (A) , September 2022 (Summer) (B) and October 2020 (Fall) (C), Note the different scales for each season The data in grey in plot A was also plotted in Figure 1 (also in grey).

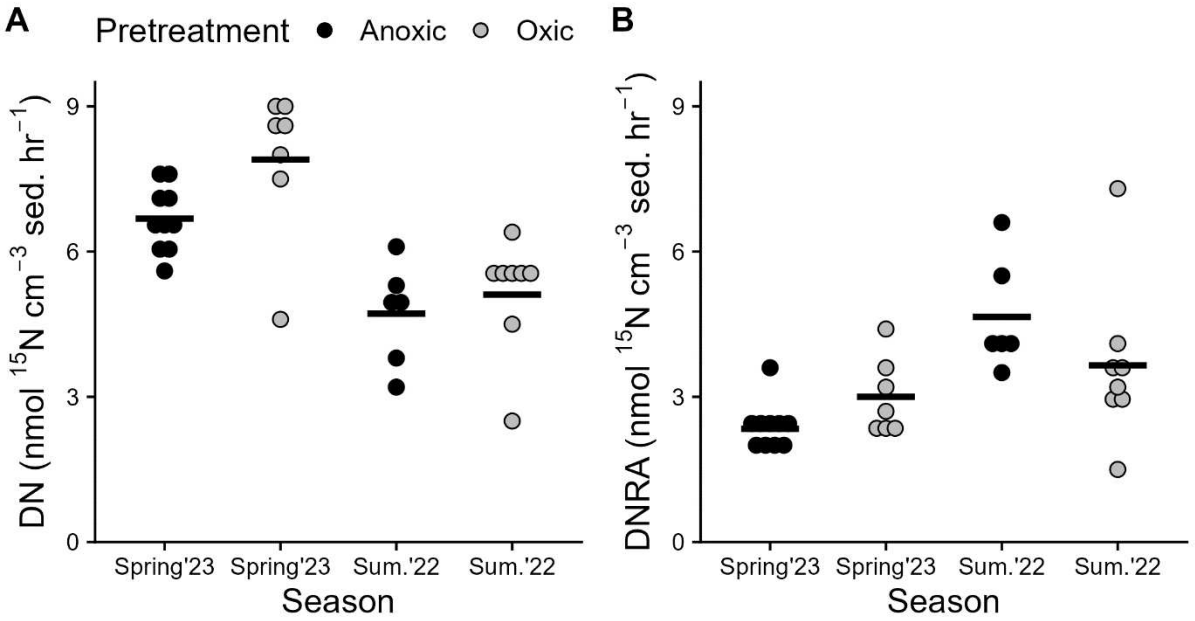

Figure 4. The impact of transient oxygenation on nitrate reduction A) The rate of denitrification in incubations started anoxically (black) or oxically (grey) in sediments collected in May 2023 (Spring) and September 2022 (Summer) is plotted, in nmol of ^{15}N per cm^3 sediment per hour. B) The rate of DNRA in incubations started anoxically (black) or oxically (grey) is plotted, in nmol of ^{15}N per cm^3 sediment per hour. Rates of DNRA and denitrification were determined from the same Exetainers. Each data point is the rate in a separate Exetainer, calculated over the anoxic incubation period, while the horizontal bars are the average rate of each group.

Transient oxygenation had little to no effect on rates of denitrification and DNRA. Oxygenation may have slightly increased denitrification in the spring, and decreased DNRA in the summer, but otherwise did not change rates.

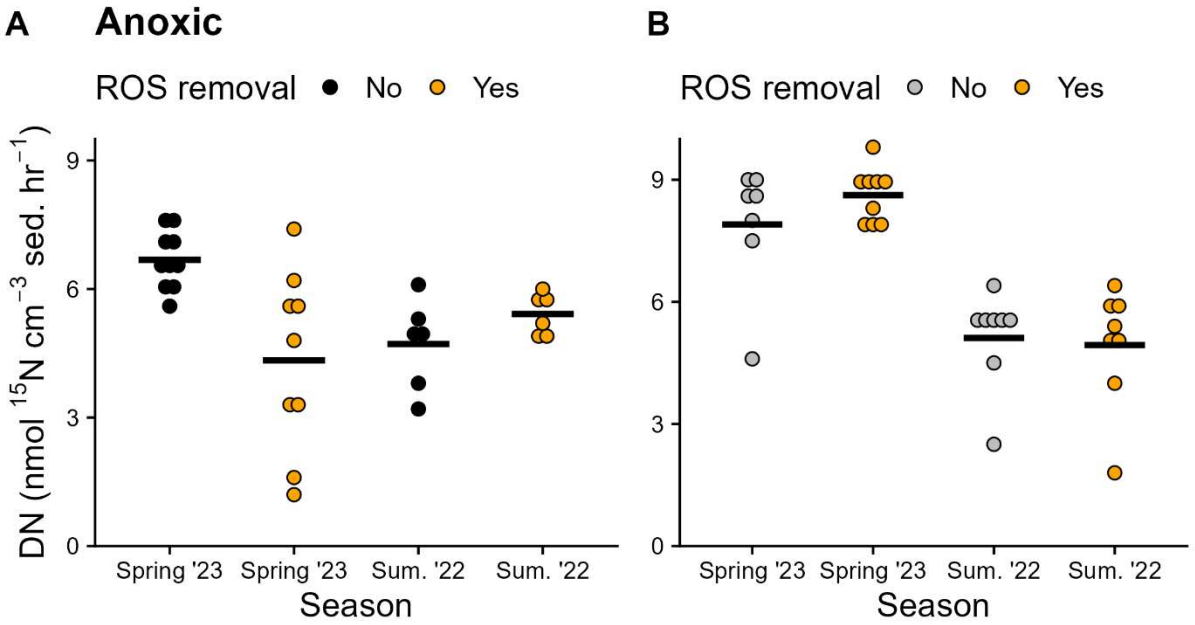

Figure 5. The impact of ROS on denitrification A) The rate of denitrification in incubations started anoxically without (black) or with (orange) catalase and superoxide dismutase in sediments collected in May 2023 (Spring) and September 2022 (Summer) is plotted, in nmol of ^{15}N per cm^3 sediment per hour. B) The rate of denitrification in incubations started oxically without (grey) or with (orange) catalase and superoxide dismutase in sediments collected in May 2023 (Spring) and September 2022 (Summer) is plotted, in nmol of ^{15}N per cm^3 sediment per hour. Each data point is the rate in a separate Exetainer, calculated over the anoxic incubation period, while the horizontal bars are the average rate of each group. Points in black and grey were also plotted in Figure 4A (also in black and grey).

ROS had no effect on rates of denitrification and DNRA (Figures 5 & 6). Incubations that started anoxically in the spring may have had a slightly lower rate of denitrification when ROS were removed but the large spread on the data in this season makes this unclear (Figure 5A).

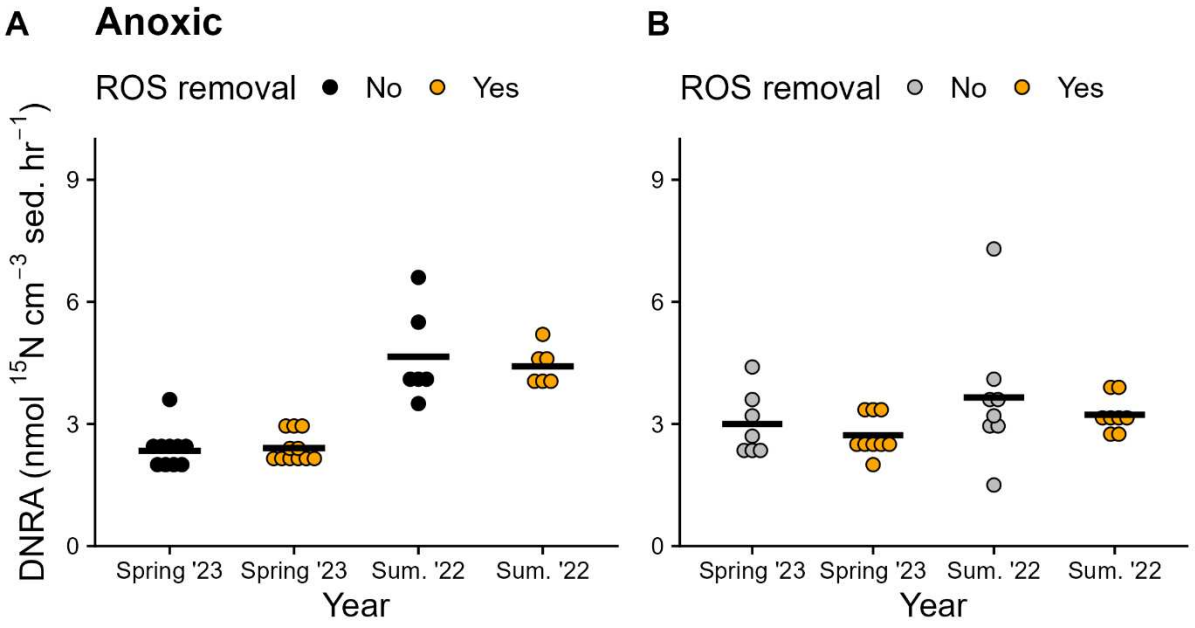

Figure 6. The impact of ROS on DNRA A) The rate of DNRA in incubations started anoxically without (black) or with (orange) catalase and superoxide dismutase in sediments collected in May 2023 (Spring) and September 2022 (Summer) is plotted, in nmol of ^{15}N per cm^3 sediment per hour. B) The rate of DNRA in incubations started oxically without (grey) or with (orange) catalase and superoxide dismutase in sediments collected in May 2023 (Spring) and September 2022 (Summer) is plotted, in nmol of ^{15}N per cm^3 sediment per hour. Each data point is the rate in a separate Exetainer, calculated over the anoxic incubation period, while the horizontal bars are the average rate of each group. Points in black and grey were also plotted in Figure 4B (also in black and grey).

Discussion

Impact of transient oxygenation on mineralization

In the fall and summer, transient oxygenation increased subsequent sulfate reduction by 3-10x, but not in spring (**Figure 1**). Rates of DNRA and denitrification were generally not affected by transient oxygenation (**Figure 4**). The rapid recovery of sulfate reduction upon anoxia is consistent with previous experiments on these sediments, which found that sulfate reduction resumes immediately upon anoxia (van Erk *et al.*, 2023). This recovery is also expected given that sulfate reducers living in the upper sediment of the tidal flat would have to be tolerant to twice daily tidal inundation and oxygen exposure. Similarly, the rapid recovery of denitrification and DNRA from oxygen exposure is expected based on the relatively high oxygen tolerance of these processes in other sediments (Cojean *et al.*, 2019), and especially as complete denitrifiers are also aerobes (Chen and Strous, 2013). Furthermore, in these sediments oxygen-

tolerant denitrification has been observed (Gao *et al.*, 2010; Marchant *et al.*, 2017). However, there is no reason to expect that oxygen would directly improve the capacity for sulfate reduction, as sulfate reduction proteins and gene transcription are inhibited by oxygen (Dolla *et al.*, 2006; Lu and Imlay, 2021). Similarly, the transcription of denitrification and DNRA genes is generally inhibited by oxygen (Pandey *et al.*, 2020).

Instead, the increase in sulfate reduction rates after oxygenation in the summer and fall was most likely due to oxygen indirectly affecting the capacity for sulfate reduction. The most obvious way of doing this would be through increasing the bioavailability of electron donor. Hydrolysis is the rate-limiting step of carbon degradation, and while the hydrolysis of labile organic carbon is not affected by the presence of oxygen, the hydrolysis of more resistant organic carbon is expected to be boosted by the presence of oxygen (Arndt *et al.*, 2013). In other words, oxygen is expected to have different impacts on hydrolysis rates depending on the lability of the carbon pool (Arndt *et al.*, 2013). It may be that under carbon-limited conditions, transient oxygenation boosts subsequent sulfate reduction due to increased availability of electron donor. Indeed, we see the biggest effect of oxygenation on sulfate reduction in the fall, when sulfate reduction rates were the lowest, suggesting electron donor limitation (**Figure 1**). ROS also substantially decreased sulfate reduction at this time, as would be expected if ROS decrease the availability of the carbon pool (**Figures 2 & 3**), discussed below. However, if carbon hydrolysis were boosted overall, it should have also lead to an increase in denitrification and DNRA. That it did not suggests that there is an additional, unknown factor at play. It is possible that oxygenation more meaningfully increased bioavailability of electron donors for sulfate reducers than nitrate reducers, as nitrate reducers generally have a higher affinity for electron donors than sulfate reducers, and a given community may have preference for one electron donor over the other (Achtnich *et al.*, 1995; Grigoryan *et al.*, 2008). The type of carbon source has previously been found to influence rates and partitioning of nitrate reduction (Morley and Baggs, 2010). Without

tracking the carbon pool over the course of incubations, it is not possible to definitively rule this in or out.

Impact of ROS on sulfate reduction

The effect of ROS on sulfate reduction was modulated by prior oxygen exposure. ROS decreased sulfate reduction in anoxically started incubations, i.e. the removal of ROS increased sulfate reduction rates (**Figure 2**). ROS were less likely to affect sulfate reduction after an oxic pretreatment than anoxic pretreatment, where the removal of ROS increased sulfate reduction by about nothing, 30, or 60% (**Figure 3**). This was somewhat lower and less consistent than other recent experiments in these sediments, which found sulfate reduction rates after transient oxygenation to be increased by ~1.5x by the removal of ROS (van Erk *et al.*, 2023). The cause of this difference may be either variation in the porewater chemistry which results in different rates of ROS production, or in differing sizes of the carbon pool, discussed further below. Overall, we found that not only do ROS have the potential to impact respiration even without a recent exposure to oxygen, but the impact of ROS is sometimes greater in incubations started anoxically than oxically.

ROS in sediments are generally expected to be formed from the reaction of reduced iron with oxygen (Zhang *et al.*, 2020; Zhao *et al.*, 2022, 2023). Nevertheless, we found that ROS impacted mineralization in sediments without recent oxygen exposure, and even tended to have a greater impact on mineralization in anoxically treated sediments than in oxygen-exposed sediments (**Figure 2 & 3**). This reconciles with recently collected profiles of hydrogen peroxide from the same sandbank, which demonstrated that concentrations peaked in the anoxic zone (van Erk *et al.*, 2023). Where this ROS comes from is unclear, but the best current explanation for ROS in this zone is the reaction of pyrite with water (Borda *et al.*, 2001; Cohn *et al.*, 2006). The scale of this process, and other mechanisms for the anoxic generation of ROS, merit further attention and research, especially as they have the potential to impact mineralization. The effect

of ROS on anoxically started incubations were visible even in sediment that was kept at 4°C for six days before incubation (October 2020, **Figure 2C**) and so are not due to the residual effects of recent oxygen exposure during tidal inundation.

ROS could potentially decrease sulfate reduction via reaction with the organic carbon pool. ROS are expected to change the nature and availability of the carbon pool in sediments (Goldstone *et al.*, 2002; Waggoner *et al.*, 2015; Patel *et al.*, 2021). They can directly react with organic carbon, mineralizing it all the way to CO_2 or simply breaking it into smaller molecules (Page *et al.*, 2012; Trusiak *et al.*, 2018; Yu and Kuzyakov, 2021). Removing bioavailable organic carbon could lead to lower rates of sulfate reduction, especially if the environment is limited in electron donor. This fits with the observation that ROS had a larger impact in sulfate reduction rates in incubations started anoxically than oxically. Oxygenation can boost the hydrolysis of resistant carbon, so it is likely that organics would be more bioavailable following exposure to oxygen (Arndt *et al.*, 2013). Removing a portion of organic carbon with ROS would have less of impact following an influx of freshly hydrolyzed carbon than without. Unfortunately, we did not gather data on the transformation of organic matter, so we are unable to confirm this hypothesis. Furthermore, denitrification and DNRA were not affected by ROS, undermining the hypothesis that ROS affect sulfate reduction via the carbon pool, although hydrogen accumulation, iron reduction, and aerobic respiration rates were previously found to be affected (van Erk *et al.*, 2023).

ROS could also directly inhibit sulfate reduction via directly damaging sulfate reducing enzymes. Many enzymes involved in sulfate reduction and anaerobic metabolism are sensitive to oxygen and ROS (Dolla *et al.*, 2006; Lu and Imlay, 2021). Sulfate reducers, like many anaerobes, do have multiple mechanisms of detoxifying ROS, but due to high numbers of reactive iron-sulfur cluster proteins, remain sensitive to ROS infiltration (Dolla *et al.*, 2006; Johnson and Hug, 2019; Lu and Imlay, 2021). In particular, hydrogen peroxide can diffuse across cell membranes,

so internal enzymatic removal may not keep cell concentrations sufficiently low when a cell is exposed to high extracellular peroxide concentrations.

It may also be that our experimental setup conflates the effects of reactive sulfur species and reactive oxygen species in the experiments enzymatically removing ROS. Reactive sulfur species can be produced through a variety of mechanisms, including from sequential one electron reductions of sulfide in an analogous way to reactive oxygen species, and exert a similar stress on organisms (Olson, 2019). As sulfate reducers produce sulfide as part of their metabolism, they likely are exposed to higher concentrations of sulfide than nitrate reducers. Furthermore, both catalase and superoxide dismutase can detoxify reactive sulfur species, for example they can react with sulfide using oxygen or hydrogen peroxide to produce polysulfides or persulfides, and may have originally evolved to moderate reactive sulfur species (Olson *et al.*, 2017, 2018; Olson, 2019). Catalase can also aerobically metabolize polysulfides, without producing sulfide (Olson *et al.*, 2017). Anoxically, catalase can also produce sulfide from thioredoxin, dithiothreitol, and sulfur dioxide (Olson, 2019). These reactions could potentially decrease complete sulfide oxidation back to sulfate by transforming sulfide into a less usable form, making it falsely seem that sulfate reduction increased. However, sulfur species produced from incomplete sulfide oxidation should still be detected by the acid-chromium distillation used to determine sulfate reduction rates, and ^{35}S should only have entered the reduced sulfur pool via sulfate reduction (Røy *et al.*, 2014). Furthermore, sulfide oxidation by catalase was found to be an oxygen and hydrogen peroxide-dependent process, and we observed effects even in anaerobically treated sediments (Olson *et al.*, 2017; Olson, 2019). Additionally, catalase and superoxide dismutase were also previously found to increase iron accumulation, hydrogen accumulation, and aerobic respiration in these sediments (van Erk *et al.*, 2023). Nevertheless, it is necessary to determine how sulfide oxidation is affected by catalase and superoxide dismutase, and the concentration and activity of reactive sulfur species in these sediments in order to confirm the observed effects were caused directly by reactive oxygen species.

Variation between seasons

The impact of ROS and transient oxygenation differed depending on the season (**Figures 1-3**). The availability of organic carbon and temperature are two of the most important regulators of sulfate reduction rates, apart from the availability of oxygen and sulfate (Goldhaber and Kaplan, 1982; Westrich and Berner, 1984; Robador *et al.*, 2016) both of which differ substantially seasonally. Higher temperatures result in higher rates of sulfate reduction (Robador *et al.*, 2016), and as expected the rates of sulfate reduction in our study were highest in the summer. The constituents of the porewater of the flat vary based on the season, largely due to variations in organic carbon input, based on timeseries of a nearby beach (Grunwald *et al.*, 2010; Seidel *et al.*, 2015; Ahrens *et al.*, 2020). The organic carbon pool varies not only in quantity, but also in composition and lability (Seidel *et al.*, 2015). Organic carbon supply was highest in the early spring in one campaign, with particularly highly labile organic carbon in the summer and spring (Seidel *et al.*, 2015) and it was inferred to be highest in summer based on oxygen consumption rates in another campaign (Ahrens *et al.*, 2020). This matches with our data, which found higher rates of sulfate reduction in the spring and summer. It may also explain why the greatest effect of ROS and oxygenation was found in the fall, as the organic carbon pool then is less labile. Variations in porewater chemistry can also vary the microbial community composition, which may also impact how mineralization rates respond to ROS (Degenhardt *et al.*, 2020).

The heterogeneity of the sandflat may also contribute to the variation between seasons that we observed. The Janssand tidal flat is subject to both surface advective flow that varies depending on the movement of the overlying water column, and deeper flow through the body of the flat due to pressure differences (Billerbeck *et al.*, 2006). Together these cause a high variation in the porewater chemistry of the flat, with points only meters away having very different chemistries, especially depending on their elevation within the flat (Jansen *et al.*, 2009). Sediment sampled only a small distance apart may thus have very different histories, which may

influence its response to ROS and oxygenation. Furthermore, the precise mineral composition can determine the rate of ROS production, so sediment with different porewater chemistry, even if close by, would be expected to have different rates of ROS production (Yu and Kuzyakov, 2021; Zhao *et al.*, 2023).

Environmental impact

The impact of ROS on microbes was heretofore expected to be largely confined to oxic and oxic-anoxic transition zones (Imlay, 2019; Zhao *et al.*, 2022). We found that ROS can impact sulfate reduction even when sediments were kept anoxic and may even have a larger effect on anoxic sediments than sediments exposed to oxygen. ROS in anoxic zones are an unaccounted for control on microbial respiration. Both the anaerobic formation of ROS, and their impact on anaerobic respiration deserve additional attention. Additionally, the impact of ROS and oxygenation appears to vary seasonally, so further investigations should be conducted over the course of the year to better estimate the impact of ROS.

Limitations

We found interesting effects of ROS and oxygenation on sulfate reduction, but the mechanism behind these effects is not clear based on our experiments. As we did not measure organic carbon concentrations or transformation, we cannot conclude whether sulfate reduction is inhibited by ROS primarily directly via protein damage, or indirectly, via the carbon pool. These experiments should be repeated, along with measuring the size and content of the carbon pool, as well as the concentration of reactive oxygen species. Additionally, incubations with lactate/acetate addition, alongside removing or not removing ROS, could provide insight into whether ROS impose a carbon limitation on sulfate reduction in these sediments, via abiotically mineralizing organic carbon. Finally, the interaction of superoxide dismutase and catalase with reactive sulfur species presents a major hurdle to determining the direct impact of ROS via enzyme addition. Further investigation into how these enzymes might directly impact measured

rates of sulfate reduction is necessary. Verification of our results with an alternative method of ROS removal/addition is necessary.

Summary

Our results indicate that ROS and oxygen impact sulfate reduction rates in opposing ways, where oxygen exposure increases sulfate reduction in the subsequent anoxic period, but ROS decrease it. This is surprising, given that the mechanism through which oxygen harms anaerobes involves the formation of ROS (Lu and Imlay, 2021). Furthermore, we found that the impact of ROS and oxygenation on sulfate reduction varied according to the season. Additionally, we found that neither oxygenation nor the removal of reactive oxygen species greatly affected denitrification or DNRA. We propose that these effects are due either to the interaction of ROS with different size carbon pools, or to an increased sensitivity of sulfate reducers to ROS. Further work is necessary to confirm our findings, particularly tracking the carbon pool during incubations and determining the impact of reactive sulfur species.

Achtnich, C., Bak, F., and Conrad, R. (1995) Competition for electron donors among nitrate reducers, ferric iron reducers, sulfate reducers, and methanogens in anoxic paddy soil. *Biol Fertil Soils* **19**: 65–72.

Ahrens, J., Beck, M., Marchant, H.K., Ahmerkamp, S., Schnetger, B., and Brumsack, H.-J. (2020) Seasonality of Organic Matter Degradation Regulates Nutrient and Metal Net Fluxes in a High Energy Sandy Beach. *J Geophys Res Biogeosciences* **125**: e2019JG005399.

Arndt, S., Jørgensen, B.B., LaRowe, D.E., Middelburg, J.J., Pancost, R.D., and Regnier, P. (2013) Quantifying the degradation of organic matter in marine sediments: A review and synthesis. *Earth-Sci Rev* **123**: 53–86.

de Beer, D., Wenzhöfer, F., Ferdelman, T.G., Boehme, S.E., Huettel, M., van Beusekom, J.E.E., et al. (2005) Transport and mineralization rates in North Sea sandy intertidal sediments, Sylt-Rømø Basin, Wadden Sea. *Limnol Oceanogr* **50**: 113–127.

Billerbeck, M., Werner, U., Polerecky, L., Walpersdorf, E., deBeer, D., and Huettel, M. (2006) Surficial and deep pore water circulation governs spatial and temporal scales of nutrient recycling in intertidal sand flat sediment. *Mar Ecol Prog Ser* **326**:.

Borda, M.J., Elsetinow, A.R., Schoonen, M.A., and Strongin, D.R. (2001) Pyrite-Induced Hydrogen Peroxide Formation as a Driving Force in the Evolution of Photosynthetic Organisms on an Early Earth. *Astrobiology* **1**: 283–288.

Bourceau, O.M., Ferdelman, T., Lavik, G., Mussmann, M., Kuypers, M.M.M., and Marchant, H.K. (2023) Simultaneous sulfate and nitrate reduction in coastal sediments. *ISME Commun* **3**: 17.

Canfield, D.E. and Des Marais, D.J. (1991) Aerobic Sulfate Reduction in Microbial Mats. *Science* **251**: 1471–1473.

Chen, J. and Strous, M. (2013) Denitrification and aerobic respiration, hybrid electron transport chains and co-evolution. *Evol Asp Bioenerg Syst* **1827**: 136–144.

Cohn, C.A., Mueller, S., Wimmer, E., Leifer, N., Greenbaum, S., Strongin, D.R., and Schoonen, M.A. (2006) Pyrite-induced hydroxyl radical formation and its effect on nucleic acids. *Geochem Trans* **7**: 3.

Cojean, A.N.Y., Zopfi, J., Gerster, A., Frey, C., Lepori, F., and Lehmann, M.F. (2019) Direct O2 control on the partitioning between denitrification and dissimilatory nitrate reduction to ammonium in lake sediments. *Biogeosciences* **16**: 4705–4718.

Cypionka, H. (2000) Oxygen Respiration by Desulfovibrio Species. *Annu Rev Microbiol* **54**: 827–848.

Degenhardt, J., Dlugosch, L., Ahrens, J., Beck, M., Waska, H., and Engelen, B. (2020) Seasonal Dynamics of Microbial Diversity at a Sandy High Energy Beach Reveal a Resilient Core Community. *Front Mar Sci* **7**:.

Dilling, W. and Cypionka, H. (1990) Aerobic respiration in sulfate-reducing bacteria. *FEMS Microbiol Lett* **71**: 123–127.

Dolla, A., Fournier, M., and Dermoun, Z. (2006) Oxygen defense in sulfate-reducing bacteria. *Asp Prokaryotic Genome Res* **126**: 87–100.

van Erk, M.R., Bourceau, O.M., Moncada, C., Basu, S., Hansel, C.M., and Beer, D. (2023) Reactive oxygen species affect the potential for mineralization processes in permeable intertidal flats. *Nat Commun* **14**: 938.

Ezraty, B., Gennaris, A., Barras, F., and Collet, J.-F. (2017) Oxidative stress, protein damage and repair in bacteria. *Nat Rev Microbiol* **15**: 385–396.

Gao, H., Schreiber, F., Collins, G., Jensen, M.M., Kostka, J.E., Lavik, G., et al. (2010) Aerobic denitrification in permeable Wadden Sea sediments. *ISME J* **4**: 417–426.

García-Robledo, E., Corzo, A., and Papaspyrou, S. (2014) A fast and direct spectrophotometric method for the sequential determination of nitrate and nitrite at low concentrations in small volumes. *Mar Chem* **162**: 30–36.

Gligorovski, S., Strekowski, R., Barbati, S., and Vione, D. (2015) Environmental Implications of Hydroxyl Radicals (•OH). *Chem Rev* **115**: 13051–13092.

Goldhaber, M.B. and Kaplan, I.R. (1982) Controls and Consequences of Sulfate Reduction Rates in Recent Marine Sediments. In *Acid Sulfate Weathering*. SSSA Special Publications. pp. 19–36.

Goldstone, J.V., Pullin, M.J., Bertilsson, S., and Voelker, B.M. (2002) Reactions of Hydroxyl Radical with Humic Substances: Bleaching, Mineralization, and Production of Bioavailable Carbon Substrates. *Environ Sci Technol* **36**: 364–372.

Grigoryan, A.A., Cornish, S.L., Buziak, B., Lin, S., Cavallaro, A., Arensdorf, J.J., and Voordouw, G. (2008) Competitive Oxidation of Volatile Fatty Acids by Sulfate- and Nitrate-Reducing Bacteria from an Oil Field in Argentina. *Appl Environ Microbiol* **74**: 4324–4335.

Grunwald, M., Dellwig, O., Kohlmeier, C., Kowalski, N., Beck, M., Badewien, T.H., et al. (2010) Nutrient dynamics in a back barrier tidal basin of the Southern North Sea: Time-series, model simulations, and budget estimates. *J Sea Res* **64**: 199–212.

Hansel, C.M. and Diaz, J.M. (2021) Production of Extracellular Reactive Oxygen Species by Marine Biota. *Annu Rev Mar Sci* **13**: 177–200.

Holtappels, M., Lavik, G., Jensen, M.M., and Kuypers, M.M.M. (2011) Chapter ten - 15N-Labeling Experiments to Dissect the Contributions of Heterotrophic Denitrification and Anammox to Nitrogen Removal in the OMZ Waters of the Ocean. In *Methods in Enzymology*. Klotz, M.G. (ed). Academic Press, pp. 223–251.

Huettel, M., Berg, P., and Kostka, J.E. (2014) Benthic Exchange and Biogeochemical Cycling in Permeable Sediments. *Annu Rev Mar Sci* **6**: 23–51.
Imlay, J.A. (2013) The molecular mechanisms and physiological consequences of oxidative stress: lessons from a model bacterium. *Nat Rev Microbiol* **11**: 443–454.
Imlay, J.A. (2019) Where in the world do bacteria experience oxidative stress? *Environ Microbiol* **21**: 521–530.
Jansen, S., Walpersdorf, E., Werner, U., Billerbeck, M., Böttcher, M.E., and de Beer, D. (2009) Functioning of intertidal flats inferred from temporal and spatial dynamics of O2, H2S and pH in their surface sediment. *Ocean Dyn* **59**: 317–332.
Johnson, L.A. and Hug, L.A. (2019) Distribution of reactive oxygen species defense mechanisms across domain bacteria. *Early Life Earth Oxidative Stress* **140**: 93–102.
Jørgensen, B.B. (1994) Sulfate reduction and thiosulfate transformations in a cyanobacterial mat during a diel oxygen cycle. *FEMS Microbiol Ecol* **13**: 303–312.
Kraft, B., Tegetmeyer, H.E., Sharma, R., Klotz, M.G., Ferdelman, T.G., Hettich, R.L., et al. (2014) The environmental controls that govern the end product of bacterial nitrate respiration. *Science* **345**: 676–679.
Lu, Z. and Imlay, J.A. (2021) When anaerobes encounter oxygen: mechanisms of oxygen toxicity, tolerance and defence. *Nat Rev Microbiol* **19**: 774–785.
Marchant, H.K., Ahmerkamp, S., Lavik, G., Tegetmeyer, H.E., Graf, J., Klatt, J.M., et al. (2017) Denitrifying community in coastal sediments performs aerobic and anaerobic respiration simultaneously. *ISME J* **11**: 1799–1812.
Miranda, K.M., Espey, M.G., and Wink, D.A. (2001) A Rapid, Simple Spectrophotometric Method for Simultaneous Detection of Nitrate and Nitrite. *Nitric Oxide* **5**: 62–71.
Morley, N. and Baggs, E.M. (2010) Carbon and oxygen controls on N2O and N2 production during nitrate reduction. *Soil Biol Biochem* **42**: 1864–1871.
Morris, J.J., Rose, A.L., and Lu, Z. (2022) Reactive oxygen species in the world ocean and their impacts on marine ecosystems. *Redox Biol* **52**: 102285.
Olson, K.R. (2019) Hydrogen sulfide, reactive sulfur species and coping with reactive oxygen species. *Free Radic Biol Med* **140**: 74–83.
Olson, K.R., Gao, Y., Arif, F., Arora, K., Patel, S., DeLeon, Eric.R., et al. (2018) Metabolism of hydrogen sulfide (H2S) and Production of Reactive Sulfur Species (RSS) by superoxide dismutase. *Redox Biol* **15**: 74–85.
Olson, K.R., Gao, Y., DeLeon, E.R., Arif, M., Arif, F., Arora, N., and Straub, K.D. (2017) Catalase as a sulfide-sulfur oxido-reductase: An ancient (and modern?) regulator of reactive sulfur species (RSS). *Redox Biol* **12**: 325–339.
Page, S.E., Kling, G.W., Sander, M., Harrold, K.H., Logan, J.R., McNeill, K., and Cory, R.M. (2013) Dark Formation of Hydroxyl Radical in Arctic Soil and Surface Waters. *Environ Sci Technol* **47**: 12860–12867.
Page, S.E., Sander, M., Arnold, W.A., and McNeill, K. (2012) Hydroxyl Radical Formation upon Oxidation of Reduced Humic Acids by Oxygen in the Dark. *Environ Sci Technol* **46**: 1590–1597.
Pandey, C.B., Kumar, U., Kaviraj, M., Minick, K.J., Mishra, A.K., and Singh, J.S. (2020) DNRA: A short-circuit in biological N-cycling to conserve nitrogen in terrestrial ecosystems. *Sci Total Environ* **738**: 139710.
Patel, K.F., Tejnecký, V., Ohno, T., Bailey, V.L., Sleighter, R.L., and Hatcher, P.G. (2021) Reactive oxygen species alter chemical composition and adsorptive fractionation of soil-derived organic matter. *Geoderma* **384**: 114805.
Preisler, A., de Beer, D., Lichtschlag, A., Lavik, G., Boetius, A., and Jørgensen, B.B. (2007) Biological and chemical sulfide oxidation in a Beggiatoa inhabited marine sediment. *ISME J* **1**: 341–353.

Pullin, M.J., Bertilsson, S., Goldstone, J.V., and Voelker, B.M. (2004) Effects of sunlight and hydroxyl radical on dissolved organic matter: Bacterial growth efficiency and production of carboxylic acids and other substrates. *Limnol Oceanogr* **49**: 2011–2022.

Robador, A., Müller, A.L., Sawicka, J.E., Berry, D., Hubert, C.R.J., Loy, A., et al. (2016) Activity and community structures of sulfate-reducing microorganisms in polar, temperate and tropical marine sediments. *ISME J* **10**: 796–809.

Roberts, K.L., Kessler, A.J., Grace, M.R., and Cook, P.L.M. (2014) Increased rates of dissimilatory nitrate reduction to ammonium (DNRA) under oxic conditions in a periodically hypoxic estuary. *Geochim Cosmochim Acta* **133**: 313–324.

Robertson, E.K. and Thamdrup, B. (2017) The fate of nitrogen is linked to iron(II) availability in a freshwater lake sediment. *Geochim Cosmochim Acta* **205**: 84–99.

Røy, H., Weber, H.S., Tarpgaard, I.H., Ferdelman, T.G., and Jørgensen, B.B. (2014) Determination of dissimilatory sulfate reduction rates in marine sediment via radioactive 35S tracer. *Limnol Oceanogr Methods* **12**: 196–211.

Schutte, C.A., Huanca-Valenzuela, P., Lavik, G., Marchant, H.K., and de Beer, D. (2021) Advection Drives Nitrate Past the Microphytobenthos in Intertidal Sands, Fueling Deeper Denitrification. *Front Microbiol* **12**:.

Seidel, M., Beck, M., Greskowiak, J., Riedel, T., Waska, H., Suryaputra, IG.N.A., et al. (2015) Benthic-pelagic coupling of nutrients and dissolved organic matter composition in an intertidal sandy beach. *Mar Chem* **176**: 150–163.

Tong, M., Yuan, S., Ma, S., Jin, M., Liu, D., Cheng, D., et al. (2016) Production of Abundant Hydroxyl Radicals from Oxygenation of Subsurface Sediments. *Environ Sci Technol* **50**: 214–221.

Trusiak, A., Treibergs, L.A., Kling, G.W., and Cory, R.M. (2018) The role of iron and reactive oxygen species in the production of CO2 in arctic soil waters. *Geochim Cosmochim Acta* **224**: 80–95.

Waggoner, D.C., Chen, H., Willoughby, A.S., and Hatcher, P.G. (2015) Formation of black carbon-like and alicyclic aliphatic compounds by hydroxyl radical initiated degradation of lignin. *Org Geochem* **82**: 69–76.

Wang, W., Qu, Y., Yang, B., Liu, X., and Su, W. (2012) Lactate oxidation in pyrite suspension: A Fenton-like process in situ generating H2O2. *Chemosphere* **86**: 376–382.

Warembourg, F.R. (1993) 5 - Nitrogen Fixation in Soil and Plant Systems. In *Nitrogen Isotope Techniques*. Knowles, R. and Blackburn, T.H. (eds). San Diego: Academic Press, pp. 127–156.

Werner, U., Billerbeck, M., Polerecky, L., Franke, U., Huettel, M., van Beusekom, J.E.E., and de Beer, D. (2006) Spatial and temporal patterns of mineralization rates and oxygen distribution in a permeable intertidal sand flat (Sylt, Germany). *Limnol Oceanogr* **51**: 2549–2563.

Westrich, J.T. and Berner, R.A. (1984) The role of sedimentary organic matter in bacterial sulfate reduction: The G model tested1. *Limnol Oceanogr* **29**: 236–249.

Yu, G.-H. and Kuzyakov, Y. (2021) Fenton chemistry and reactive oxygen species in soil: Abiotic mechanisms of biotic processes, controls and consequences for carbon and nutrient cycling. *Earth-Sci Rev* **214**: 103525.

Zhang, Y., Tong, M., Yuan, S., Qian, A., and Liu, H. (2020) Interplay between iron species transformation and hydroxyl radicals production in soils and sediments during anoxic-oxic cycles. *Geoderma* **370**: 114351.

Zhao, G., Tan, M., Wu, B., Zheng, X., Xiong, R., Chen, B., et al. (2023) Redox Oscillations Activate Thermodynamically Stable Iron Minerals for Enhanced Reactive Oxygen Species Production. *Environ Sci Technol* **57**: 8628–8637.

Zhao, G., Wu, B., Zheng, X., Chen, B., Kappler, A., and Chu, C. (2022) Tide-Triggered Production of Reactive Oxygen Species in Coastal Soils. *Environ Sci Technol* **56**: 11888–11896.

Manuscript 4:

High resolution functional analysis and community structure of photogranules

Lukas M. Trebuch [1,2,7], **Olivia M. Bourceau** [3,7], Stijn M. F. Vaessen[1,2], Thomas R. Neu [4], Marcel Janssen2, Dirk de Beer [3], Louise E. M. Vet[5], René H. Wijffels[2,6] and Tânia V. Fernandes[1]

Published in **The ISME Journal**

doi: https://doi.org/10.1038/s41396-023-01394-0

Supplementary information is available in the online version of this article

[1]Department of Aquatic Ecology, Netherlands Institute of Ecology (NIOO-KNAW), Droevendaalsesteeg 10, 6708 PB Wageningen, The Netherlands. [2]Bioprocess Engineering, AlgaePARC Wageningen University, P.O. Box 16, 6700 AA Wageningen, The Netherlands. [3]Max-Plank-Institute for Marine Microbiology, Celsiusstrasse 1, 28359 Bremen, Germany. [4]Microbiology of Interfaces, Department River Ecology, Helmholtz Centre for Environmental Research - UFZ, Brueckstrasse 3A, 39114 Magdeburg, Germany. [5]Department of Terrestrial Ecology, Netherlands Institute of Ecology (NIOO-KNAW), Droevendaalsesteeg 10, 6708 PB Wageningen, The Netherlands. [6]Faculty of Biosciences and Aquaculture, Nord University, N-8049 Bodø, Norway. [7]**These authors contributed equally: Lukas M. Trebuch, Olivia M. Bourceau.**

www.nature.com/ismej

ISME

ARTICLE OPEN

Check for updates

High resolution functional analysis and community structure of photogranules

Lukas M. Trebuch[1,2,7✉], Olivia M. Bourceau[3,7], Stijn M. F. Vaessen[1,2], Thomas R. Neu[4], Marcel Janssen[2], Dirk de Beer[3], Louise E. M. Vet[5], René H. Wijffels[2,6] and Tânia V. Fernandes[1]

© The Author(s) 2023

Photogranules are spherical aggregates formed of complex phototrophic ecosystems with potential for "aeration-free" wastewater treatment. Photogranules from a sequencing batch reactor were investigated by fluorescence microscopy, 16S/18S rRNA gene amplicon sequencing, microsensors, and stable- and radioisotope incubations to determine the granules' composition, nutrient distribution, and light, carbon, and nitrogen budgets. The photogranules were biologically and chemically stratified, with filamentous cyanobacteria arranged in discrete layers and forming a scaffold to which other organisms were attached. Oxygen, nitrate, and light gradients were also detectable. Photosynthetic activity and nitrification were both predominantly restricted to the outer 500 µm, but while photosynthesis was relatively insensitive to the oxygen and nutrient (ammonium, phosphate, acetate) concentrations tested, nitrification was highly sensitive. Oxygen was cycled internally, with oxygen produced through photosynthesis rapidly consumed by aerobic respiration and nitrification. Oxygen production and consumption were well balanced. Similarly, nitrogen was cycled through paired nitrification and denitrification, and carbon was exchanged through photosynthesis and respiration. Our findings highlight that photogranules are complete, complex ecosystems with multiple linked nutrient cycles and will aid engineering decisions in photogranular wastewater treatment.

The ISME Journal (2023) 17:870–879; https://doi.org/10.1038/s41396-023-01394-0

INTRODUCTION

Wastewater treatment reactors continuously select for functional traits in their microbial communities. Manipulating operating conditions allows for the selection of desired traits, including conversion processes to purify water and self-aggregation of microbial biomass. Self-aggregation (i.e., forming biogranules, spherical aggregates of microorganisms) enables stratification (oxic and anoxic zones) and facilitates biomass harvesting because dense aggregates rapidly sink once reactor mixing is stopped. Generally, biogranules are formed in reactors where the liquid residence time is shorter than the doubling time of the microorganisms. This washes out suspended cells and generates selective pressure for biomass retention [1, 2]. Although the aggregated biomass in biogranules is subject to mass transfer resistances that reduce the activity per cell, efficient biomass retention and the ensuing increased biomass assures strongly elevated volumetric conversion rates in biogranule reactors.

Phototrophic biogranules, called photogranules, were first observed in cultures of photosynthetic mats from the North Sea [3]. The granules were composed of filamentous cyanobacteria, diatoms, and heterotrophic bacteria. Spherical geometry is rare in phototrophic communities, but some examples of photogranules in nature have been reported. For example, photogranules composed of cyanobacteria and heterotrophic bacteria called cryoconites are found in glaciers [4, 5]. Green and pink microbial "berries" are found in salt marshes, formed through a symbiosis of cyanobacteria and diatoms, and of communities of sulfur-oxidizing purple sulfur bacteria and sulfur-reducing bacteria, respectively [6, 7].

In phototrophic biofilms in nature, as in photogranules, concentration gradients of various dissolved chemical species (e.g., oxygen, substrates) are formed due to diffusional limitation. Similarly, light intensity gradients are formed by light absorption and scattering [8]. These intersecting gradients create a varied environment that can support the simultaneous growth of diverse microorganisms filling different niches, such as photoautotrophs, chemoautotrophs, and heterotrophs, exhibiting aerobic, and anaerobic metabolisms [9]. Complex interactions between these microbial groups take place, that may stabilize the functioning of the consortium [10]. For example, heterotrophs may grow on extracellular organic compounds excreted by phototrophs. The latter, in turn, may fix the inorganic CO_2 produced in heterotrophic growth. Aerobic chemoautotrophs, such as nitrifiers, may benefit from photosynthesis-enhanced oxygen levels while simultaneously competing with phototrophs for inorganic carbon and nitrogen. Unlike in biofilms, photogranules are free living, so their

[1]Department of Aquatic Ecology, Netherlands Institute of Ecology (NIOO-KNAW), Droevendaalsesteeg 10, 6708 PB Wageningen, The Netherlands. [2]Bioprocess Engineering, AlgaePARC Wageningen University, P.O. Box 16, 6700 AA Wageningen, The Netherlands. [3]Microsensor Research Group, Max-Plank-Institute for Marine Microbiology, Celsiusstrasse 1, 28359 Bremen, Germany. [4]Microbiology of Interfaces, Department River Ecology, Helmholtz Centre for Environmental Research - UFZ, Brueckstrasse 3A, 39114 Magdeburg, Germany. [5]Department of Terrestrial Ecology, Netherlands Institute of Ecology (NIOO-KNAW), Droevendaalsesteeg 10, 6708 PB Wageningen, The Netherlands. [6]Faculty of Biosciences and Aquaculture, Nord University, N-8049 Bodø, Norway. [7]These authors contributed equally: Lukas M. Trebuch, Olivia M. Bourceau.
✉email: L.Trebuch@nioo.knaw.nl

Received: 30 July 2022 Revised: 28 February 2023 Accepted: 3 March 2023
Published online: 30 March 2023

Downloaded from https://academic.oup.com/ismej/article/17/6/870/7474056 by guest on 24 May 2024

biomass is not limited to the surface area of their container. Furthermore, the surface to volume ratio of a sphere is such that for small spheres, there is capacity for a higher biomass-water exchange than in a plane of the same volume. This relationship holds so long as the radius of the sphere is less than one third of the thickness of the plane.

Recently, photogranules were cultivated with selection pressure to remove and recover nitrogen, phosphorus, and carbon from wastewater [11–17]. This involved a regular exchange of the medium after settling of biomass, thus with a selection pressure towards formation of fast-settling granules. The granules exhibited indeed excellent settling properties, and their in-situ photosynthetic oxygen production fuelled oxygen-demanding microbial processes such as nitrification and respiration. This linked the O_2, and CO_2 cycles within the treatment process, making progress towards "aeration-free" wastewater treatment. Initial studies have investigated the physical structure and metabolic functions of single photogranules from wastewater, but were limited in focus to phototrophic organisms and oxygen profiles [18–20]. A modelling approach predicted the distribution of microorganisms and extracellular polymeric substances (EPS) within photogranules and the bulk turnover of chemical compounds and reactor functions based on varying nutrient inputs, but has not yet been tested in real photogranules [21, 22].

Photogranules experience both varying external environmental conditions (i.e., light intensity, nutrient concentrations) during reactor operation, and internal conditions, as nutrient gradients are created and eliminated in response to microbial activity and external variation. Therefore, a full understanding of the microbial ecology within photogranules requires detailed investigation under various and varying conditions in vivo. Here, we studied the physical and biological stratification and functioning of these same photogranules with microscopic imaging, metataxonomics, microsensors, and incubations with radio- and stable-isotope labels. Our findings provide insight into the spatial and temporal distribution of functional activity (photosynthesis, nitrification, and denitrification) within photogranules and their dependency on external factors (light, nutrients). Further, the results can be used to support engineering decisions in photogranular wastewater treatment.

MATERIALS AND METHODS

Cultivation and sample preparation

Photogranules were obtained from bioreactors as described previously [12] (Fig. S1). The bioreactors were bubble columns 38 cm high, 10 cm in diameter and with a bottom cone 10 cm high. The working volume was 1.6 L, standing 28 cm from the bottom of the cone. Mixing was achieved by gassing with air enriched with 5% v/v CO_2 at a rate of 500 mL min^{-1}. Temperature was kept at 35 °C using an external water bath and pH at 6.8 ± 0.1 by automatic addition of 1 M HCl or 1 M NaOH. Bioreactors were operated in sequencing batch mode with a settling time of 5 min, a hydraulic retention time (HRT) of 0.67 days, and an operating cycle of 12 h. Day:night cycles of 12 h were superimposed on the sequencing batch cycle such that each batch cycle was subjected to 6 h light and 6 h darkness. Warm white light (4000 K) LED lamps (Avago ASMT-MY22-NMP00, Broadcom Inc., USA), positioned at one side of the bioreactor, were providing an incident light intensity of 500 µmol m^{-2} s^{-1} at the surface of the bioreactor during the light phase. A sludge retention time (SRT) of 7 days was achieved by automatically removing 114 ml of the mixed liquor at the end of every batch cycle via a peristaltic pump. The influent contained 100 mg_N L^{-1} (7.1 $mmol_N$ L^{-1}) as ammonium, 10 mg_P L^{-1} (0.3 $mmol_P$ L^{-1}) and 200 mg_{COD} L^{-1} (3.2 mmol L^{-1} of sodium acetate). The bioreactors were operated for 299 days. Photogranules were sampled during stable operational periods at day 105, 186, 214, 270, and 299 from the mixed phase of the bioreactor and were either directly analyzed or fixed in paraformaldehyde (PFA) in 5% phosphate buffered saline (PBS) for later microscopic analysis. Photogranules ranged from 0.4 to 5 mm wide with an average diameter of 2.6 mm. Photogranules ranging from 2 to 4 mm wide were used for analysis.

White light microscopy and confocal laser scanning microscopy (CLSM)

A stereomicroscope (Leica M205C, Germany) was used to visualize whole and sectioned photogranules under white light. Images were obtained with the Leica Application Suite (LAS version 4.13, Germany). The 3-dimensional structure of the granules was examined by multi-channel CLSM (Leica TCS SP5X, Germany). The system with an upright microscope and a super continuum light source was controlled by the LAS-AF 2.4.1 software. Image data stacks were recorded with 25× NA 0.95 and 63× NA 1.2 water immersion lenses. Samples were mounted in a cover well chamber with spacers. For this purpose, the photogranules were cut in half and stained inside the chamber, which was then filled up with water and closed with a coverslip. For identifying a suitable lectin, a screening with all commercially available lectins was performed. Glycoconjugates were detected by fluorescence lectin-binding analysis (FLBA), according to Staudt et al. and Zippel and Neu [22, 23]. After testing several lectins, the BAN lectin labelled with Alexa-568 was selected for imaging. BAN is a lectin derived from banana (*Musa paradisiaca*), which has single-carbohydrate binding specificity for D-mannose and D-glucose [24]. The fluorochrome Syto9 was used as a counterstain to visualize nucleic acids. Cyanobacteria and eukaryotic algae were identified based on their pigments [25, 26]. The settings for recording image data stacks sequentially were as follows: Excitation: 480, 635 nm and 565 nm, emission: 500–550 nm (Syto9), 585–650 nm (BAN-A568, phycobilins), 650–720 nm (Chl A). Images were processed with the imaging software Fiji [27] and individual image data stacks were stitched together using Photoshop (version CS6).

16S/18S rRNA gene amplicon sequencing

DNA samples were taken to assess the microbial community. Specifically, 15 mL of harvested photogranules were homogenized by a glass/Teflon tissue grinder, aliquoted into five 2 mL microcentrifuge tubes, centrifuged at 14.87 × 10^3 rcf for 10 min and the supernatant discarded. The cell pellets were immediately frozen at −80 °C until further processing. DNA of 200 mg of wet cell pellet was extracted in triplicate by using the DNeasy PowerSoil Pro Isolation Kit (Qiagen GmbH, Hilden, Germany) according to the manufacturer's protocol. The quantity and quality of DNA were spectrophotometrically determined with a NanoDrop One (ThermoFisher Scientific, USA). The DNA samples were submitted for sequencing to Génome Québec (McGill University, Montreal, CA). The 16S rRNA gene V3/V4 variable region was amplified using primer pair 341F (CCTACGGGNGGCWGCAG) and 805R (GACTACHVGGGTATCTAATCC) [28]. The 18S rRNA gene V4 variable region was amplified using the primer pair 616*F (TTAAARVGYTCGTAGTYG) and 1132R (CCGTCAATTHCTTYAART) [29]. Both sets of primers were modified to add Illumina adaptor overhang nucleotides sequences to the gene-specific sequences. Sequencing was performed using a MiSeq system (Illumina, USA) with 300-bp reads (v3 chemistry). Primers were removed from the raw sequences using *cutadapt* (version 1.18) [30]. The obtained sequences were processed further with DADA2 programme [31]. Taxonomic alignment of the sequences was done to the SILVA database (release 138) using SINA (https://www.arb-silva.de). The 16S and 18S dataset was normalized using the cumulative sums scaling (CSS) function of the R package *metagenomSeq* version 1.24.1 [32]. The analysis of the microbiome data was performed with the R-package *phyloseq* (version 1.26.1) [33]. The raw 16S and 18S rRNA gene sequence data is available in the EBI database under project number PRJEB54633.

Microsensor measurements

Photogranules were pinned with glass needles to a nylon mesh fitted over a small petri dish (Fig. S2). The Petri dish was submerged in tap water (Table S1) and amended with acetate, medium stocks, and nitrate as indicated. Oxygen concentration was determined using a Clark-type oxygen microsensor [34] fitted to a motorized micromanipulator and two-point calibrated in oxygen-saturated water and basic sodium ascorbate (oxygen-free baseline). Nitrate concentrations were determined using a nitrate LIX membrane sensor manufactured in house (Max Planck Institute for Marine Microbiology, Bremen, Germany), calibrated in a nitrate dilution series [35]. Light profiles were determined with a scalar irradiance light microsensor with an 80 µm spherical tip (Zensor, Denmark) [36], connected to a USB4000 fibre optic spectrophotometer (Ocean Optics, USA) [37]. To collect profiles, microsensors pierced the granule, propelled stepwise by a motorized micromanipulator.

Using the oxygen and nitrate profiles generated from the microsensor measurements, the net consumption/production rates of reactants were calculated by segregating the granule into "shells," with each shell the

Downloaded from https://academic.oup.com/ismej/article/17/6/870/7474056 by guest on 24 May 2024

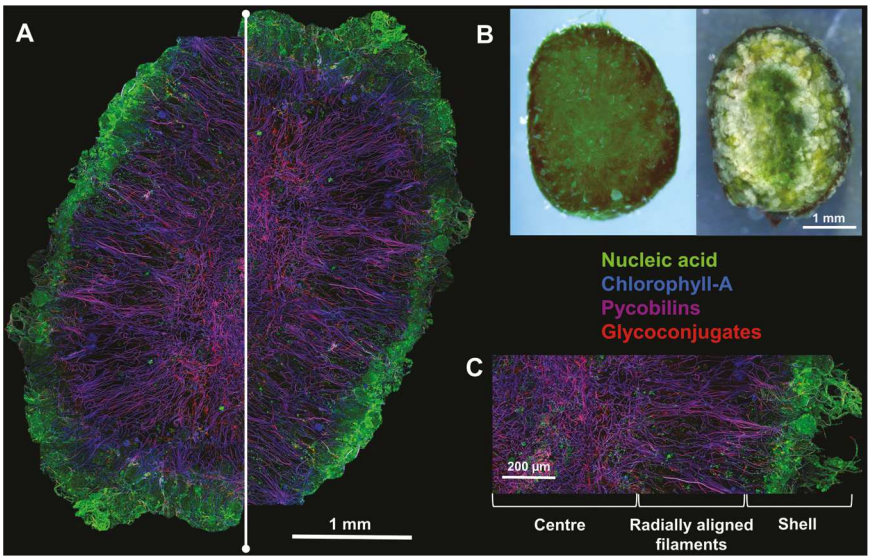

Fig. 1 Macro-photographs and CLSM of photogranules. A CLSM image of a photogranule cross section showing the nucleic acid staining (green), photopigments of filamentous cyanobacteria as an overlay of phycobilins (red) and chlorophyll A (blue) resulting in purple, the chlorophyll A of eukaryotic microalgae (blue), and the lectin signal of glycoconjugates (red). The CLSM images are made of 14 individual images stitched together. Due to limitations of the CLSM technique only half of the photogranule could be captured and for representation purposes the image was mirrored over the white vertical line. **B** Macro-photography of a photogranule under white light. The left image shows the whole photogranule and the right image the cross section of the same photogranule. **C** Close-up of the CLSM cross section from the centre to the surface of the photogranule. The cross section can be divided into three distinct zones: (1) the centre, (2) radially aligned filaments and (3) the shell.

width of the distance between measurements, and assuming a spherical geometry. The flux between a point on the outer part of the shell and a point on the inner part of the shell was calculated, then multiplied by the surface area of the shell.

$$P = D \times \frac{dC_r}{dx_r} \times 4 \times \mathrm{pi} \times r^2 \quad (1)$$

with P as the conversion rate per shell of aggregate (expressed in this paper in nmol/h), with D as diffusion coefficient, dC_r/dx_r the concentration gradient of the reactant at location r, and r the radial distance from the shell surface to the centre of the aggregate. The total conversion rates were obtained by addition of activities in all shells, since the rates represent total activities, not activities normalized to volume. To produce the volumetric rate the production rate of each shell was divided by the volume of that shell. The diffusion coefficient used for oxygen was 2000 $\mu m^2\ s^{-1}$, (Bionumbers ID 104440) [38, 39] and the coefficient used for nitrate was 1700 $\mu m^2\ s^{-1}$ (Bionumbers ID 104439) [38, 39].

Separate photosynthesis rates were determined by placing the microsensor at a set depth, then covering the light for 5–10 s. The rate of the decrease in oxygen concentration is equivalent to the rate of photosynthesis at that depth.

^{14}C carbon fixation incubations

Photogranules were incubated without headspace in 5.9 mL glass vials at pH 6.5 in tap water amended with either 3 mM or 10 mM sodium bicarbonate, and amended with 8 mM ammonium, 3 mM phosphate, and/or 3 mM acetate as indicated. There were 3–4 photogranules per vial, with one vial per condition, except for the incubation with ammonium and phosphate, which had 2 vials. Additionally, photogranules were provided with ~60 kBq ^{14}C bicarbonate. Vials were constantly rotated and incubated for 6 h at room temperature in the dark (nitrification experiment) or in the light (photosynthesis, ~250 µmol $m^{-2}\ s^{-1}$). Incubations were performed simultaneously. Incubations were stopped by removing 600 µL supernatant and replacing it with a 20% paraformaldehyde (PFA) solution, achieving a final concentration of 2% PFA. Photogranules used for control (blanks) were killed first in PFA and then exposed to the tracer for 6 h.

The photogranules were washed twice in 10 mM carbonate buffer to remove unreacted carbonate tracer and embedded by immersing in optimal cutting temperature compound (OCT, Leica) overnight, then frozen in 1 ml plastic cups at −20 °C and sectioned in 20 µm thick slices in a cryomicrotome. The slices were caught on polylysine slides, and the radioactivity distribution was imaged in a radio-imager (BioSpaceLab, Paris), until 10^6 counts were obtained. Blanks were counted for 12 h, as 10^6 counts could not be obtained in a reasonable time. The produced images were then analyzed with M3Vision (BioSpaceLab, Paris). The CO_2 uptake of the whole granule was obtained, subsequently normalized per mm^2 and then divided by the thickness of the aggregate section to obtain volumetric rates (see Fig. S6).

^{15}N nitrogen incubations

Photogranules were incubated in 6 mL gas-tight glass vials in tap water amended with 3 mM sodium bicarbonate and either 1 mM ^{15}N ammonium or 1 mM ^{15}N nitrate and incubated without headspace at room temperature in the dark or light as indicated. Two photogranules were placed in each vial, one small and one large. Four separate vials were prepared per condition, and the photogranules in one vial per group were killed at 4 separate time points (~0, 2, 4.5, and 5.5 h incubation). Photogranules were killed with a 1:1 w/v ZnCl solution. Timepoint 0 was used as the blank.

After killing the photogranule, a 2 mL helium headspace was created in each vial. The vials were shaken vigorously and allowed to equilibrate for 5 days. Subsequently, 150 µL of headspace was injected into an IR-MS and analyzed for ^{15}N-N_2. Injections were calibrated against a series of ambient air injections, allowing calculation of the excess ^{15}N nitrogen content. Total excess ^{15}N was calculated as (excess $^{29}N_2 + (2 \times$ excess $^{30}N_2)$). Rates of denitrification were calculated by fitting a linear equation to the excess ^{15}N production [40].

NO_x, the sum of nitrate and nitrite, was converted to NO with acidic vanadium chloride and measured with a CLD 60 Chemiluminescence NO/NO_x analyser [41]. NO_x content was calibrated against a dilution series of nitrate. The rate of nitrification was then determined by fitting a linear equation to the sum of the excess ^{15}N at each time point and the NO_x concentration.

RESULTS

Physical structure of photogranules

The photogranules were physically robust and exhibited a clear stratification (Fig. 1). Filamentous cyanobacteria (phycobilin and Chl A autofluorescence) with gliding motility formed a complex network that functioned as a scaffold for other microorganisms. A

Downloaded from https://academic.oup.com/ismej/article/17/6/870/7474056 by guest on 24 May 2024

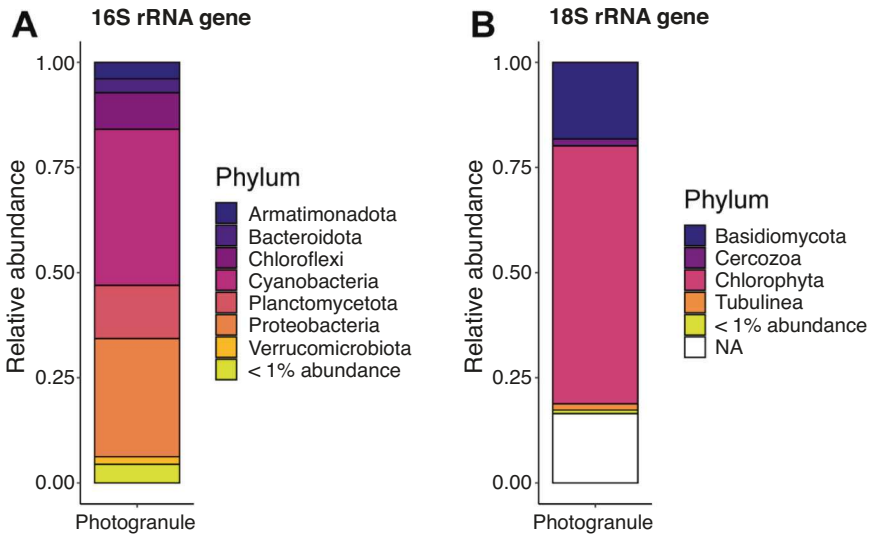

Fig. 2 Microbial community composition obtained by 16S/18S rRNA gene amplicon sequencing. The relative abundance is given at the Phylum level. All ASVs with abundances lower than 1% are grouped together and displayed as "< 1% abundance" in the two bar plots."NA" are ASVs that are not assigned at phylum level. **A** 16S dataset and **B** 18S dataset.

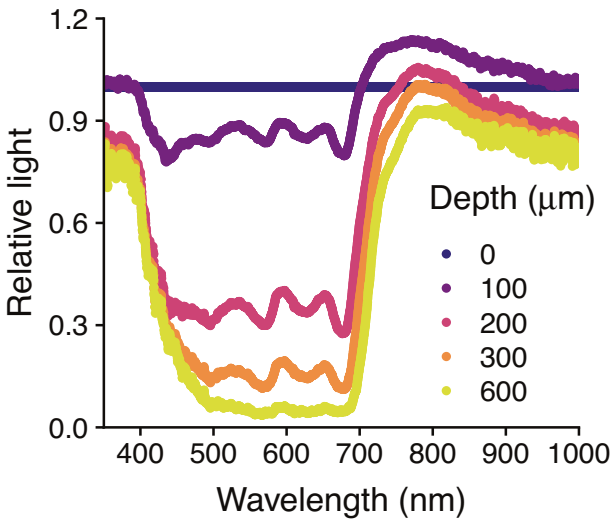

Fig. 3 The light relative to the photogranule surface, measured with a light microsensor, is plotted for five different depths. Surface illumination was approximately 250 µmol m^{-2} s^{-1}.

dense shell of both phototrophic and non-phototrophic organisms (stained by SYTO9) formed the outer 300–500 µm of the granule. Below this shell was a zone of radially aligned filamentous cyanobacteria followed by a dense and jumbled centre. Coccoid eukaryotic algae (Chl-a autofluorescence) were present in microcolonies throughout the photogranule (Fig. S4). Glycoconjugates (visualized by lectin staining) surrounded the filamentous cyanobacteria throughout the entire photogranule (Fig. S4D). Glycoconjugates indicate the excretion of extracellular polymeric substances (EPS) by phototrophic and non-phototrophic organisms and can contribute to the physical structure of the photogranule, serving as a "glue." The BAN lectin used in this study visualizes glycoconjugates with D-glucose and D-mannose monosaccharide building blocks.

Microbial community composition

The microbial community consisted of both phototrophic organisms, including motile filamentous cyanobacteria and eukaryotic algae, and non-phototrophic organisms (Fig. 2A). The 16S rRNA gene sequences were dominated by amplicon sequencing variants (ASV) attributed to phototrophic organisms from the phylum *Cyanobacteria* (37%) and non-phototrophic organisms from the class *Proteabacteria* (28%). The two most abundant ASV were the cyanobacteria *Leptolyngbya boryana* with 15% relative abundance and *Alkalinema pantanalense* with 13% relative abundance. The nitrifiers *Nitrosomonas* sp., *Nitrobacter* sp. and *Nitrospira* sp. made up about 2% of the prokaryotic community, while the aerobic chemoheterotrophs and denitrifiers *Thauera* sp. and *Zoogloea* sp. made up 15% relative abundance. Strict anaerobic prokaryotes from the Family *Anaerolineaceae* and *Caldilineaceae* together made up 5% of ASVs, suggesting that part of the photogranule was anoxic. This is indeed confirmed by microsensing in the following section. The 18S rRNA gene sequences were dominated by ASVs attributed to eukaryotic microalgae (58%), fungi (18%), and protists (2%) (Fig. 2B). The eukaryotic algae present were *Chlorella* sp. (39%), *Chlorococcum* sp. (13%), *Botryoshaerella* sp. (1%), and *Tetradesmus* sp. (1%). The fungi present was *Trichosporon* sp. (18%).

Light absorption

The photogranules effectively absorbed light across the visible light spectrum (Fig. 3). Within 600 µm depth 90% of the surface light was completely absorbed. There was an increase in scalar irradiance in the range of 700–800 nm especially at 100 and 200 µm depth when compared to the reference light intensity at 0 µm depth, suggesting fluorescence by photopigments, or high light scattering paired with little absorbance by pigments at these bandwidths [36, 37].

Photosynthesis and carbon fixation

The photogranules had a high capacity for both oxygen production by photosynthesis and oxygen consumption (Fig. 4A–C). In the presence of acetate, oxygen consumption surpassed oxygen production, leading to anoxia throughout the majority of the photogranule, even in the light. In the absence of acetate, the photogranule was saturated with oxygen throughout (Fig. 4A) and had a maximum oxygen production of 738 nmol-O_2 photogranule^{-1} h^{-1}, integrating the oxygen production rate with depth (Eq. 1). Although the oxygen concentration was lower in the presence of acetate, photosynthesis did not decrease, resulting in carbon fixation comparable to in the absence of acetate (Fig. 4E).

Downloaded from https://academic.oup.com/ismej/article/17/6/870/7474056 by guest on 24 May 2024

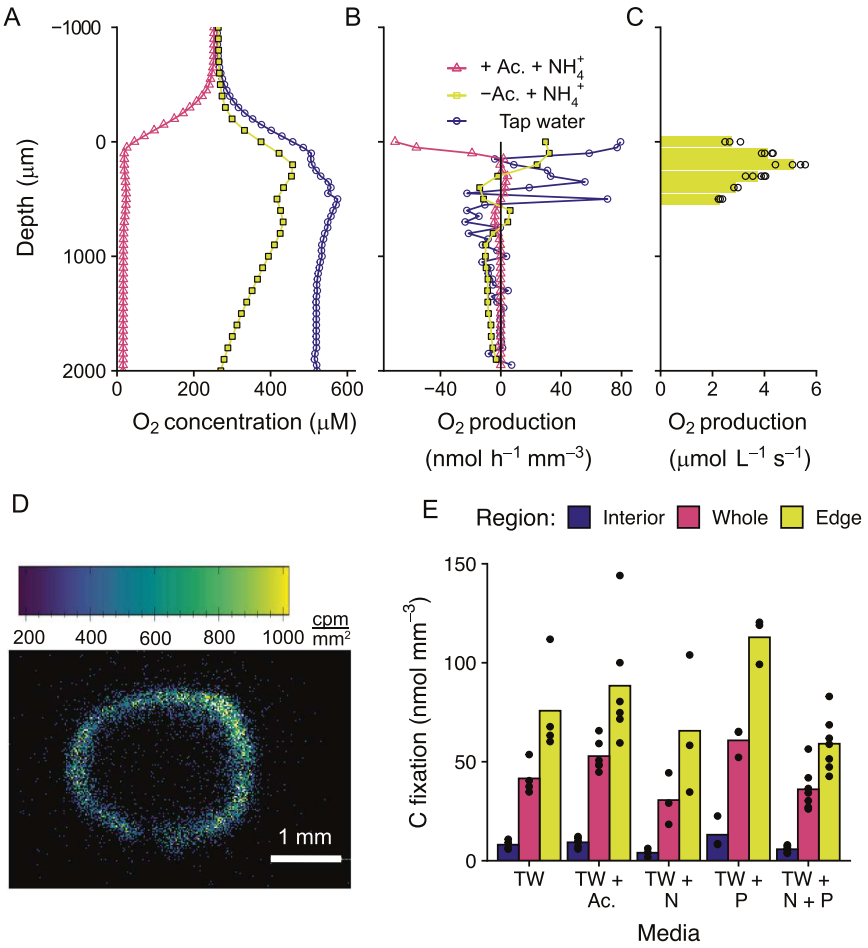

Fig. 4 Photosynthesis. A Oxygen profiles were measured in the same photogranule under three different conditions: untreated tap water (blue circles), growth media without acetate but with ammonium (yellow squares), and growth media with acetate and with ammonium (pink triangles). **B** The total oxygen production at each depth of the photogranule, calculated from the profiles in figure A, assuming a spherical aggregate 4 mm in diameter. **C** Instantaneous oxygen production, determined by the change in oxygen concentration after 5–8 s dark shift, at six different depths, in media with ammonium but no acetate. The bars represent the mean oxygen production of 3–4 measurements, and the open circles are each individual measurement. **D** A representative microradiograph image of the distribution of ^{14}C from carbon fixation in a photogranule (incubated with acetate). White scale bar is 1 mm. **E** Carbon fixation in photogranules incubated in the light in untreated tap water (TW), tap water amended with 3 mM acetate (TW + Ac.), with 8 mM NH_4^+ (TW + N), with 3 mM PO_4^{3-}, and with both 8 mM NH_4^+ and 3 mM PO_4^{3-}. Carbon fixation was measured by incubating photogranules with ^{14}C–CO_2 then determining ^{14}C fixation with a microradiograph. The carbon fixation was segregated by region, using activity to mark boundaries within the aggregate: the interior of the photogranule (blue), the entire photogranule (purple) and the outer edge of the photogranule (yellow). The black dots represent measurements of individual photogranules. These light-exposed incubations were carried out simultaneously to incubations in the dark, which are displayed in (**A**). The results from incubations with 3 mM and 10 mM bicarbonate were combined, since there was no substantial difference between groups.

This indicates that oxygen is rapidly, nearly instantaneously cycled in the photogranule and that during periods of acetate exposure, respiration is oxygen-limited, despite high oxygen production through photosynthesis. The interior of the photogranule is also likely light-limited, as light is rapidly attenuated within the photogranule (Fig. 3), and thus the majority of the light-driven carbon fixation in the photogranule occurs in the outer edges (Fig. 4D, E). Nevertheless, the highest photosynthesis rates were ~200 μm below the surface of the granule (Fig. 4C), consistent with the microscope images showing a higher density of photosynthetic bacteria slightly below the surface of the granule (Figs. S3 and S4). Considering a photogranule with a diameter of 4 mm, a maximum carbon fixation rate of 383 nmol-C photogranule^{-1} h^{-1} was calculated (Eq. 1).

Carbon fixation in the photogranule was insensitive to short-term changes in nutrient concentration (Fig. 4D). Carbon fixation was similar in all photogranules incubated in untreated tap water, in tap water with 3 mM acetate, in tap water with 8 mM ammonium, in tap water with 3 mM phosphate, as well as in tap water with both 8 mM ammonium and 3 mM phosphate. This indicates that the rate of carbon fixation, driven by photosynthesis, is constant over the entire light phase of the reactor batch cycle. However, the rate of aerobic respiration and other oxygen-consuming processes, such as nitrification, varies substantially, due to the variable carbon supply.

Nitrification/denitrification and carbon fixation

Autotrophic nitrification occurred largely in the outer edges (0–500 μm) of the photogranule in dark incubations with ^{14}C-labelled carbonate, with or without ammonium and the nitrification inhibitor ATU (Fig. 5B). Carbon fixation was highest in the incubations containing ammonium (0.9 nmol mm^{-3}) although there was still detectable carbon fixation in the incubations without ammonium and with ATU. The slightly higher level of

Downloaded from https://academic.oup.com/ismej/article/17/6/870/7474056 by guest on 24 May 2024

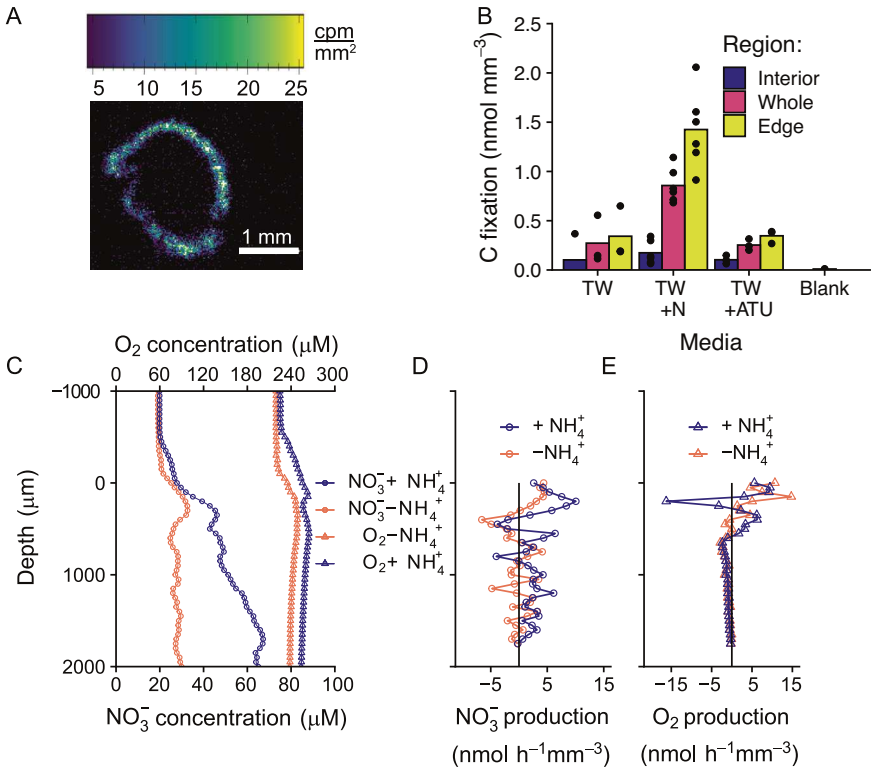

Fig. 5 Nitrogen cycling. A representative microradiograph image of the distribution of ^{14}C from carbon fixation in a photogranule incubated with 8 mM NH_4^+. **B** Carbon fixation in photogranules incubated in the dark in untreated tap water (TW), tap water amended with 8 mM NH_4^+ (TW + N), with 8 mM NH_4^+ and the nitrification inhibitor ATU (TW + ATU), and in photogranules killed with paraformaldehyde before tracer addition (Blank). Carbon fixation was measured by incubating photogranules with ^{14}C-bicarbonate then determining ^{14}C fixation by microradiography. The carbon fixation was segregated by region, using activity to mark boundaries within the aggregate: the interior of the photogranule (blue), the entire photogranule (orange) and the outer edge of the photogranule (yellow). **C** The average of three microprofiles of nitrate (circles) and oxygen (triangles) concentrations in the same photogranule incubated in the light first without NH_4^+ (orange) then with 100 μM NH_4^+ (blue) after reaching steady state. **D** Nitrate production at each depth calculated from the profiles in (**B**), in nmol h^{-1}, assuming a spherical photogranule with a radius of 1800 μm. Positive values indicate zones of production, while negative values indicate zones of consumption. **E** Instantaneous oxygen production, determined by the change in oxygen concentration after 5–8 s dark shift, at six different depths, in tap water with ammonium. The bars represent the mean oxygen production of 3–4 measurements, and the open triangles are each individual measurement.

carbon fixation (0.4 nmol mm^{-3}) in photogranules incubated in untreated tap water compared to the photogranules incubated with ATU (0.3 nmol mm^{-3}) suggests that the photogranules may have stored some residual ammonium or used the low concentrations of ammonium (<0.03 mg_{NH4} L^{-1} or <1.66 μmol L^{-1}) available in the tap water (Table S1). The higher level of carbon fixation in photogranules incubated with ATU compared to dead photogranules (Blank, 0.06 nmol mm^{-3}), indicates there is significant anaplerotic carbon fixation in the photogranule (0.2 nmol mm^{-3}).

Profiles of nitrate concentrations in the light and dark partially confirm the distribution of nitrification predicted by the dark carbon-fixation distribution (Fig. 5B, C). While the absolute concentration of nitrate peaks in the photogranule centre (Fig. 5B), the volumetric rate of nitrate production, calculated from the same profiles, had has two peaks at the outer edge, and a relatively steady production in the centre. These peaks corresponded to a dip in oxygen concentration, and a peak in oxygen consumption, observed in multiple other photogranules as well (Fig. 5C–E). Nitrate consumption peaked in between the nitrification peaks, rather than at the photogranule centre. Note that diffusive flux through a sphere is dependent on the radius of the sphere (Eq. 1) which changes with depth. Thus, a linear gradient does not indicate that the system is controlled by diffusion, as it would in a flat biofilm. To aid interpretation of the profiles, reference gradients controlled by diffusive flux through a sphere and plane are plotted together (Fig. S5). Summing up the nitrate production rates at each depth an overall nitrate production rate of 93.7 nmol photogranule^{-1} h^{-1} (with NH_4^+) and 25.1 nmol photogranule^{-1} h^{-1} (without NH_4^+) was observed, which corresponded well with ^{15}N-NH_4^+ incubations.

Nitrogen cycling in the photogranules was either oxygen or carbon-limited, depending on the incubation conditions (Fig. 6A, B). In the presence of acetate there was no nitrification when photogranules were incubated with ^{15}N-ammonium in the dark (Fig. 6A), due to an absence of oxygen. Some nitrification in the presence of acetate occurred in the light, as indicated by the production of ^{15}N-N_2 (black bar, Fig. 6A), although net nitrate was consumed from the background concentration of 10 μM (white bar, Fig. 6A). In the absence of acetate, nitrification was much higher, especially when incubated in the light (max. 150 nmol-N photogranule^{-1} h^{-1}) (Fig. 6B). Denitrification was also higher in the absence of acetate, although the photogranules were always oxic in the absence of acetate, and there should be little free organic carbon (Fig. 6A). This indicates that there is significant carbon recycling within the photogranules, and that denitrification is tolerant to oxygen. Nonetheless, denitrification was clearly carbon-limited or depressed by oxygen in the absence of acetate, as indicated by the much higher rate of denitrification in photogranules incubated with ^{15}N-nitrate in the dark, with acetate (max. 480 nmol-N photogranule^{-1} h^{-1}) (Fig. 6B).

Downloaded from https://academic.oup.com/ismej/article/17/6/870/7474056 by guest on 24 May 2024

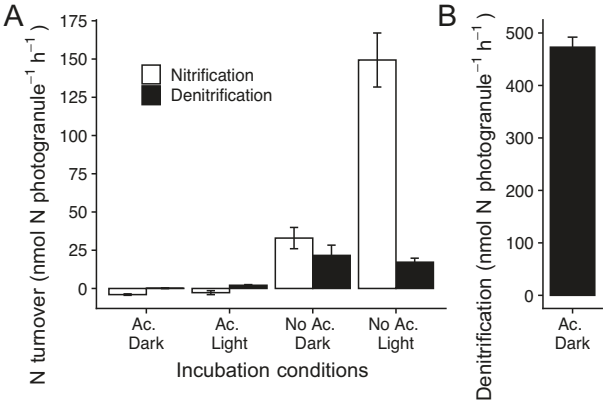

Fig. 6 Rates of N-cycling processes. A Nitrification (white bars) and denitrification (black bars) in photogranules incubated with 1 mM ^{15}N-labelled ammonium, either in the dark or the light, and with or without the addition of 3 mM acetate. Rates are a linear fit of the production of nitrate and nitrite or $^{15}N–N_2$ in 4 separate vials stopped at different points. Nitrification represents rate of production of extracellular nitrate and nitrite plus the production of $^{15}N–N_2$. Denitrification denotes the production of ^{15}N-N_2. Error bars indicate the standard error of the slope. **B** The rate of denitrification in photogranules incubated with $^{15}N–NO_3^-$ with acetate in the dark. The error bar represents the standard error of the slope.

DISCUSSION

Physical, biological, and structural features of photogranules

The stratification pattern in photogranules closely resembled that of photosynthetic microbial mats (Fig. 1). Motile filamentous cyanobacteria (e.g., *Alkalinema pantanalense*, *Leptolyngbya boryana*, *Cephalothrix komarekiana* and *Limnothrix* sp.) and excreted extracellular polymeric substances (EPS) generated a complex net of filaments that provided structural rigidity, similar to that observed in cyanobacterial mats [42, 43]. The proliferation of microbial communities within biofilms is dependent on the EPS matrix [44]. The lectin stain revealed that a large fraction of glycoconjugates in the EPS matrix was attributed to D-glucose and D-mannose. The glucose constituents were likely produced by filamentous cyanobacteria, as it is the dominant monosaccharide in the glycoconjugate fraction of their EPS matrix [23, 45, 46]. Both glucose- (especially α(1–4) glucans) and mannose-containing polysaccharides have been shown to play a key role in biofilm cohesion in both aerobic granules and phototrophic microbial mats [47, 48]. The lectin-specific BAN glycoconjugates reported show only a part of the total glycoconjugates present. Nevertheless, we anticipate that there are other types of glycoconjugates and matrix compounds present such as extracellular proteins and eDNA [49].

The importance of filamentous cyanobacteria in photogranule formation was highlighted previously [12, 19, 50]. It was proposed that initially, filamentous, and motile cyanobacteria form a nucleus of filaments (a bundle) that can harbour other organisms. As it grows this structure becomes more and more physically and biologically stratified and finally results in a photogranule, with a large diversity of microenvironments and associated microbial processes. In natural systems, as well as in photogranules, physical and biological stratification occurs according to the availability and gradients of light and nutrients [8]. Thus, while young and small photogranules (<0.5 mm) do not have a defined structure, photogranules grown to sizes of several millimetres show a clear stratification. Others have also observed microbial stratification in large (>2.5 mm) photogranules, with cyanobacteria forming a layer close to the surface [19]. In our study we found that independent of photogranule size, the filamentous cyanobacteria were present throughout the whole photogranule. However, they showed different arrangements of the filaments from surface to centre. While the cyanobacterial filaments were densely packed and jumbled at the surface and centre, in the area in between they aligned themselves radially. One explanation for this phenomenon is the competition for space within the photogranule, as radially arranging the filaments would facilitate movement between regions with higher exposure to light (phototaxis) and higher levels of other substrates (chemotaxis) [43]. This would be especially useful to "pierce" through the thick shell of non-phototrophic organisms in the first 500 µm of the photogranule, the region with the highest light availability. Such radial movement was previously observed in biogranules derived from subcultures of microbial mats composed of cyanobacteria (*Cephalotrix* sp. formerly known as *Phormidium* sp.) diatoms and heterotrophic bacteria originating from the North Sea [3]. Their movement was shown to be triggered by light and substrates.

Functional stratification in photogranules

The photogranules also exhibited a functional stratification similar to phototrophic biofilms in nature. The photogranule surface was exposed to the highest light and substrate levels and supported the highest photosynthetic and nitrifying activities. In the presence of acetate, the photogranule harboured anoxic zones that allowed anaerobic processes such as denitrification to occur. Most of the microbial activity was concentrated in the outer 500 µm of the photogranule. In that region phototrophs (cyanobacteria and eukaryotic algae) attenuated about 90% of all incoming light and showed the highest photosynthetic activity at around 400–500 µm (max. 100 nmol/h).

In addition, to the high concentration of cyanobacteria in the outer part of the photogranule, there was also a large population of non-phototrophic organisms, including nitrifiers (*Nitrosomonas* sp., *Nitrobacter* sp. and *Nitrospira* sp.) and chemoheterotrophic bacteria/denitrifiers (*Thauera* sp. and *Zoogloea* sp.). This high microbial density supported high oxygen production/consumption and nitrate production, as well as carbon fixation (Figs. 4 and 5). However, the ^{14}C incubations may underestimate the nitrification activity as they were performed in the dark (in the light carbon fixation by photosynthesis would be orders of magnitude higher than by nitrification, Figs. 4E, 5B) and nitrification was much higher in the light (Fig. 6). Nitrate profiles within the granules did indicate nitrification within the centre of the granule, although the highest rates were confined to the outer edge (peak ~200 µm) of the granule (Fig. 5D), which is slightly closer to the surface than in similar-sized cryoconites (peak ~400 µm) [5]. Similarly, the oxygen profiles in the absence of acetate but presence of ammonium also indicate some nitrification (i.e., oxygen consumption) in the centre of the granules, although again the highest rates were at the outer portion of the granule (Figs. 4B and 5D). Nevertheless, the nitrate accumulation observed in the profile (Fig. 5C) was not caused by increased nitrification rates at lower depth but mostly due to the reducing rate of nitrate consumption towards the centre. The peak in nitrification just below the surface also aligns with a model of photogranules grown without DOC, but the same level of ammonium as in this study. Given that DOC is rapidly consumed in the bulk liquid, of the scenarios modelled, this scenario most closely fits our data [21].

Although the centre of the photogranule seemed to be relatively inactive, it may serve important functions. These could include substrate storage (e.g., as lipids, starch or EPS), fermentative processes, or decomposition of dead organic constituents, which all contribute to internal nutrient cycling in the photogranule. The centre has a lower oxygen concentration and may shelter less oxygen-tolerant microbes. Anaerobic prokaryotes such as *Anaerolineaceae* and *Caldilineaceae* and the fungi *Trichosporon* sp. found in the photogranule can ferment carbohydrates and mineralize organic phosphorus and nitrogen, comprised in EPS or necrotic biomass, to H_2, alcohols (e.g., butanol, ethanol), ketones (e.g., acetone), PO_4^{3-}, and NH_4^-, which in turn can be reused

Downloaded from https://academic.oup.com/ismej/article/17/6/870/7474056 by guest on 24 May 2024

within the photogranule [51–53]. Cyanobacteria are also adapted to anoxic conditions and can ferment six-carbon sugars (e.g., glucose) to e.g., lactate or ethanol [54]. Such internal nutrient cycling likely increases in significance the larger the photogranule becomes and may fuel metabolic processes despite external substrate limitation.

Nutrient removal and microbial activity during a sequencing batch cycle

The photosynthetic activity of the photogranule was insensitive to the short-term nutrient fluctuations typical of the wastewater batch process, although other microbial activities were substantially impacted. Combining our results with data collected from the wastewater reactor allowed us to build a timeline of the shifting nutrient limitations and metabolic processes that occurred over the course of a batch cycle (Fig. S9). At the beginning of a batch, nutrients such as ammonium (NH_4^+), phosphate (PO_4^{3-}), and acetate were available in high concentrations. In this phase, the photogranules could maintain high photosynthetic and heterotrophic activities, resulting in ammonium, phosphate, acetate, carbon dioxide, and oxygen consumption, and oxygen production. Only limited nitrification occurred during this phase, due to the low oxygen concentrations generated by aerobic respiration of acetate. Rapid growth of microorganisms during this phase fuelled ammonium and phosphorous uptake. As acetate concentrations decreased and oxygen concentrations increased, nitrification and subsequently denitrification kicked off. In the dark phase, the phototrophs switched from photosynthesis to respiration on internally stored photosynthates. Nitrification continued until all ammonium was converted to nitrate, even though nitrifiers made up only 2% of the total community. Since all acetate was already consumed, denitrification was fuelled by intracellularly stored carbon (e.g., as polyhydroxyalkanoates) [55] or internally recycled carbon by decomposition of organic matter [56] but was not able to completely remove all nitrate, due to carbon limitation.

The ^{15}N incubations showed that denitrification can also occur under oxic conditions. Thus, denitrification was likely performed in part by the aerobic denitrifier *Thauera* sp. [57]. Further, the incubations showed that even in the absence of acetate the internally cycled organic carbon (e.g., organic carbon from phototrophs, or internally stored and recycled carbon) can sustain denitrification (Fig. 6A). Compared to the maximum denitrification rate with addition of acetate in the dark, the denitrification rate sustained on internally cycled carbon was about 25x lower (Fig. 6B). Nevertheless, these rates were sufficient to keep removing nitrogen from the bioreactor in the dark period.

From ecology to application

The fundamental knowledge of how photogranules are structured and function will allow engineers to replicate this novel ecosystem for wastewater treatment. In our study we investigated an active phototrophic, nitrifying, and denitrifying community that exhibited high nitrogen and carbon removal/conversion rates and showed internally linked processes (exchange of oxygen, nitrogen, and carbon dioxide).

Introducing a phototrophic community to the wastewater treatment process will ultimately allow closure of the CO_2 and oxygen cycles of the conventional activated sludge process. Oxygen would be produced through photosynthesis and CO_2 by the heterotrophic conversion of organic matter, making an external supply of oxygen unnecessary. The oxygen production and consumption in the aggregate was calculated to be 13.6 mmol L^{-1} d^{-1} and 13.1 mmol L^{-1} d^{-1}, respectively (Equation S1–S4), resulting in a net oxygen production. The oxygen produced by photosynthesis is quickly used by consumption processes, demonstrating closely coupled processes in the aggregate. In the beginning of the batch cycle when acetate was still present, the photogranule was oxygen limited, i.e., photosynthesis could not supply heterotrophic respiration and nitrification with sufficient oxygen to achieve maximal rates (Fig. 4A). This was also apparent from the hourly oxygen production rate of 1.1 mmol L^{-1} h^{-1} and oxygen consumption rate of 1.4 mmol L^{-1} h^{-1} in the first 4 h of the cycle (considering full removal of acetate after 4 h into the cycle and high nitrification activity). After acetate was fully consumed, photosynthesis would likely become carbon limited without external CO_2 supply. To optimize oxygen demand versus oxygen production in a system without external oxygen or CO_2 supply, the light supply and specific acetate load could be altered. This will be especially important when wastewater characteristics (N, P, COD) or light conditions change.

As stated before, most activity was in the edge (outer 500 µm) of the photogranule due to light penetration and nutrient diffusion limitation. The photogranules (2–4 mm) investigated in this study thereby contained a considerable relatively inactive zone, which reduced the overall conversion rate of an individual photogranule. Smaller sizes would optimize the conversion rate per individual photogranule and could consequently increase the maximal conversion rate of a photogranule treatment system. In previous studies, an ideal granule size was determined to be 1.25–1.5 mm for aerobic granules [58, 59] and 0.5–1.7 mm for photogranules [19]. While the light and carbon load of the system influence photogranule size, the solid retention time (SRT) ultimately controls the size of photogranules as it provides an upper ceiling to the age of a photogranule. A shorter SRT would result in smaller granules and higher photogranule-specific conversion rates but might be detrimental for some slow growing organisms (e.g. nitrifiers) and compromise settleability of the photogranule if granule sizes become too small (<0.5 mm) [60]. Therefore, granule size must be carefully evaluated with all these different aspects in mind.

Finally, our results indicate the need to change the operating conditions of the reactor to further increase nitrification rates. Nitrification was strongly controlled by the availability of oxygen, where rates were 3–4 times higher in the light than in the dark (Fig. 6A). In the presence of acetate, nitrification is expected to be completely inhibited, as the entire photogranule was anoxic under this condition. Nevertheless, during reactor operation, photogranules always completely removed ammonium from the supernatant, both when the batch started with a light cycle and when it started with a dark cycle. Since acetate consumption takes ~4 h (Fig. S8) the conditions for optimal nitrification would only be available for ~2 h in a cycle starting with a light phase. In contrast, in a cycle starting with a dark phase that consumes all acetate, nitrification would be optimized for a full 6 h. This indicates that there is substantial unused nitrification capacity in the cycle starting with a dark phase. An additional, partial exchange of the reactor liquid could be supported at this time, to increase reactor activity. This would also allow for the denitrification of more of the converted nitrate, which is otherwise carbon-limited, as most nitrate is produced after the removal of the acetate (Figs. 6B, S8). Another option would be to pulse an external carbon source (e.g., methanol, acetate, or molasses) to promote carbon-limited denitrification, which is a common practice in conventional wastewater treatment plants [61].

CONCLUSIONS

Photogranules contain complete ecosystems in only a few cubic millimetres. A scaffold of motile filamentous cyanobacteria and EPS supports a diverse array of phototrophs and heterotrophs capable of nitrification, denitrification, photosynthesis, aerobic respiration, and phosphate uptake. This diverse community internally cycles at least three nutrients important in wastewater treatment: oxygen, nitrogen, and carbon. Oxygen from

Downloaded from https://academic.oup.com/ismej/article/17/6/870/7474056 by guest on 24 May 2024

photosynthesis is immediately consumed by aerobic respiration and nitrification in the presence of acetate or ammonium, respectively. Nitrifiers convert ammonium to nitrate and nitrite, which is subsequently rapidly denitrified. Organic carbon fixed through photosynthesis is used to fuel denitrification after acetate is depleted. Conditions within the photogranule vary dramatically over time, from completely anoxic to oxygen concentrations three times above saturation, with even larger variation in nitrate and organic carbon availability. Nevertheless, photogranules maintain high, robust activity levels, supported by a dense network of interconnected cells that exchange nutrients. This dense network and nutrient exchange allow for denitrification in the absence of external organic carbon, small amounts of nitrification without the provision of external ammonium, and nitrification under nearly anoxic conditions. Photogranules thus offer an opportunity to utilize the sun's energy to clean wastewater and decrease the energy requirement of conventional wastewater treatment, by reducing or eliminating the need to aerate treatment reactors.

DATA AVAILABILITY

The raw 16S and 18S rRNA gene sequence data is available in the EBI database under project number PRJEB54633. The other data that support the findings of this study are available from the corresponding author upon reasonable request.

REFERENCES

1. Beeftink HH, van den Heuvel JC. Novel anaerobic gas-lift reactor (AGLR) with retention of biomass: Start-up routine and establishment of hold up. Biotechnol Bioeng. 1987;30:233–8.
2. de Beer D, van den Heuvel JC, Ottengraf SPP. Microelectrode measurements of the activity distribution in nitrifying bacterial aggregates. Appl Environ Microbiol. 1993;59:573–9.
3. Brehm U, Krumbein WE, Palińska KA. Microbial spheres: a novel cyanobacterial–diatom symbiosis. Naturwissenschaften. 2003;90:136–40.
4. Langford H, Hodson A, Banwart S, Bøggild C. The microstructure and biogeochemistry of Arctic cryoconite granules. Ann Glaciol. 2010;51:87–94.
5. Segawa T, Takeuchi N, Mori H, Rathnayake RMLD, Li Z, Akiyoshi A, et al. Redox stratification within cryoconite granules influences the nitrogen cycle on glaciers. FEMS Microbiol Ecol. 2020;96:1–13.
6. Wilbanks EG, Salman-Carvalho V, Jaekel U, Humphrey PT, Eisen JA, Buckley DH, et al. The Green Berry Consortia of the Sippewissett Salt Marsh: millimeter-sized aggregates of diazotrophic unicellular cyanobacteria. Front Microbiol. 2017;8:1623.
7. Wilbanks EG, Jaekel U, Salman V, Humphrey PT, Eisen JA, Facciotti MT, et al. Microscale sulfur cycling in the phototrophic pink berry consortia of the Sippewissett Salt Marsh. Environ Microbiol. 2014;16:3398–415.
8. Wolf G, Picioreanu C, van Loosdrecht MCM. Kinetic modeling of phototrophic biofilms: The PHOBIA model. Biotechnol Bioeng. 2007;97:1064–79.
9. Flemming HC, Wingender J, Szewzyk U, Steinberg P, Rice SA, Kjelleberg S. Biofilms: an emergent form of bacterial life. Nat Rev Microbiol. 2016;14:563–75.
10. Ataeian M, Liu Y, Kouris A, Hawley AK, Strous M. Ecological interactions of cyanobacteria and heterotrophs enhances the robustness of cyanobacterial consortium for carbon sequestration. Front Microbiol. 2022;13:780346.
11. Abouhend AS, McNair A, Kuo-Dahab WC, Watt C, Butler CS, Milferstedt K, et al. The oxygenic photogranule process for aeration-free wastewater treatment. Environ Sci Technol. 2018;52:3503–11.
12. Trebuch LM, Oyserman BO, Janssen M, Wijffels RH, Vet LEM, Fernandes TV. Impact of hydraulic retention time on community assembly and function of photogranules for wastewater treatment. Water Res. 2020;173:115506.
13. Zhang M, Ji B, Liu Y. Microalgal-bacterial granular sludge process: a game changer of future municipal wastewater treatment? Sci Total Environ. 2021;752:141957.
14. Gikonyo JG, Ansari AA, Abouhend AS, Tobiason JE, Park C. Hydrodynamic granulation of oxygenic photogranules. Environ Sci Water Res Technol. 2021;7:427–40.
15. Ansari AA, Abouhend AS, Park C. Effects of seeding density on photogranulation and the start-up of the oxygenic photogranule process for aeration-free wastewater treatment. Algal Res. 2019;40:101495.
16. Ji B, Zhang M, Wang L, Wang S, Liu Y. Removal mechanisms of phosphorus in non-aerated microalgal-bacterial granular sludge process. Bioresour Technol. 2020;312:123531.
17. Ji B, Zhu L, Wang S, Liu Y. Temperature-effect on the performance of non-aerated microalgal-bacterial granular sludge process in municipal wastewater treatment. J Environ Manag. 2021;282:111955.
18. Ouazaite H, Milferstedt K, Hamelin J, Desmond-Le Quéméner E. Mapping the biological activities of filamentous oxygenic photogranules. Biotechnol Bioeng. 2021;118:601–11.
19. Abouhend AS, Milferstedt K, Hamelin J, Ansari AA, Butler C, Carbajal-González BI, et al. Growth progression of oxygenic photogranules and its impact on bioactivity for aeration-free wastewater treatment. Environ Sci Technol. 2020;54:486–96.
20. Meng F, Xi L, Liu D, Huang WW, Lei Z, Zhang Z, et al. Effects of light intensity on oxygen distribution, lipid production and biological community of algal-bacterial granules in photo-sequencing batch reactors. Bioresour Technol. 2019;272:473–81.
21. Tenore A, Mattei MR, Frunzo L. Multiscale modelling of oxygenic photogranules. arXiv preprint arXiv:2104.12273. 2021.
22. Staudt C, Horn H, Hempel DC, Neu TR. Volumetric measurements of bacterial cells and extracellular polymeric substance glycoconjugates in biofilms. Biotechnol Bioeng. 2004;88:585–92.
23. Zippel B, Neu TR. Characterization of glycoconjugates of extracellular polymeric substances in tufa-associated biofilms by using fluorescence lectin-binding analysis. Appl Environ Microbiol. 2011;77:505–16.
24. Singh DD, Saikrishnan K, Kumar P, Surolia A, Sekar K, Vijayan M. Unusual sugar specificity of banana lectin from *Musa paradisiaca* and its probable evolutionary origin. Crystallographic and modelling studies. Glycobiology. 2005;15:1025–32.
25. Neu TR, Woelfl S, Lawrence JR. Three-dimensional differentiation of photoautotrophic biofilm constituents by multi-channel laser scanning microscopy (single-photon and two-photon excitation). J Microbiol Methods. 2004;56:161–72.
26. Lawrence J, Neu T, Swerhone GD. Application of multiple parameter imaging for the quantification of algal, bacterial and exopolymer components of microbial biofilms. J Microbiol Methods. 1998;32:253–61.
27. Schindelin J, Arganda-Carreras I, Frise E, Kaynig V, Longair M, Pietzsch T, et al. Fiji: an open-source platform for biological-image analysis. Nat Methods. 2012;9:676–82.
28. Herlemann DPR, Labrenz M, Jürgens K, Bertilsson S, Waniek JJ, Andersson AF. Transitions in bacterial communities along the 2000 km salinity gradient of the Baltic Sea. ISME J. 2011;5:1571–9.
29. Hugerth LW, Muller EEL, Hu YOO, Lebrun LAM, Roume H, Lundin D, et al. Systematic design of 18S rRNA gene primers for determining eukaryotic diversity in microbial consortia. PLoS One. 2014;9:e95567.
30. Martin M. Cutadapt removes adapter sequences from high-throughput sequencing reads. EMBnet J. 2011;17:10.
31. Callahan BJ, McMurdie PJ, Rosen MJ, Han AW, Johnson AJA, Holmes SP. DADA2: High-resolution sample inference from Illumina amplicon data. Nat Methods. 2016;13:581–3.
32. Paulson JN, Stine OC, Bravo HC, Pop M, Colin Stine O, Bravo HC, et al. Differential abundance analysis for microbial marker-gene surveys. Nature Methods. 2013;10:1200–1202. https://doi.org/10.1038/nmeth.2658.
33. McMurdie PJ, Holmes S. phyloseq: an R package for reproducible interactive analysis and graphics of microbiome census data. PLoS ONE. 2013;8:e61217.
34. Revsbech NP. An oxygen microsensor with a guard cathode. Limnol Oceanogr. 1989;34:474–8.
35. de Beer D, Schramm A, Santegoeds CM, Kuhl M. A nitrite microsensor for profiling environmental biofilms. Appl Environ Microbiol. 1997;63:973–7.
36. Lassen C, Ploug H, JÃ¸rgensen BB. A fibre-optic scalar irradiance microsensor: application for spectral light measurements in sediments. FEMS Microbiol Lett. 1992;86:247–54.
37. Kühl M, Jørgensen BB. Spectral light measurements in microbenthic phototrophic communities with a fiber-optic microprobe coupled to a sensitive diode array detector. Limnol Oceanogr. 1992;37:1813–23.
38. Picioreanu C, van Loosdrecht MCM, Heijnen JJ. Modelling the effect of oxygen concentration on nitrite accumulation in a biofilm airlift suspension reactor. Water Sci Technol. 1997;36:147–56.
39. Kreft J-U, Picioreanu C, van Loosdrecht MCM, Wimpenny JWT. Individual-based modelling of biofilms. Microbiology. 2001;147:2897–912.
40. Holtappels M, Lavik G, Jensen MM, Kuypers MMM. 15N-Labeling experiments to dissect the contributions of heterotrophic denitrification and anammox to nitrogen removal in the OMZ waters of the ocean. In: Klotz MG, Methods in enzymology. 1st ed. 2011. Cambridge, Massachusetts, USA: Academic Press; 2011. p. 223–51.
41. Braman RS, Hendrix SA. Nanogram nitrite and nitrate determination in environmental and biological materials by vanadium(III) reduction with chemiluminescence detection. Anal Chem. 1989;61:2715–8.
42. Tamulonis C, Kaandorp J. A model of filamentous cyanobacteria leading to reticulate pattern formation. Life. 2014;4:433–56.
43. Stal LJ. Physiological ecology of cyanobacteria in microbial mats and other communities. N. Phytol. 1995;131:1–32.
44. Wingender J, Neu TR, Flemming H-C. Microbial extracellular polymeric substances. Berlin, Heidelberg:Springer Berlin Heidelberg; 1999.

Downloaded from https://academic.oup.com/ismej/article/17/6/870/7474056 by guest on 24 May 2024

45. Li P, Harding SE, Liu Z. Cyanobacterial exopolysaccharides: their nature and potential biotechnological applications. Biotechnol Genet Eng Rev. 2001;18:375–404.
46. Nicolaus B, Panico A, Lama L, Romano I, Manca MC, De Giulio A, et al. Chemical composition and production of exopolysaccharides from representative members of heterocystous and non-heterocystous cyanobacteria. Phytochemistry. 1999;52:639–47.
47. McSwain BS, Irvine RL, Hausner M, Wilderer PA. Composition and distribution of extracellular polymeric substances in aerobic flocs and granular sludge. Appl Environ Microbiol. 2005;71:1051–7.
48. Rossi F, De Philippis R. Role of cyanobacterial exopolysaccharides in phototrophic biofilms and in complex microbial mats. Life. 2015;5:1218–38.
49. Neu TR, Lawrence JR. The extracellular matrix - an intractable part of biofilm systems. In: Flemming H-C, Neu TR, Wingender J, editors. The perfect slime: microbial extracellular polymeric substances (EPS). London, England: IWA Publishing; 2017.
50. Milferstedt K, Kuo-Dahab WC, Butler CS, Hamelin J, Abouhend AS, Stauch-White K, et al. The importance of filamentous cyanobacteria in the development of oxygenic photogranules. Sci Rep. 2017;7:17944.
51. Middelhoven WJ. Trichosporon wieringae sp.nov., an anamorphic basidiomycetous yeast from soil, and assimilation of some phenolic compounds, polysaccharides and other non-conventional carbon sources by saprophytic Trichosporon species. Antonie Van Leeuwenhoek. 2004;86:329–37.
52. Yamada T, Sekiguchi Y, Hanada S, Imachi H, Ohashi A, Harada H, et al. Anaerolinea thermolimosa sp. nov., Levilinea saccharolytica gen. nov., sp. nov. and Leptolinea tardivitalis gen. nov., sp. nov., novel filamentous anaerobes, and description of the new classes Anaerolineae classis nov. and Caldilineae classis nov. in the. Int J Syst Evol Microbiol. 2006;56:1331–40.
53. Zhang B, Xu X, Zhu L. Structure and function of the microbial consortia of activated sludge in typical municipal wastewater treatment plants in winter. Sci Rep. 2017;7:17930.
54. Stal L. Fermentation in cyanobacteria. FEMS Microbiol Rev. 1997;21:179–211.
55. Alzate Marin JC, Caravelli AH, Zaritzky NE. Nitrification and aerobic denitrification in anoxic-aerobic sequencing batch reactor. Bioresour Technol. 2016;200:380–7.
56. Nielsen LP, Sloth NP. Denitrification, nitrification and nitrogen assimilation in photosynthetic microbial mats. In: Microbial mats. Berlin, Heidelberg: Springer Berlin Heidelberg; 1994. p. 319–24.
57. Wang Q, He J. Complete nitrogen removal via simultaneous nitrification and denitrification by a novel phosphate accumulating Thauera sp. strain SND5. Water Res. 2020;185:116300.
58. de Kreuk MK, Heijnen JJ, van Loosdrecht MCM. Simultaneous COD, nitrogen, and phosphate removal by aerobic granular sludge. Biotechnol Bioeng. 2005;90:761–9.
59. Baeten JE, van Loosdrecht MCM, Volcke EIP. Modelling aerobic granular sludge reactors through apparent half-saturation coefficients. Water Res. 2018;146:134–45.
60. Bradley IM, Sevillano-Rivera MC, Pinto AJ, Guest JS. Impact of solids residence time on community structure and nutrient dynamics of mixed phototrophic wastewater treatment systems. Water Res. 2019;150:271–82.
61. Monteith HD, Bridle TR, Sutton PM. Industrial waste carbon sources for biological denitrification. In: Jenkins SH, editor. Water pollution research and development. Oxford, England: Pergamon Press; 1981. p. 127–41.

ACKNOWLEDGEMENTS

The authors would like to thank Ute Kuhlicke from UFZ Magdeburg for her excellent support with confocal laser scanning microscopy, the technicians of the microsensor group at the MPI in Bremen for their help and the production of microsensors, and Elisa Merz for her help with ^{15}N incubation measurements. This research was supported by the Dutch Technology Foundation (STW) under the grant number STW-15424.

AUTHOR CONTRIBUTIONS

LMT: Conceptualization, methodology, investigation, formal analysis, writing - original draft; OMB: Conceptualization, methodology, investigation, formal analysis, writing- original draft; SMFV: Methodology, investigation; TRN: Methodology, investigation, writing- review & editing; MJ: Supervision, conceptualization, writing- review & editing; DB: Conceptualization, methodology, investigation, writing- review & editing; RHW: Supervision, writing- review & editing; LMV: Supervision, funding acquisition, Writing- Review & Editing; TVF: Supervision, conceptualization, funding acquisition, writing- review & editing

COMPETING INTERESTS

The authors declare no competing interests.

ADDITIONAL INFORMATION

Supplementary information The online version contains supplementary material available at https://doi.org/10.1038/s41396-023-01394-0.

Correspondence and requests for materials should be addressed to Lukas M. Trebuch.

Reprints and permission information is available at http://www.nature.com/reprints

Publisher's note Springer Nature remains neutral with regard to jurisdictional claims in published maps and institutional affiliations.

Open Access This article is licensed under a Creative Commons Attribution 4.0 International License, which permits use, sharing, adaptation, distribution and reproduction in any medium or format, as long as you give appropriate credit to the original author(s) and the source, provide a link to the Creative Commons license, and indicate if changes were made. The images or other third party material in this article are included in the article's Creative Commons license, unless indicated otherwise in a credit line to the material. If material is not included in the article's Creative Commons license and your intended use is not permitted by statutory regulation or exceeds the permitted use, you will need to obtain permission directly from the copyright holder. To view a copy of this license, visit http://creativecommons.org/licenses/by/4.0/.

© The Author(s) 2023

Downloaded from https://academic.oup.com/ismej/article/17/6/870/7474056 by guest on 24 May 2024

Discussion

The impact of electron acceptor variation on respiration

This thesis supports the emerging notion that carbon remineralization in dynamic environments is loosely rather than strictly thermodynamically sorted (Chen *et al.*, 2017). In the Wadden Sea, for example, while oxygen greatly decreases denitrification, it does not completely inhibit it (Gao *et al.*, 2010; Marchant *et al.*, 2017); while nitrate somewhat decreases sulfate reduction rates, it does not completely inhibit it (**Manuscript 1,** (Laverman *et al.*, 2012)); and sulfate and iron reduction occur simultaneously (**Manuscript 2**). In wastewater photogranules, oxygen similarly did not completely inhibit denitrification (**Manuscript 4**). Under the strict sorting observed in other environments, microbial carbon degradation proceeds using the most electronegative acceptor available (Richards *et al.*, 1965; Fenchel and Jørgensen, 1977). Strict sorting would allow microbes to conserve the most energy thermodynamically possible during the breakdown of organic carbon (Richards *et al.*, 1965; Fenchel and Jørgensen, 1977). This sorting is naturally complicated by the kinetics of biological reactions, as the cellular machinery of different processes is more or less efficient, or faster or slower. Inhibitors and metabolic warfare may further complicate such sorting, as does high variability, as investigated in this thesis. In regularly varying environments like the intertidal sediments and batch reactor photogranules tested in this thesis, the most electronegative acceptor available may change multiple times a day ((Jansen *et al.*, 2009), **Manuscript 4**). This frequent switching appears to select for a community that maintains some residual reduction of less electronegative acceptors in the presence of more favorable acceptors((Chen *et al.*, 2017), **Manuscripts 1 & 4, Figure 1**). This residual reduction of less electronegative acceptors produces reduced products that can fed into the reduction of more electronegative acceptors, creating a metabolic "braid"(Chen *et al.*, 2017). It also selects for flexible microbes, for example sulfate reducers capable of DNRA and able to begin sulfate reduction immediately upon anoxia (**Manuscript 1 & 2, Figure 1**) and the rapid increase in DNRA and denitrification upon anoxia (**Manuscript 3**). Nonetheless, there is still a large degree of sorting. Even in the variable sediments we tested from the Wadden Sea, for example, sulfate reduction was completely inhibited by oxygen, although it swiftly recovered upon anoxia (**Manuscripts 2 & 3**).

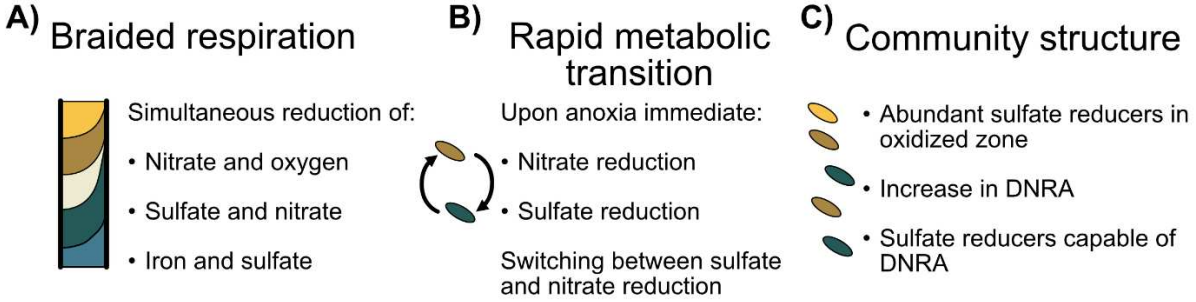

Figure 1: Long-term impacts of redox fluctuation in permeable sediments of the Wadden Sea. Over the long term, redox fluctuation supports a microbial community that performs braided metabolism, with the simultaneous respiration of nitrate and oxygen, sulfate and nitrate, and iron and sulfate. It also selects for a community that can rapidly adapt to changes in electron acceptor availability, such as sulfate reducers performing DNRA, and the immediate initiation of nitrate and sulfate reduction upon anoxia. Finally, it also impacts community structure, with redox fluctuation increasing DNRA (Manuscript 1) and preserving sulfate reducers in the oxidized zone, as well as sulfate reducers capable of using other electron acceptors, such as nitrate.

This thesis also found that reactive oxygen species substantially impact rates of microbial metabolism in Wadden Sea sediments, and that there are large concentrations of hydrogen peroxide in these sediments. ROS are rapidly formed when reduced substances like iron II, H_2S, Mn II, and reduced organic matter come into contact with oxygen (Yu and Kuzyakov, 2021) and alternating oxic-anoxic conditions can result in cyclical bursts of ROS (Zhao *et al.*, 2022, 2023). ROS have the potential to directly damage microbes, degrade and alter organic matter, and transform the chemical species a microbe might interact with (Trusiak *et al.*, 2018; Ma *et al.*, 2019; Dong *et al.*, 2023). In the presence of soluble and solid iron II, present in abundance in sediments, hydrogen peroxide can kick off pseudo-Fenton cycling, producing highly reactive hydroxyl radicals that can directly remineralize organic carbon (Trusiak *et al.*, 2018; Yu and Kuzyakov, 2021). We found that enzymatically removing ROS increased rates of aerobic respiration, hydrogen accumulation, iron reduction, and sulfate reduction, but not nitrate reduction (**Manuscripts 2 & 3**). We hypothesized that this was due to ROS remineralizing organic substrates, decreasing the availability of electron donor used to fuel respiration. This hypothesis is supported by initial experiments testing rates of the extracellular hydrolysis of 4-Methylumbelliferyl α-D-Glucopyranosid, a fluorescently labeled substrate of alpha-glucosidases, in syringe cores of sediment from the sandflat Engelsmanplaat in the Dutch Wadden Sea (**Figure 2**). Rates of hydrolysis were higher in the presence of ROS, suggesting that ROS may have been directly hydrolyzing the Methylumbelliferyl α-D-Glucopyranosi This would be consistent with the work of other researchers, who found that hydroxyl radicals directly mineralize carbon in soils (Trusiak *et al.*, 2018). It is crucial to determine the type of products of this so far hypothetical hydrolysis by ROS to clarify its impact on microbial respiration rates. For example, if the products were bioavailable monomers or oligomers rather than CO_2 or unavailable compounds, ROS would actually stimulate biodegradation, despite also directly inhibiting microbial processes by acting on the cellular machinery of e.g. the fermenters. Could ROS make organic polymers more bioavailable or does inhibition of microbes prevail? Tracking the carbon pool over an oxic-anoxic cycle with abiotic controls, as well as incubations with organic carbon amendments are necessary.

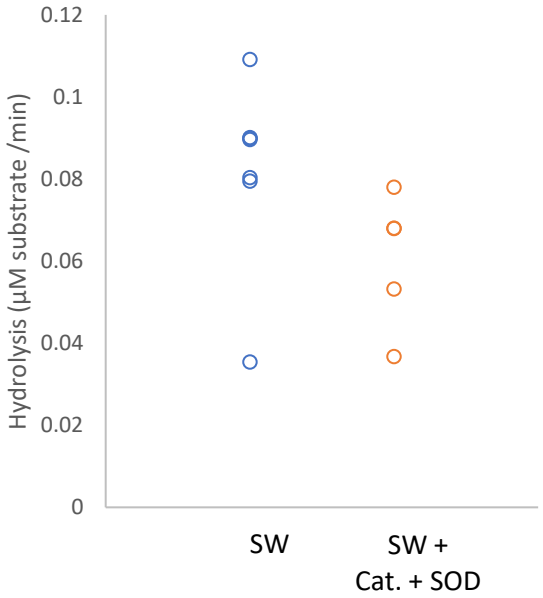

Figure 2 alpha-glucosidase activity: The rate of hydrolysis of 4-Methylumbelliferyl α-D-Glucopyranosid, a fluorescently labeled substrate of alpha-glucosidases, in syringe cores of sandy sediment, provided alone in seawater (blue circles) or alongside catalase and superoxide dismutase.

Curiously, this thesis also found that while oxygen did inhibit sulfate reduction, oxygenation boosted rates of sulfate reduction but not nitrate reduction in the subsequent anoxic period (**Manuscript 3**). As sulfate reduction is generally inhibited by oxygen, we had expected that the opposite would occur. We hypothesize that this increase in sulfate is due to aerobic carbon hydrolysis increasing bioavailabile monomers and fermentation products in the subsequent anoxic period. Oxygenation can particularly increase the degradation of more recalcitrant, aged organic matter (Arndt *et al.*, 2013). That nitrate reduction is not also increased by the increase in electron donors does not exclude this hypothesis, but rather likely reflects different limiting conditions, i.e. electron acceptor vs electron donor limitation. Nitrate reduction in the Wadden Sea is likely nitrate limited. Nitrate concentrations around Spiekeroog are negligible (e.g. <5 µM) in the summer and reach maximums of up to 60-120 µM in the winter during low tide (Grunwald *et al.*, 2010). In contrast, sulfate concentrations are about 28 mM, or 1000 times higher. Additionally, nitrate reduction can also use sulfide and iron II as an electron donor (An and Gardner, 2002; Liu *et al.*, 2019), both of which are abundant in the sediments of Janssand ((Jansen *et al.*, 2009), **Manuscript 2**), while sulfate and iron reduction are unable to use these donors. An increase in available electron donor such as might occur if oxygen boosted hydrolysis, would therefore increase sulfate reduction rates, but not nitrate reduction. Removal of ROS also increased hydrogen accumulation (**Manuscript 2**) indicating that fermentation is

inhibited by ROS, or again, that ROS reduced the organic carbon available for fermentation. This boost in hydrogen, a good electron donor, would also contribute to increased sulfate reduction rates. Differing limiting conditions explain the diverging responses of sulfate and nitrate reduction to ROS removal and oxygen pulses observed in **Manuscript 3**. In order to confirm these hypotheses, it would be beneficial to track how the carbon pool and inorganic electron donor concentrations change over an oxic-anoxic cycle. Additionally, it should be confirmed that nitrate reducers are acceptor limited by incubating sediment with additional electron donor and monitoring nitrate and sulfate reduction rates.

In the immediate aftermath of the advection of fresh oxygenated seawater into anoxic sediment, the chemical environment and metabolic activity within the sediment immediately changes (**Figure 3**). Iron II reacts with oxygen and is immediately converted to iron III, in the process producing ROS. These ROS inhibit aerobic respiration, and in the subsequent anoxic period, hydrogen accumulation, iron reduction, and sulfate reduction. Importantly, hydrogen can directly fuel iron and sulfate reduction. We expect that the inhibitory effect of ROS is mediated primarily by the abiotic interaction of ROS with the organic carbon pool, and possibly via a direct inhibitory effect on fermentation. The input of oxygenated seawater to the sediment also triggers denitrifiers to switch their metabolism to aerobic respiration, and through an unclear mechanism also increases sulfate reduction in the following anoxic period. This may be by increasing the hydrolysis of more recalcitrant organic carbon. If the input of fresh seawater also contains nitrate, this would prompt some sulfate reducers to switch their metabolism to DNRA.

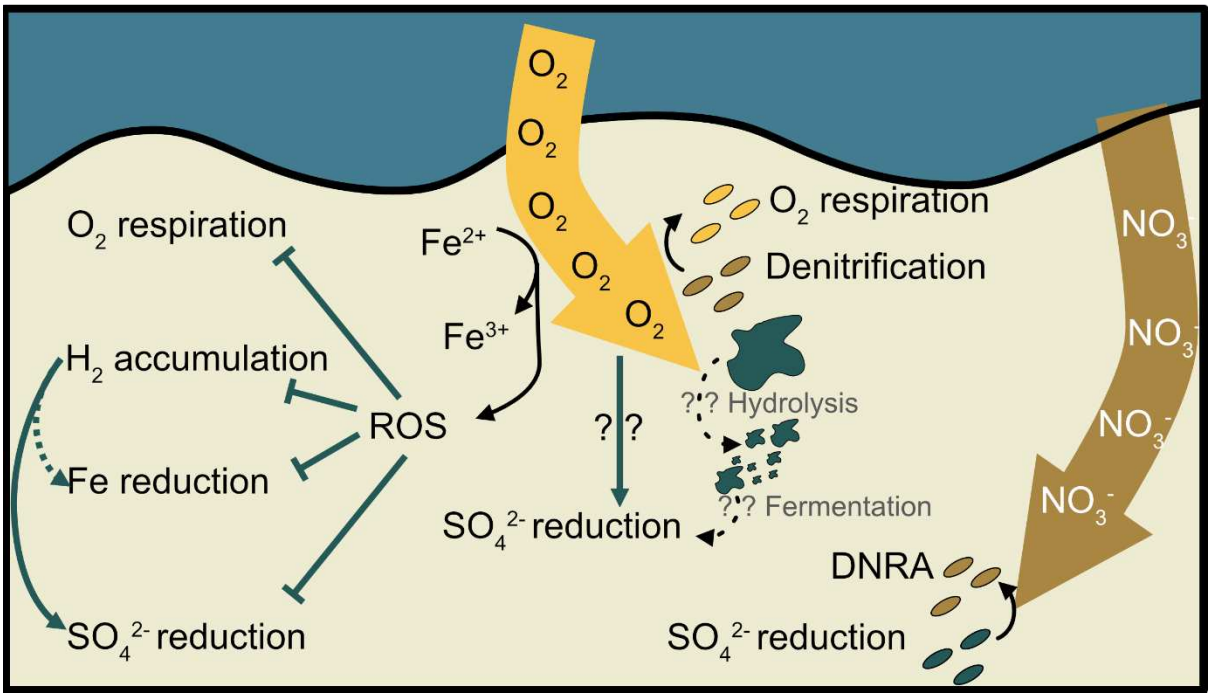

Figure 3: Short-term impacts of redox variation in permeable sediments of the Wadden Sea. An input of oxic, nitrate-rich seawater into anoxic sediment has immediate effects on microbial metabolism. Oxygen

abiotically reacts with iron II, producing iron III and reactive oxygen species in the process. Reactive oxygen species depress the rate of sulfate, iron reduction, and hydrogen accumulation once the sediments become anoxic, as well as aerobic respiration before the sediments become anoxic (Manuscripts 2 & 3). It is important to note that hydrogen can fuel sulfate and iron reduction, so a decrease in hydrogen accumulation would also affect rates of iron and sulfate reduction. Additionally, an influx of nitrate causes capable sulfate reducers to switch their metabolism to DNRA in the zone with nitrate but without oxygen. Similarly, an influx of oxygen causes denitrifiers to switch their metabolism to aerobic respiration. Through a mechanism possibly involving the aerobic hydrolysis of organic carbon transient oxygenation increases sulfate reduction rates in the subsequent anoxic period.

Environmental Implications

Redox fluctuation causes extensive changes to biogeochemical turnover rates, both in the immediate aftermath of a redox switch (**Manuscripts 1 - 3**), and over the long term when integrating the repeated effects. In the short term, the previously suppressed or depressed process rapidly increases, e.g. when sulfate reduction begins immediately upon anoxia, or increases after nitrate depletion (**Manuscripts 1 & 2**). Repeated cycling results in communities that can not only rapidly recover from redox switching, but also simultaneously employ multiple electron acceptors, e.g. aerobic denitrification (**Manuscript 4**, (Gao *et al.*, 2010)) or denitrification and DNRA occurring at the same time as sulfate reduction (**Manuscripts 1 & 3**). Redox fluctuation can also cause the generation of ROS, especially in iron-rich sediments (Zhao *et al.*, 2022). ROS in turn can decrease the rates of microbial respiration (**Manuscript 2 & 3**). Redox fluctuation and the associated ROS can also affect the lability of the carbon pool both by its degradation and by affecting its sorbtion to minerals (Chen *et al.*, 2021). Environmental redox fluctuation often occurs in areas of high microbial activity, since a high microbial activity is usually required to drive down oxygen and other electron acceptor concentrations. Thus, environmental redox fluctuation has the potential to impact a larger percentage of microbial carbon turnover than would be suggested by the geographic size of these regions.

This thesis found high levels of ROS in the anoxic zone of sediments and also that these ROS can decrease rates of sulfate reduction (**Manuscripts 2 & 3**). This greatly expands the zones in which ROS are relevant. Previously, ROS were expected in the oxic zone and in the oxic-anoxic transition zone, where reduced substances come into contact with oxygen (Imlay, 2019; Zhao *et al.*, 2022). ROS in the anoxic zone of sediments have the potential to be particularly potent, as large quantities of reduced iron would enable Fenton and pseudo-Fenton cycling (Gil-Lozano *et al.*, 2017). **Manuscript 3** found that the effects of ROS were more consistent in sediments that had been kept anoxic than those that were exposed to oxygen. While oxygenation produces large amounts of ROS in previously anoxic sediments, it may also increase availability of electron donor, decreasing the net effect of ROS compared to sediments kept anoxic. The response of sulfate reduction to ROS indicates that anaerobes in these sediments must constantly deal with some level of ROS exposure which is harmful to their metabolisms (Lu and Imlay,

2021). Fresh inputs of seawater such as through deep advection likely spur large bursts of ROS production and consequently decease rates of sulfate reduction, probably through decreasing availability of electron donor. This ROS production can occur even if the water input is anoxic, as replacing water around pyrite triggers another round of ROS production (Wang *et al.*, 2012).

ROS in photogranules

The role of ROS within photogranules was also briefly investigated using microsensors, revealing that the granules had an extremely high capacity for hydrogen peroxide degradation, with undetectable levels within the granule (**Figure 4**). This high capacity for degradation has previously been observed for other cyanobacterial consortia (de Beer *et al.*, 2018). These observations would indicate that ROS are highly regulated in Cyanobacteria, suggesting that in these environments they are frequently exposed to ROS. This is expected, as ROS can be produced directly by photosystem proteins under high-light conditions, both through the Mehler reaction involving photosystem I and directly in photosystem II (Asada, 1999; Pospíšil, 2016). In the Mehler reaction Photosystem I donates electrons from Photosystem II to molecular oxygen to form superoxide, which is immediately converted to hydrogen peroxide by superoxide dismutase (Asada, 1999). Ascorbate peroxidase or another antioxidant then converts the hydrogen peroxide to water. Together with the Hill reaction, which produces oxygen from water, these four reactions comprise the Water-Water Cycle (Asada, 1999). The Water-Water Cycle allows organisms to cope with excess electron flow under high-light conditions, and also generates a pH gradient which allows for ATP generation without NADPH generation (Asada, 1999; Cardol *et al.*, 2011). Photosystem II generates superoxide, singlet oxygen, and hydrogen peroxide under high-light conditions through various mechanisms, due to electron leakage to oxygen, electron transfer from triplet chlorophyll, and incomplete water oxidation (Pospíšil, 2016). All this is to say, photosynthetic organisms should be well prepared to remove ROS. Nevertheless, hydrogen peroxide can severely impair cyanobacteria and control toxic cyanobacterial blooms (Piel *et al.*, 2019).

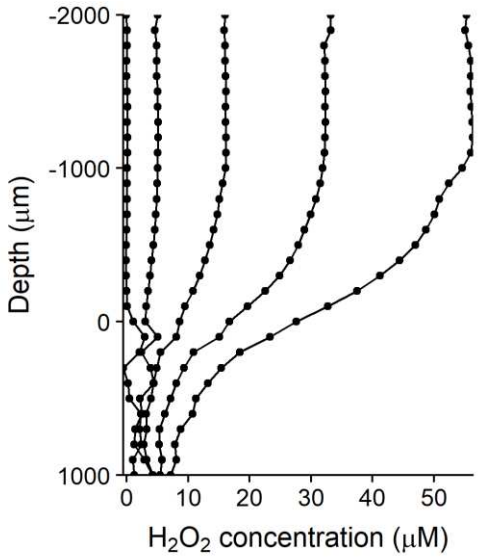

Figure 4 H_2O_2 degradation by photogranules: Profiles of the concentration of hydrogen peroxide above and within a photogranule after additions of hydrogen peroxide bringing the media concentration to 0, 5, 15, 30, and 55 µM hydrogen peroxide. The hydrogen peroxide is almost entirely consumed by the photogranule.

Follow up questions

The details of the rates and mechanisms of ROS formation in the Wadden Sea remain unresolved. While we found that ROS were quickly produced and consumed after the injection of oxic water into anoxic sediment, the typical rates of ROS consumption and production in these sediments remains unknown (**Manuscript 2**). Remarkably, the concentration of hydrogen peroxide peaked in the anoxic zone, indicating that anoxic processes produce large quantities of ROS. These anoxically produced ROS can also influence rates of mineralization within the sediment to a sometimes larger degree than in sediments exposed to oxygen (**Manuscript 3**). It has been previously shown that pyrite can react with water to produce ROS (Borda *et al.*, 2001; Cohn *et al.*, 2006; Gil-Lozano *et al.*, 2017). The "patchyness" of pyrite minerals influences how much ROS are produced from oxygenating pyrite, i.e. the more Fe (III)-oxide or -hydroxides the more ROS produced, which would be impacted by oxic-anoxic cycling and water replacement (Schoonen *et al.*, 2010; Gil-Lozano *et al.*, 2017). Determining the dynamics of anoxic ROS formation via long term in-situ measurements would help us further understand the role of ROS in the flats. The incubations in this thesis should also be repeated while simultaneously measuring the concentrations of ROS, to determine what concentration of hydrogen peroxide and superoxide are necessary to impact biogeochemical rates. Additional incubations with added ROS would be helpful to determine how different concentrations of ROS affect metabolism.

Several mechanisms could explain how ROS affect biogeochemical processes. ROS could be directly inhibiting, damaging, or killing microbes and their proteins, leading to lower rates of consumption (Ma *et al.*, 2019; Zhang *et al.*, 2020). On the other hand, hydrogen peroxide reacts

with minerals to form hydroxyl radicals that directly react with the carbon pool, remineralizing some of it to CO_2 and altering the structure of other parts (Trusiak *et al.*, 2018; Remucal *et al.*, 2020; Yu and Kuzyakov, 2021). Altering the size and composition of the carbon pool also has the potential to change mineralization rates. For example, a solution of pyrite and water generated enough ROS to degrade lactate, which is a good electron donor for sulfate reducers (Wang *et al.*, 2012). Furthermore, enzymes, including those performing hydrolysis of carbon molecules, are usually extremely specific, and any alteration may make a molecule no longer fit into an enzyme's active site (Robinson, 2015). In order to determine the mechanism through which ROS affects the carbon pool, organic carbon composition and concentration should be tracked over the course of an incubation, with and without enzymatic removal of ROS. This could be done with ultra-performance liquid chromatography (UPLC) for selected carbon molecules, and with mass spectrometry for a broader class of molecules. Additionally, live cell counts and examining transcriptomes of sediments should elucidate whether cells are undergoing oxidative stress that inhibits their metabolisms. Incubations with and without the provision of additional organic carbon should also be performed, to determine whether rates are electron donor limited. This would be particularly helpful for determining why sulfate reduction rates are impacted by oxygenation and ROS, but nitrate reduction rates are not, i.e. confirming that nitrate reduction rates are acceptor-limited and sulfate reduction rates are donor-limited.

Acquiring sediment profiles of superoxide and the hydroxyl radical and comparing them to oxygen and hydrogen peroxide would also be particularly interesting. The hydroxyl molecule is the species that directly reacts with organic carbon, and like superoxide and peroxides, is both a oxidant and reductant. Hydroxyl radicals and superoxide have short half-lives, making analysis difficult, with superoxide having a half-life in seawater of seconds to minutes, and the hydroxyl radical around 250 nanoseconds (Morris *et al.*, 2022). Initial attempts to acquire superoxide profiles were made by Marit van Erk and Subhajit Basu during a cruise in 2022. Porewater was extracted into a syringe containing superoxide dismutase. Superoxide dismutase converts superoxide dismutase to hydrogen peroxide and oxygen, which are more much more stable. The hydrogen peroxide was then measured using the fluorometric method described in Manuscript 2. These initial attempts proved promising, with a difference between the hydrogen peroxide concentrations detected in porewater with and without added superoxide dismutase. Detecting hydroxyl radical concentrations is considerably more difficult, due to its shorter half-life and the lack of enzymes able to convert it to a more stable product. Currently methods for detecting hydroxyl radical production rely on its reaction with dyes, which give the total production over a given time period, but not the standing concentration (Zhang *et al.*, 2020; Zhao *et al.*, 2022).

Conclusion

Varying electron acceptor availability directly impacts microbial respiration. It results in a more flexible metabolic sorting than under more stable conditions, with multiple electron acceptors being respired at once. It also selects for microbes that can quickly initiate anaerobic respiration in the anoxic period following oxygen exposure. This allows anaerobes like sulfate reducers to thrive even at depths regularly exposed to nitrate and oxygen. Varying electron acceptor availability also results in ROS production, which directly depresses respiration rates. The fascinating interplay of electron acceptor variation, ROS, and microbial respiration is fertile ground for further investigation and an underexplored control on carbon turnover in variable environments.

An, S. and Gardner, W.S. (2002) Dissimilatory nitrate reduction to ammonium (DNRA) as a nitrogen link, versus denitrification as a sink in a shallow estuary (Laguna Madre/Baffin Bay, Texas). *Mar Ecol Prog Ser* **237**: 41–50.

Arndt, S., Jørgensen, B.B., LaRowe, D.E., Middelburg, J.J., Pancost, R.D., and Regnier, P. (2013) Quantifying the degradation of organic matter in marine sediments: A review and synthesis. *Earth-Sci Rev* **123**: 53–86.

Asada, K. (1999) The Water-Water Cycle in Chloroplasts: Scavenging of Active Oxygens and Dissipation of Excess Photons. *Annu Rev Plant Physiol Plant Mol Biol* **50**: 601–639.

de Beer, D., Meyer, V., Klatt, J., and Li, T. (2018) Photosynthesis under very high oxygen concentrations in dense microbial mats and biofilms. *bioRxiv* 335299.

Borda, M.J., Elsetinow, A.R., Schoonen, M.A., and Strongin, D.R. (2001) Pyrite-Induced Hydrogen Peroxide Formation as a Driving Force in the Evolution of Photosynthetic Organisms on an Early Earth. *Astrobiology* **1**: 283–288.

Cardol, P., Forti, G., and Finazzi, G. (2011) Regulation of electron transport in microalgae. *Regul Electron Transp Chloroplasts* **1807**: 912–918.

Chen, J., Hanke, A., Tegetmeyer, H.E., Kattelmann, I., Sharma, R., Hamann, E., et al. (2017) Impacts of chemical gradients on microbial community structure. *ISME J* **11**: 920–931.

Chen, N., Fu, Q., Wu, T., Cui, P., Fang, G., Liu, C., et al. (2021) Active Iron Phases Regulate the Abiotic Transformation of Organic Carbon during Redox Fluctuation Cycles of Paddy Soil. *Environ Sci Technol* **55**: 14281–14293.

Cohn, C.A., Mueller, S., Wimmer, E., Leifer, N., Greenbaum, S., Strongin, D.R., and Schoonen, M.A. (2006) Pyrite-induced hydroxyl radical formation and its effect on nucleic acids. *Geochem Trans* **7**: 3.

Dong, H., Zeng, Q., Sheng, Y., Chen, C., Yu, G., and Kappler, A. (2023) Coupled iron cycling and organic matter transformation across redox interfaces. *Nat Rev Earth Environ* **4**: 659–673.

Fenchel, T. and Jørgensen, B. (1977) Detritus Food Chains of Aquatic Ecosystems: The Role of Bacteria. In *Adv. Microb. Ecol.*, pp. 1–58.

Gao, H., Schreiber, F., Collins, G., Jensen, M.M., Kostka, J.E., Lavik, G., et al. (2010) Aerobic denitrification in permeable Wadden Sea sediments. *ISME J* **4**: 417–426.

Gil-Lozano, C., Davila, A.F., Losa-Adams, E., Fairén, A.G., and Gago-Duport, L. (2017) Quantifying Fenton reaction pathways driven by self-generated H2O2 on pyrite surfaces. *Sci Rep* **7**: 43703.

Grunwald, M., Dellwig, O., Kohlmeier, C., Kowalski, N., Beck, M., Badewien, T.H., et al. (2010) Nutrient dynamics in a back barrier tidal basin of the Southern North Sea: Time-series, model simulations, and budget estimates. *J Sea Res* **64**: 199–212.

Imlay, J.A. (2019) Where in the world do bacteria experience oxidative stress? *Environ Microbiol* **21**: 521–530.

Jansen, S., Walpersdorf, E., Werner, U., Billerbeck, M., Böttcher, M.E., and Beer, D. (2009) Functioning of intertidal flats inferred from temporal and spatial dynamics of O2, H2S and pH in their surface sediment. *Ocean Dyn* **59**: 317–332.

Laverman, A.M., Pallud, C., Abell, J., and Cappellen, P.V. (2012) Comparative survey of potential nitrate and sulfate reduction rates in aquatic sediments. *Geochim Cosmochim Acta* **77**: 474–488.

Liu, T., Chen, D., Li, X., and Li, F. (2019) Microbially mediated coupling of nitrate reduction and Fe(II) oxidation under anoxic conditions. *FEMS Microbiol Ecol* **95**: fiz030.

Lu, Z. and Imlay, J.A. (2021) When anaerobes encounter oxygen: mechanisms of oxygen toxicity, tolerance and defence. *Nat Rev Microbiol* **19**: 774–785.

Ma, S., Tong, M., Yuan, S., and Liu, H. (2019) Responses of the Microbial Community Structure in Fe(II)-Bearing Sediments to Oxygenation: The Role of Reactive Oxygen Species. *ACS Earth Space Chem* **3**: 738–747.

Marchant, H.K., Ahmerkamp, S., Lavik, G., Tegetmeyer, H.E., Graf, J., Klatt, J.M., et al. (2017) Denitrifying community in coastal sediments performs aerobic and anaerobic respiration simultaneously. *ISME J* **11**: 1799–1812.

Morris, J.J., Rose, A.L., and Lu, Z. (2022) Reactive oxygen species in the world ocean and their impacts on marine ecosystems. *Redox Biol* **52**: 102285.

Piel, T., Sandrini, G., White, E., Xu, T., Schuurmans, J.M., Huisman, J., and Visser, P.M. (2019) Suppressing Cyanobacteria with Hydrogen Peroxide Is More Effective at High Light Intensities. *Toxins* **12**: 18.

Pospíšil, P. (2016) Production of Reactive Oxygen Species by Photosystem II as a Response to Light and Temperature Stress. *Front Plant Sci* **7**:.

Remucal, C.K., Salhi, E., Walpen, N., and von Gunten, U. (2020) Molecular-Level Transformation of Dissolved Organic Matter during Oxidation by Ozone and Hydroxyl Radical. *Environ Sci Technol* **54**: 10351–10360.

Richards, F.A., Cline, J.D., Broenkow, W.W., and Atkinson, L.P. (1965) Some consequences of the decomposition of organic matter in Lake Nitinat, an anoxic fjord. *Limnol Oceanogr* **10**: R185–R201.

Robinson, P.K. (2015) Enzymes: principles and biotechnological applications. *Essays Biochem* **59**: 1–41.

Schoonen, M.A.A., Harrington, A.D., Laffers, R., and Strongin, D.R. (2010) Role of hydrogen peroxide and hydroxyl radical in pyrite oxidation by molecular oxygen. *Geochim Cosmochim Acta* **74**: 4971–4987.

Trusiak, A., Treibergs, L.A., Kling, G.W., and Cory, R.M. (2018) The role of iron and reactive oxygen species in the production of CO2 in arctic soil waters. *Geochim Cosmochim Acta* **224**: 80–95.

Wang, W., Qu, Y., Yang, B., Liu, X., and Su, W. (2012) Lactate oxidation in pyrite suspension: A Fenton-like process in situ generating H2O2. *Chemosphere* **86**: 376–382.

Yu, G.-H. and Kuzyakov, Y. (2021) Fenton chemistry and reactive oxygen species in soil: Abiotic mechanisms of biotic processes, controls and consequences for carbon and nutrient cycling. *Earth-Sci Rev* **214**: 103525.

Zhang, Y., Tong, M., Yuan, S., Qian, A., and Liu, H. (2020) Interplay between iron species transformation and hydroxyl radicals production in soils and sediments during anoxic-oxic cycles. *Geoderma* **370**: 114351.

Zhao, G., Tan, M., Wu, B., Zheng, X., Xiong, R., Chen, B., et al. (2023) Redox Oscillations Activate Thermodynamically Stable Iron Minerals for Enhanced Reactive Oxygen Species Production. *Environ Sci Technol* **57**: 8628–8637.

Zhao, G., Wu, B., Zheng, X., Chen, B., Kappler, A., and Chu, C. (2022) Tide-Triggered Production of Reactive Oxygen Species in Coastal Soils. *Environ Sci Technol* **56**: 11888–11896.

Thank you to Dirk de Beer, for allowing me to do my PhD work your group. Thank you for your supervision, teaching, and advice. Thank you for allowing me great freedom in choosing and pursuing the questions that I found interesting, enabling me to grow as a scientist. Thank you for all of your support and enabling me to do fieldwork even with a young baby. And thank you for reviewing my thesis!

Thank you to Tim Ferdelman, for your help and advice in planning my projects both during my master's and PhD, and for getting me interested in biogeochemistry and especially sulfate reduction years ago during my internship. Thank you for also serving on my PhD committee and reviewing this thesis.

Thank you to Judith Klatt and Michael Friedrich, for serving on my PhD committee. And an additional thank you to Judith introducing me to environmental microbiology lab work!

Thank you to Hannah Marchant, for your help and supervision in relation to all things nitrogen, and for being willing to take me on as a Master's student.

Thank you to Gabi Klockgether, for her help in running samples on the Mass Spec, and for measuring samples when I could not.

Thank you to Kirsten, for her help in the lab and with distillations.

Thank you to the technicians of the former Microsensor group, Gaby, Vera, Anja, Ines, Cäcilia and Karin, for producing microsensors for my work, helping with lab work, and for being so friendly and willing to help and chat.

Thank you to the Chyrene Moncada and Nina Tölke, for your excellent work during lab rotations, as well as help you provided in the lab afterwards.

Thank you to Elisa and Marit, for your help with projects and friendly conversations.

Thank you to Gunter, for your help with hydrogen measurements.

Thank you to all my co-authors of manuscripts in the thesis for your collaboration and comradery.

Thank you to the crew members of the Linquenda during our cruise in the Dutch Wadden Sea, and to the captains of the Spiekeroog Water Taxi service, who enabled many sampling trips.

Thank you to Ulrike and the other members of administration, whose organizational skills enable our research at the institute.

Thank you to the Marmic faculty and administrators, for creating the opportunity to study at the MPI.

Thank you to my family, for your support and love.

Finally, thank you to my husband, Patric, who has been with me throughout this whole journey. Who has lent me his strength and motivation and allowed me to push through the chaos of a pandemic and two children to finish my work. Who has also given me his love and care, and with whom I spent months isolating without feeling lonely or isolated. Who and am truly blessed to have as a friend and partner.